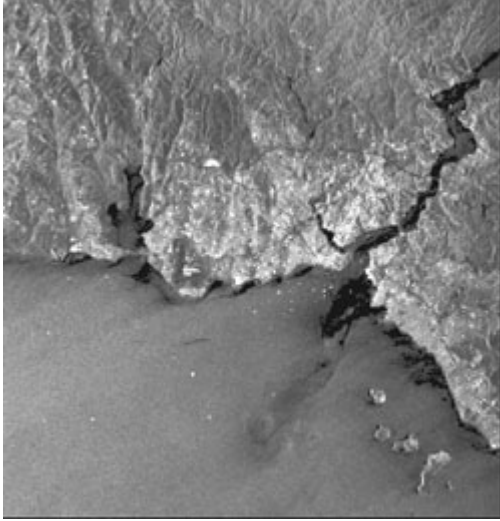


Oceanic Phenomena

Table Of Contents

- [Channel Plumes](#)
- [Coastal Discharges](#)
- [Coastal Fronts](#)
- [Coastal Rivers](#)
- [Current Fronts](#)
- [Estuaries](#)
- [Intertidal Zone](#)
- [Oceanic Eddies](#)
- [Oceanic Internal Waves](#)
- [Oceanic Wakes](#)
- [Oil Pollution](#)
- [Ship Wakes](#)
- [Underwater Bottom Topography](#)
- [Upwelling](#)

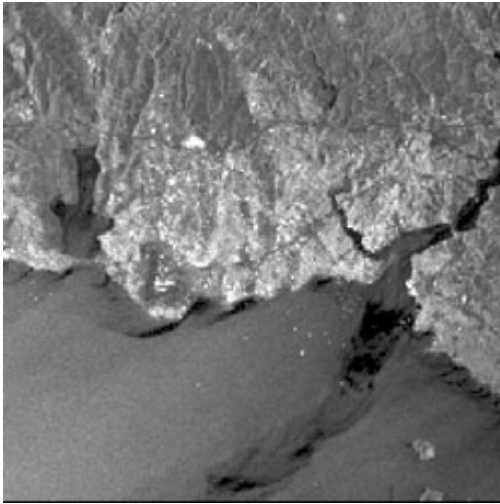
Channel Plumes



Turkey

Latitude: 41° 11' N - Longitude: 28° 32' E

The channel plume of the Bosporus is visible extending into the Sea of Marmara, which has generated at the front a vortex pair.



Turkey

Latitude: 41° 14' N - Longitude: 28° 31' E

ERS-1 SAR image of the city of Istanbul (the bright area in the lower section of the image) and of the Bosporus, which is the sea channel connecting the Black Sea with the Sea of Marmara. Surface water from the Black Sea flows into the Sea of Marmara and generates there an elongated plume. Note the numerous ships (bright spots) which anchor before the harbour of Istanbul.

#	Orbit	Frame(s)	Satellite	Date	Time	Location
1	01056	0819	ERS-2	03-Jul-1995	20:20	
2	15509	0819	ERS-1	03-Jul-1994	20:21	

References

- D.D. Ioro & Yuce, H., Observations of Mediterranean flow into the Black Sea. *J. Geophys. Res.*, **104**, No. C2, 3091-3108 (1999).
- H. Yuce. On the variability water flow into the Black Sea. *Cont. Shelf Res.*, **16**, 1399-1413 (1996).
- Ozsoy, E. & Unluata, U., The Black Sea. In: *The Sea*, Vol. 11, Chapter 31, 889-914.
- Unluata, U., Oguz, T., Latif, M.A. & Ozsoy, E., On the physical oceanography of the Turkish Straits. In: *The Physical Oceanography of Sea Straits*, edited by L.J. Pratt, Kluwer Acad., 25-60 (1990).

Coastal Discharges

Introduction

Industrial and municipal (sewage) plants located at the coast often discharge substances into the sea that float on the sea surface and damp there the short water waves that are responsible for the radar backscattering.

Therefore they often become visible on radar images as dark patches. They consist of surface-active material whose chemical composition can vary considerably. Not only mineral (petroleum) oil is surface-active, but also a countless number of natural and artificial (i.e. chemically produced) substances. It can be supposed that in many cases these discharges are not known to the authorities and that some of them are illegal.

Space-borne SAR imagery can be helpful in disclosing these coastal discharges which can be quite harmful for the coastal environment.

Mediterranean Sea

Strait of Messina

Latitude: 41° 11' N - Longitude: 28° 32' E

ERS-1 SAR image acquired on 8 September 1992 showing a section of the Mediterranean Sea (Tyrrhenian Sea) north-west of the Strait of Messina with the Golfo di Gioia (sea area where the a bright mushroom-like feature is visible which originates from a katabatic wind blowing from the mountains onto the sea); see the section " Atmospheric Phenomena", "Katabatic Winds" of this website). The dark patch marked by an arrow results from a coastal discharge from the river Budello into the Golfo di Gioia just south of the port of Gioia,Tauro. It seems that polluted waters from industrial plants are discharged into the sea via this river (see photographs).

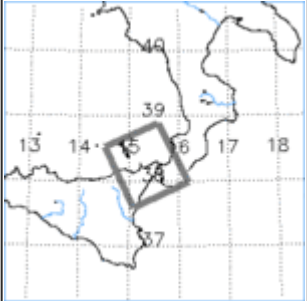


Strait of Messina

Latitude: 41° 11' N - Longitude: 28° 32' E

ERS-1 SAR image acquired on 8 September 1992 showing a section of the Mediterranean Sea (Tyrrhenian Sea) north-west of the Strait of Messina with the Golfo di Gioia (sea area where the a bright mushroom-like feature is visible which originates from a katabatic wind blowing from the mountains onto the sea); see the section " Atmospheric Phenomena", "Katabatic Winds" of this website). The dark patch marked by an arrow results from a coastal discharge from the river Budello into the Golfo di Gioia just south of the port of Gioia,Tauro. It seems that polluted waters from industrial plants are discharged into the sea via this river (see photographs).



#	Orbit	Frame(s)	Satellite	Date	Time	Location
1	6014	765	ERS-1	08-Sep-1992	21:13	
2	15079	765	ERS-1	3-Jun-1994	21:14	

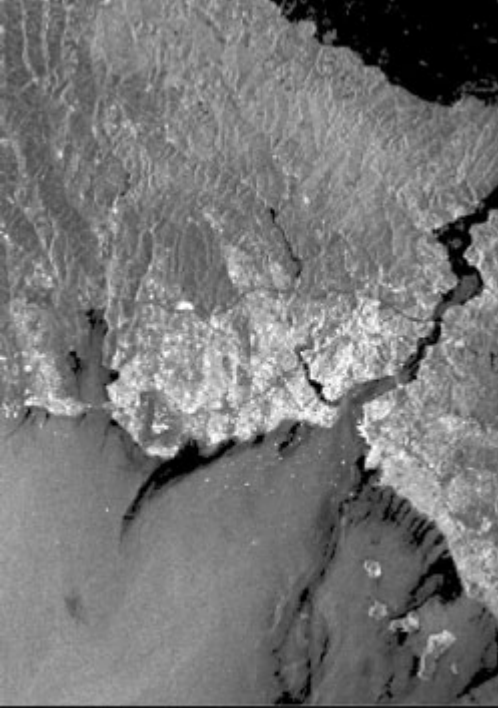
Sea of Marmara

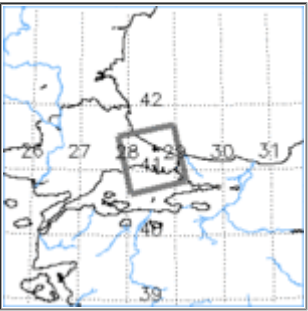
Turkey

Latitude: 41° 11' N - Longitude: 28° 32' E

ERS-1 SAR image showing a section of the Black Sea (at the top) and of the Sea of Marmara (at the bottom) with the Bosphorus in between. The bright areas visible at the southern end of the Bosphorus are the European and the Asian sections of the Turkish town of Istanbul.

The black patches and streaks visible in the coastal area adjacent to the city are very likely coastal discharges consisting sewage and industrial waste.



#	Orbit	Frame(s)	Satellite	Date	Time	Location
1	20242	3087	ERS-1	29-May-1995	20:20	

ERS SAR Views the Tropical and Subtropical Ocean

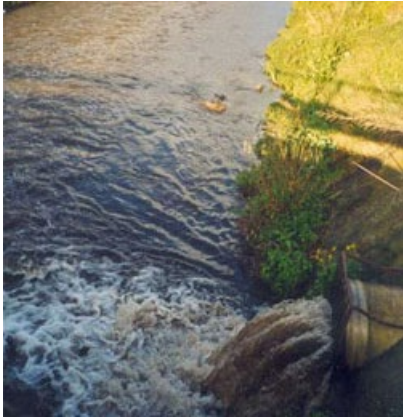


Photo of the river Budello taken on 31 January 2003, which in this part of the town of Gioia di Tauro is channelled. The view is towards west. Visible at the bottom of the photo is a spout or waste-pipe spilling "dirty water" into the river.



Another photo of the spout or waste-pipe taken on 31 January 2003.



Photo of sand bars at the mouth of the river Budello near the port of Gioia, Tauro.

Coastal Fronts

Introduction

Ocean fronts are boundaries between water masses with dissimilar properties. The dynamics by which the front is maintained between two water masses of different densities (due to different temperatures or/and salinities) causes convergences at the sea surface.

The fronts are usually marked by an increase in surface roughness due to the interaction of the convergent surface flow with the surface waves and thus appear on SAR images as bright lines. But they also can be marked by a decrease in surface roughness due to the fact that in the convergent regions surface slicks accumulate which damp the surface waves.

Ocean fronts are often located near the coast. So-called "shelf break fronts" are formed at the edges of continental shelves where waters characteristic of shallow shelf regions meet with waters of the continental slopes and the deep ocean.

So-called "shallow-sea fronts" are formed in shallow seas and estuaries where well-stratified offshore waters meet with coastal waters which are well-mixed by the action of the winds and the tides. Water near the coast often has a lower salinity than the waters further offshore because of inflow of fresh water from rivers.

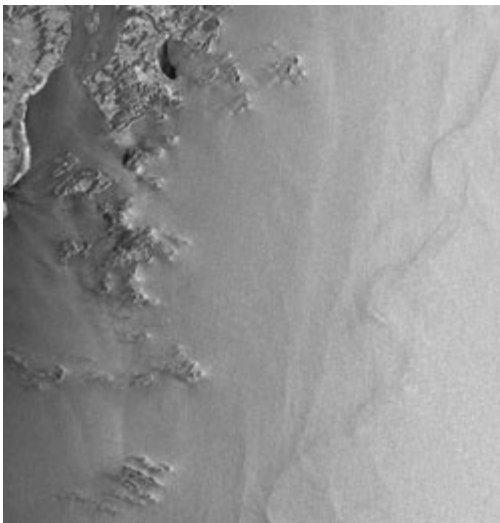
Taiwan Strait



Taiwan Strait

Latitude: 27° 19' N - Longitude: 121° 28' E

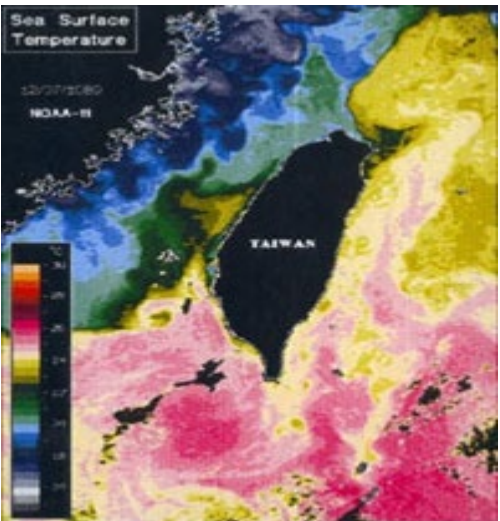
SPOT-1 image of the waters off the east coast of China. On this optical image also eddy-like structures are visible in the frontal region. © CNES 2000 - Spot Image distribution <http://www.spotimage.fr/>



Taiwan Strait

Latitude: 26° 59' N - Longitude: 120° 35' E

This ERS-1 SAR image shows a coastal front adjacent to the east coast of China. The front is a temperature front which forms in the cold season in the Taiwan Strait. The difference in sea surface temperature on both sides of the front can reach values of 8-10° C. Note that the thermal front has the form of a meander which is an often observed phenomena and which results from instabilities.

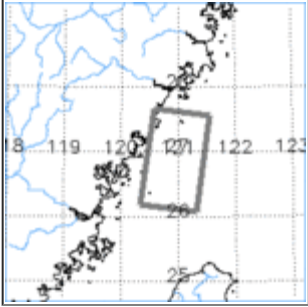
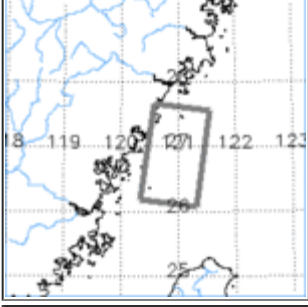
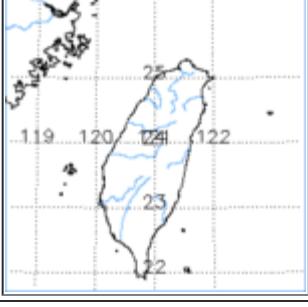


Taiwan Strait

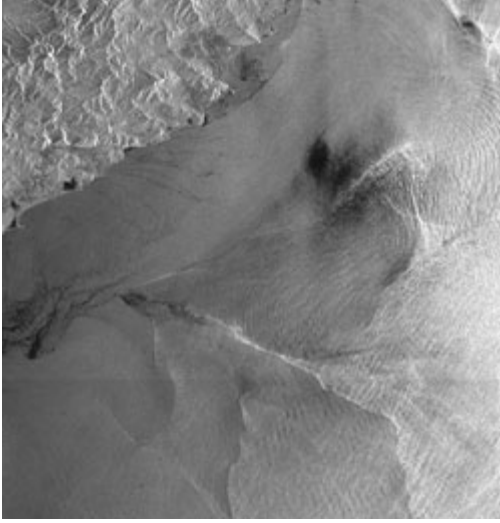
Latitude: 24° 00' N - Longitude: 121° 00' E

Sea surface temperature (SST) map of the waters surrounding Taiwan derived from NOAA-11 AVHRR data (channel 4) acquired on 7.Dec.1989 at almost cloudless sky conditions.

On this map the temperature is colour-coded (yellow/red: warm; blue: cold). Clearly visible is on this map the meandering frontal boundary in the Taiwan Strait. Note the warm waters of the Kuroshio Current adjacent to the east coast of Taiwan. Warm waters of the Kuroshio current intrude into the northern shelf of the East China Sea and from a sharp SST front north of Taiwan.

#	Orbit	Frame(s)	Satellite	Date	Time	Location
1	Path: 298	294-295-296-297	SPOT 1	28-Jan-1997	02:14	
2	23266	3151-3169	ERS-1	27-Dec-1995	02:30	
3	-	-	NOAA 11	07-Dec-1989	unknown	

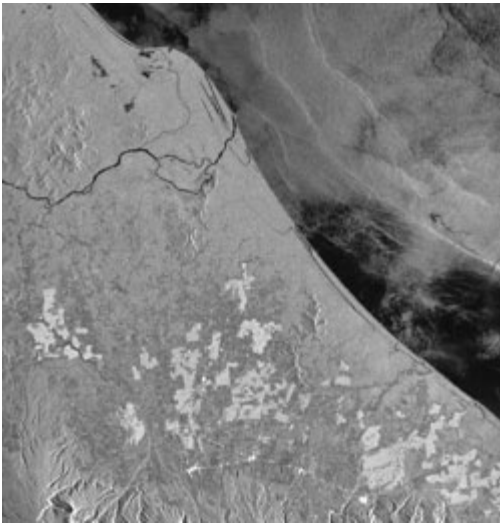
Latin American Pacific Coast



Mexico

Latitude: 15° 28' N - Longitude: 95° 29' W

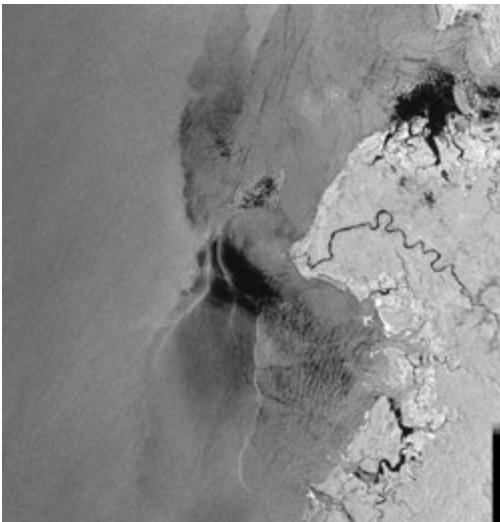
On this ERS-2 SAR image, which was acquired over the coastal waters off the Pacific coast of Mexico, several coastal fronts are visible. The large bright features visible in the lower right-hand section of the image are very likely the sea surface manifestation of an oceanic eddy.



Costa_Rica

Latitude: 10° 32' N - Longitude: 83° 38' W

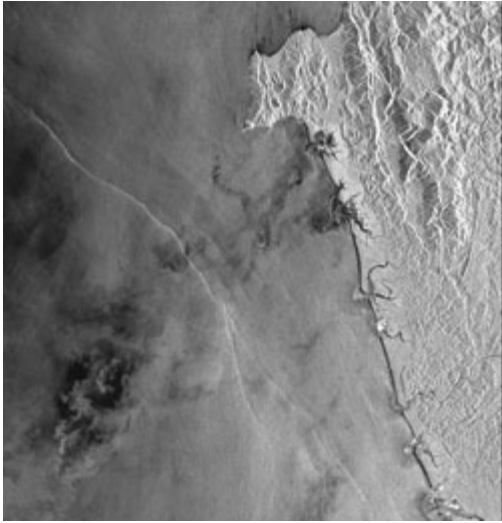
On this ERS-1 SAR image several coastal fronts are visible aligned approximately parallel to the Atlantic coast of Costa Rica in Central America.



Colombia

Latitude: 2° 06' N - Longitude: 78° 59' W

Coastal fronts in the Pacific Ocean off the coast of Colombia. The fronts visible in the lower section of the image are clearly connected with the inflow of fresh water from the rivers into the ocean.



Colombia

Latitude: 5° 14' N - Longitude: 77° 35' W

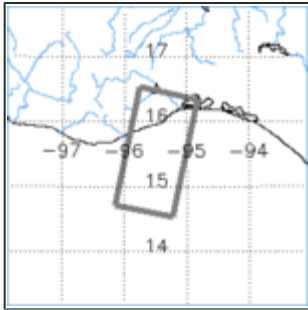
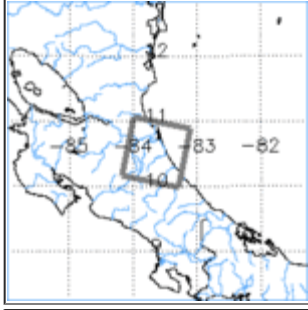
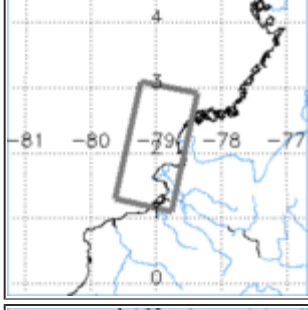
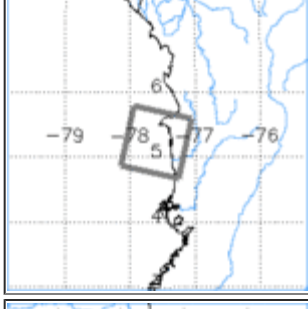
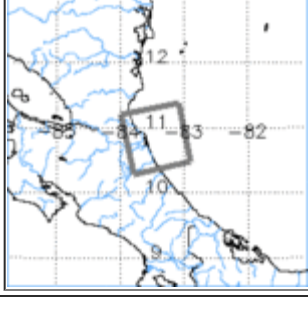
The bright line visible on this ERS-1 SAR image acquired over the coastal waters off the Pacific coast of Colombia seems to be a coastal front. Note also the small fronts at the mouths of the coastal rivers and the sea surface imprints of tropical rain cells (the dark/bright features crossing diagonally the image).



Costa Rica

Latitude: 10° 51' N - Longitude: 83° 26' W

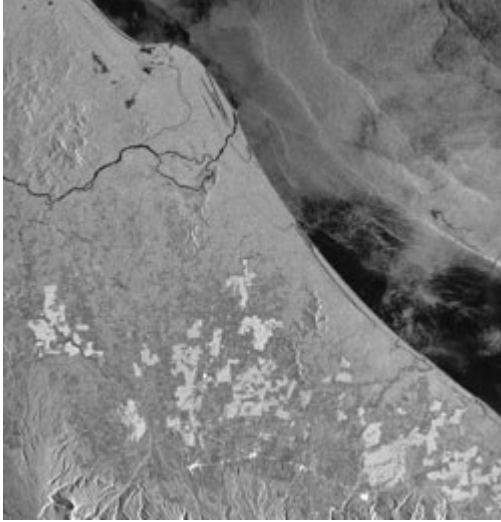
On this ERS-1 SAR image several coastal fronts and, in the right-hand section of the image, sea surface imprints of tropical rain cells are visible.

#	Orbit	Frame(s)	Satellite	Date	Time	Location
1	04990	3285-3303	ERS-2	03-Apr-1996	16:50	
2	10906	3393	ERS-1	16-Aug-1993	16:00	
3	11965	3555-3573	ERS-1	29-Oct-1993	15:26	
4	12194	3501	ERS-1	14-Nov-1993	15:32	
5	16260	0207	ERS-1	25-Aug-1994	04:07	

References

- Johannessen, J.A., Shuchman, R.A., Johannessen, O.M., Davidson, K.L. & Lyzenga, D.R., Synthetic aperture radar imaging of upper ocean circulation features and wind fronts. *J. Geophys. Res.*, **96**, No. C6, 10411-10422 (1991).
- Johannessen, J.A., Shuchman, R.A., Digranes, G., Lyzenga, D.R., Wackerman, C., Johannessen, O.M. & Vachon, P.W., Coastal ocean fronts and eddies imaged with synthetic aperture radar. *J. Geophys. Res.*, **101**, 6651-6668 (1996).
- Legeckis, R., A survey of worldwide sea surface temperature fronts detected by environmental satellites. *J. Geophys. Res.*, **83**, No. C9, 4501-4522 (1978).
- Marmorino, G.O., Thompson, D.R., Graber, H.C. & Trump, C.L., Correlation of oceanographic signatures appearing in synthetic aperture radar and interferometric synthetic aperture radar imagery with in situ measurements. *J. Geophys. Res.*, **102**, No. C8, 18723-18736 (1997).

Coastal Rivers



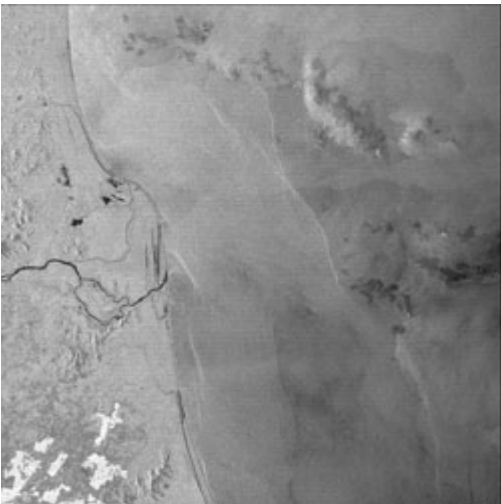
Costa Rica

Latitude: 10° 32' N - Longitude: 83° 38' W

Atlantic coast of northern Costa Rica and south Nicaragua. The river visible in the upper left-hand section of the image is the San Juan river which separates Costa Rica from Nicaragua. The dark lines near the coast are caused by a ramified river system discharging water from the tropical rain forest into the Caribbean Sea.

This river system changes strongly with time: after floods new river arms are generated and old ones are cut-off.

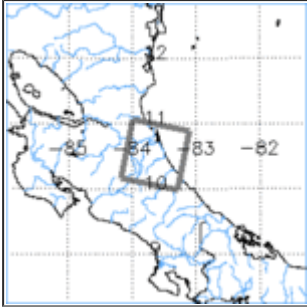
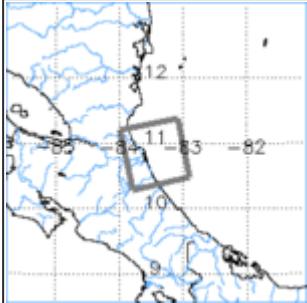
A comparison of the river system visible on this SAR image with the one drawn on a geographical map (available via internet: <http://lorenz.mur.csu.edu.au/cgi-bin/gis/Map>) reveals quite significant differences. This demonstrates that ERS SAR images can be used for monitoring changes in river systems in tropical areas.



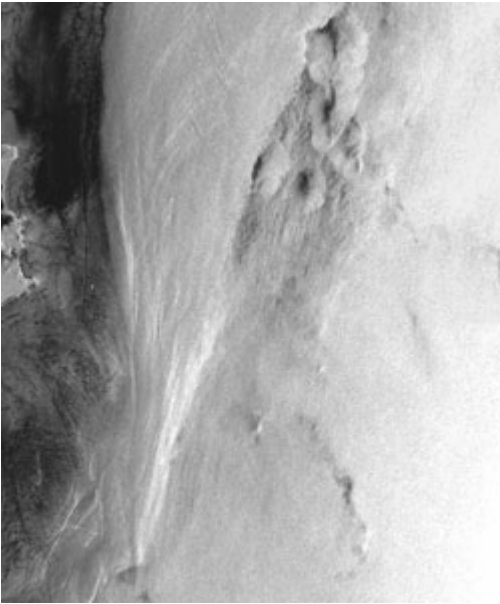
Costa Rica

Latitude: 10° 51' N - Longitude: 83° 26' W

On this image the same river system is visible as on the previous one. However, this image was acquired one year later during an ascending pass of the ERS 1 satellite, while the previous one was acquired during a descending pass. A detailed comparison of both images reveals that during the one year period the river system has changed.

#	Orbit	Frame(s)	Satellite	Date	Time	Location
1	10906	3393	ERS-1	16-Aug-1993	16:00	
2	16260	0207	ERS-1	25-Aug-1994	04:08	

Current Fronts



Australia

Latitude: 32° 10' S - Longitude: 153° 02' E

SAR strip of three ERS-1 SAR frames acquired over the coastal waters at the east coast of Australia. The East-Australian Current, which is the western boundary current of the South Pacific, is clearly visible as a broad bright band. Noteworthy are the V-shaped features visible in the northern section of this image. Their origin is unknown to us.

#	Orbit	Frame(s)	Satellite	Date	Time	Location
1	08019	4239-4257-4275	ERS-1	26-Jan-1993	23:43	

References

- Church, J.A. & Craig, P.D., Australia's shelf seas: Diversity and complexity (30,W-S). In: *The Sea*, **11**, edited by A.R. Robinson and K.H. Brink, John Wiley & Sons, Inc., Chapter 33, 933-964 (1998).
- Nilsson, C.S. & Tildesley, P.C., Imaging of oceanic fronts by ERS 1 synthetic aperture radar. *J. Geophys. Res.*, **100**, No. C1, 953-967 (1995).
- Nilsson, C.S. & Cresswell, G.R., The formation and evolution of East Australian Current warm-core eddies. In: *Progress in Oceanography*. Vol. **9**. (M.V. Angel and J. O'Brien, editors). Pergamon Press, Oxford, Frankfurt, pp. 133-183 (1982).

Estuaries

In estuaries fresh water discharged from rivers meets the salty water of the ocean. At the boundary between these two water masses a front occurs which is called "plume front" or "fresh water front". The front is associated with a narrow band of surface flow convergence where the sea surface roughness usually increases due to hydrodynamic interaction of the surface current with the short surface waves. In this case the front line is imaged by the SAR as a bright line. However, in the presence of surface slicks, slick material accumulates in the convergence zones where it damps the short surface waves. In this case the front line is imaged as a dark line.

Often the river water carries a load of sand and other terrestrial dissolutes which deposit in the estuary. Therefore in most estuaries shallow underwater sandbanks are encountered.

Often the river water is also covered with surfactants, which are either of natural (in most cases) or of anthropogenic origin. They cause a reduction of the short-scale sea surface roughness. In this case the area inside the plume front appears on the SAR image darker than the area outside this front. In addition, the river water usually has a temperature which is different from the temperature of the coastal water. This temperature difference can also give rise to a difference in grey level in the SAR image.

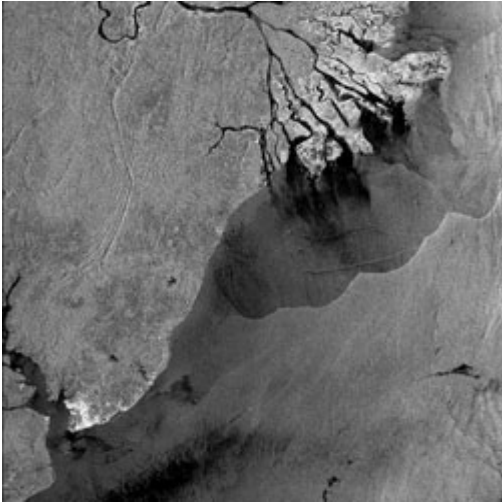
- [Mahakam \(Borneo\)](#)
- [Mekong \(Vietnam\)](#)
- [Danube \(Romania\)](#)
- [Iscuande \(Colombia\)](#)
- [Maroni \(Suriname, French Guiana\)](#)
- [Guayas \(Ecuador\)](#)
- [Ganges \(India, Bangladesh\)](#)

Mahakam (Borneo)

Kutai

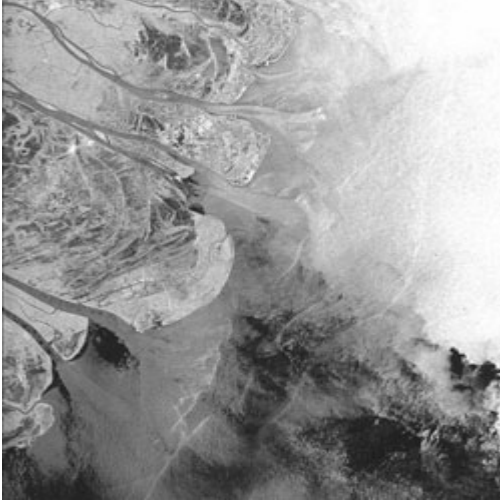
Latitude: 1° 01' S - Longitude: 117° 12' E

Frontal boundary between the fresh water outflow from the river Kutai in Borneo and the salty water of Macassar Strait. The form of the frontal boundary seems to mirror the water outflow from the various river arms.



#	Orbit	Frame(s)	Satellite	Date	Time	Location
1	24320	3627	ERS-2	12-Dec-1999	02:29	A map of the Kutai region in Borneo, Indonesia. It features a grid with latitude lines from -1 to -5 and longitude lines from -82 to -78. A blue line represents the river network. A black box highlights the specific area shown in the satellite image above, centered around 1° S and 117° E.

Mekong (Vietnam)

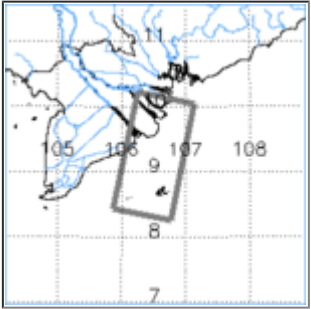


Vietnam

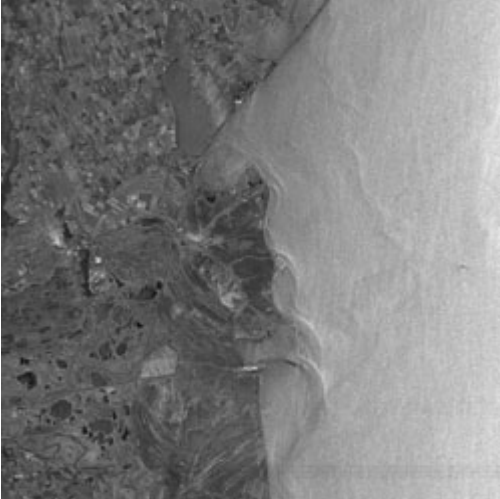
Latitude: 9° 15' N - Longitude: 106° 31' E

ERS-2 SAR image of the Mouths of the Mekong in Vietnam. Several arms of the Mekong river and several frontal boundaries (bright lines) are visible.

In the lower right-hand section of the image the Vietnamese island Con Son is visible.

#	Orbit	Frame(s)	Satellite	Date	Time	Location
1	7172	3411-3429	ERS-2	03-Sep-1996	03:18	

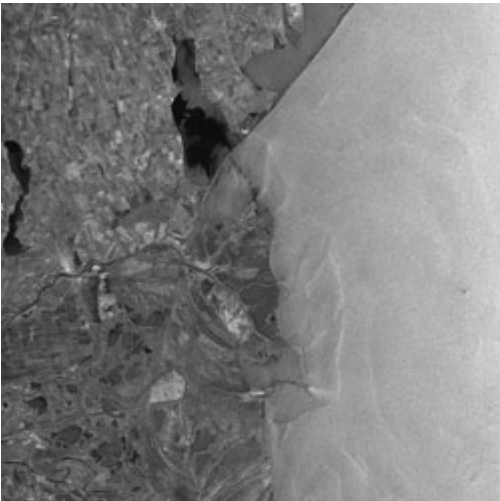
Danube (Romania)



Danube Estuary

Latitude: 45° 11' N - Longitude: 29° 32' E

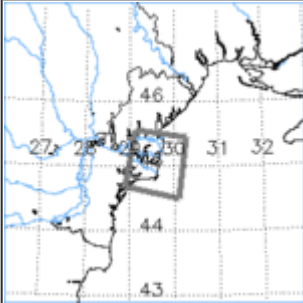
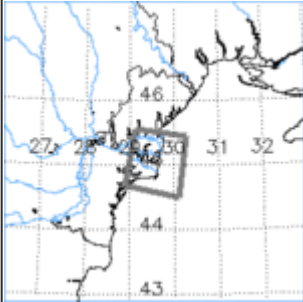
This ERS-1 SAR image shows the delta of the Danube river in Romania. The fresh water fronts at the mouths of the various river arms discharging fresh water into the Black Sea are clearly visible as bright lines.



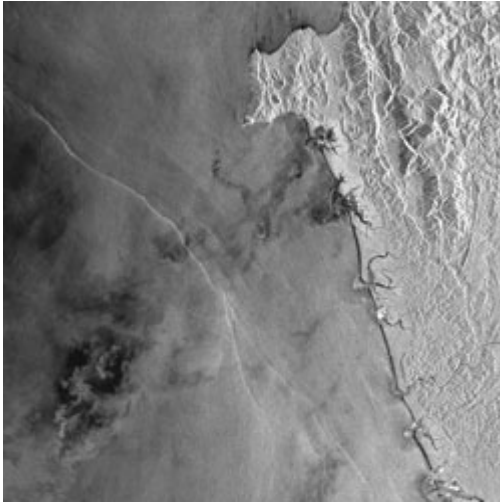
Danube Estuary

Latitude: 45° 11' N - Longitude: 29° 32' E

Another ERS-1 SAR image of the Danube Estuary. When comparing this ERS-1 SAR image with the previous one, one notes that the locations and shapes of the fresh water fronts differ significantly. This is indicative of a difference in the water volume discharged into the Black Sea at these two dates.

#	Orbit	Frame(s)	Satellite	Date	Time	Location
1	2691	6264	ERS-1	26-Nov-1992	08:50	
2	2691	6765	ERS-1	31-Oct-1992	08:50	

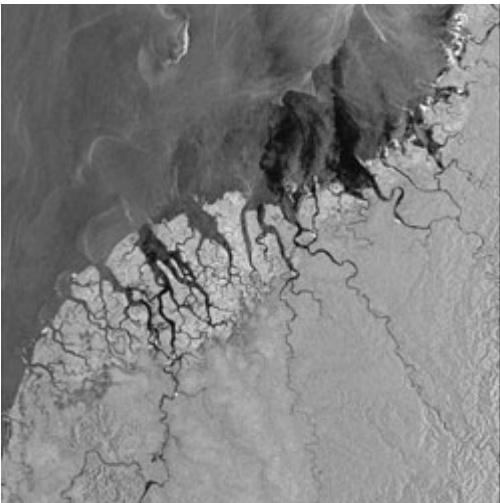
Iscuanda (Colombia)



Columbia

Latitude: 5° 14' N - Longitude: 77° 35' W

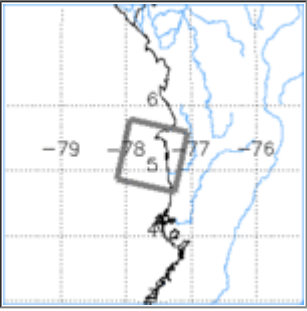
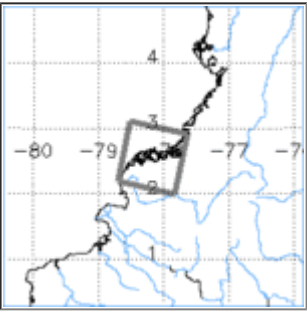
In addition to a long coastal front (the bright line crossing the whole image) several small fresh water fronts at the mouths of several small Colombian rivers discharging fresh water into the Pacific ocean can be seen on this ERS-1 SAR image.



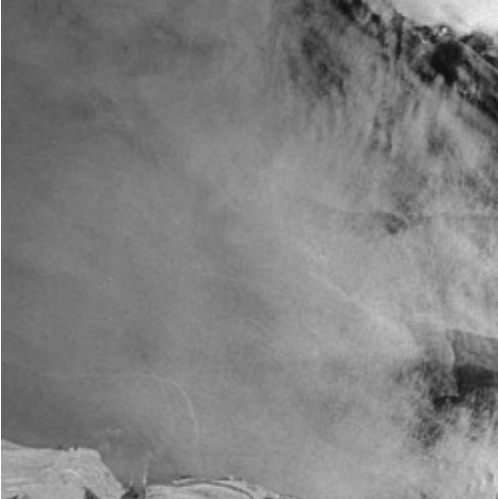
Colombia

Latitude: 2° 34' N - Longitude: 78° 10' W

River system near Punta Reyes in Colombia discharging water from the tropical rain forest into the Pacific. From the boundaries of the river plumes one may be able to obtain estimates about the precipitation in the catchment area of the river system.

#	Orbit	Frame(s)	Satellite	Date	Time	Location
1	12194	3501	ERS-1	14-NOV-1993	15:32	
2	12194	3555	ERS-1	14-Nov-1993	15:33	

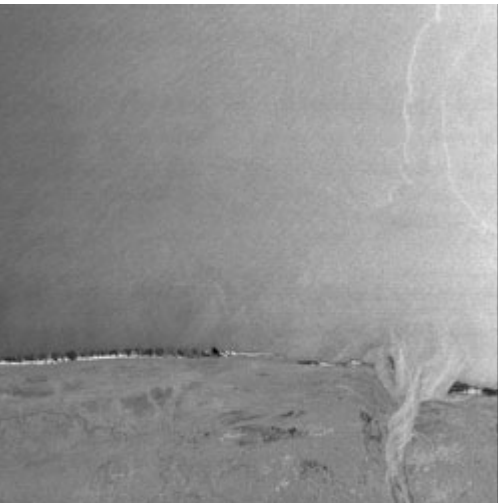
Maroni (Suriname, French Guiana)



Maroni

Latitude: 6° 08' N - Longitude: 53° 42' W

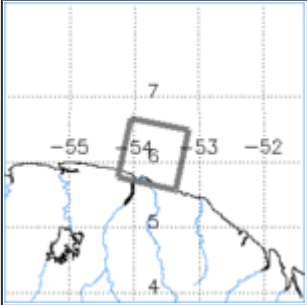
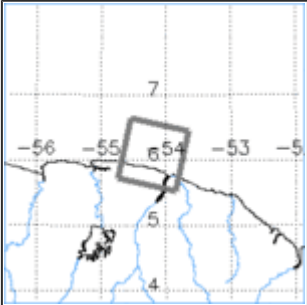
Eastuary of the river Maroni at the boundary between Surinam and French Guiana. The frontal boundary of the river plume is clearly visible extending into the Atlantic Ocean. From its arial extent one can obtain information on the water volume transported by the river which depends on rainfall in the catchment.



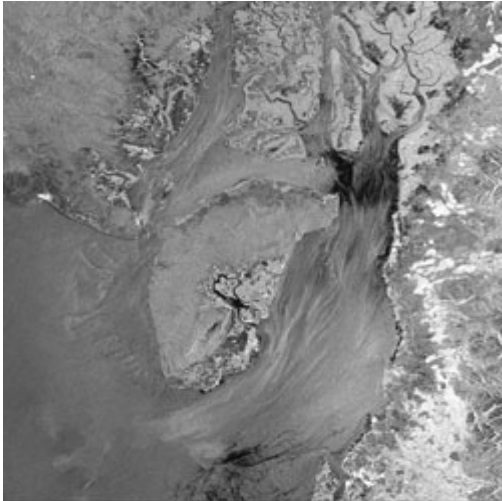
French Guiana

Latitude: 6° 05' N - Longitude: 54° 11' W

No frontal boundary of the river plume is visible on this image. The origin of the frontal lines visible in the upper right-hand section of the image is not known.

#	Orbit	Frame(s)	Satellite	Date	Time	Location
1	4721	3483	ERS-1	10-Jun-1992	13:31	
2	13253	3483	ERS-1	27-Jan-1994	13:59	

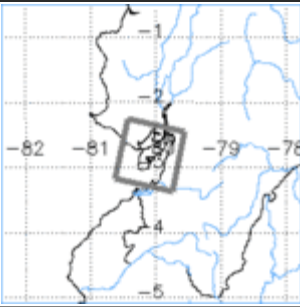
Guayas (Ecuador)



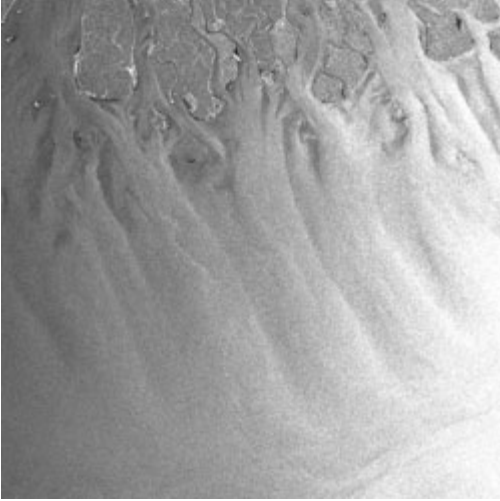
Ecuador

Latitude: 2° 48' S - Longitude: 80° 05' W

This ERS-1 SAR image shows the estuary of the river Guayas in Ecuador. The large island in the estuary is Isla Puna. The streaks on the water surface are very likely (at least partly) sea surface manifestations of underwater sandbanks.

#	Orbit	Frame(s)	Satellite	Date	Time	Location
1	06955	3663	ERS-1	13-Nov-1992	15:38	

Ganges (India, Bangladesh)

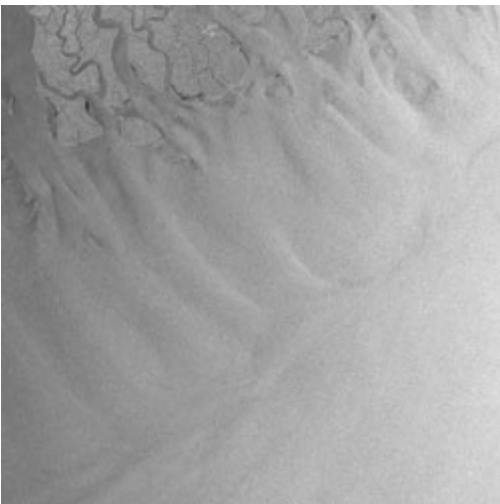


Ganges

Latitude: 21° 18' N - Longitude: 88° 17' E

Indian section of the Mouths of the Ganges. The waterway visible in the upper left-hand corner of the image is the Hugli River which connects the Indian towns Calcutta and Haldia with the Bay of Bengal.

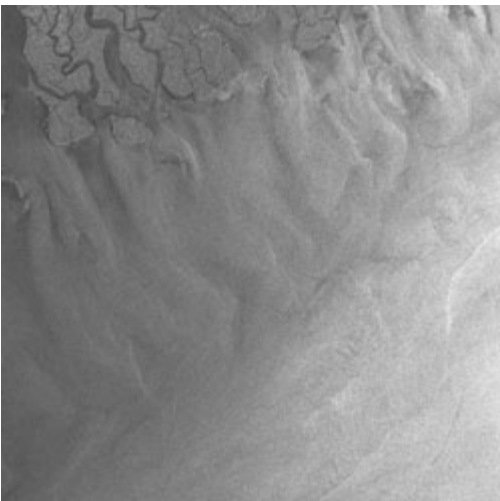
This river and the other river arms of the Ganges delta carry large amounts of suspended matter which deposit in the Bay of Bengal. The features visible on the water are sea surface manifestations of underwater sandbanks.



Ganges

Latitude: 21° 18' N - Longitude: 89° 01' E

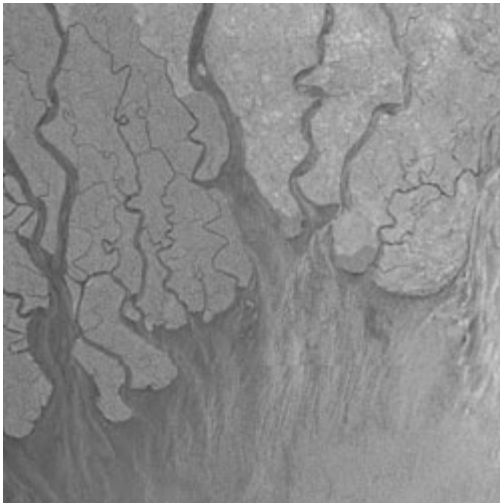
The area visible on this ERS-2 SAR image is the same as visible on the previous image, however imaged at a different time. Note the differences in the sea surface manifestations of the underwater sand banks on these two ERS SAR images.



Ganges

Latitude: 21° 18' N - Longitude: 89° 02' E

Indian section of the Mouths of the Ganges. The two islands visible in the upper left-hand section of the image are (from left to right) Dalhouse Island and Bhangaduni Island.

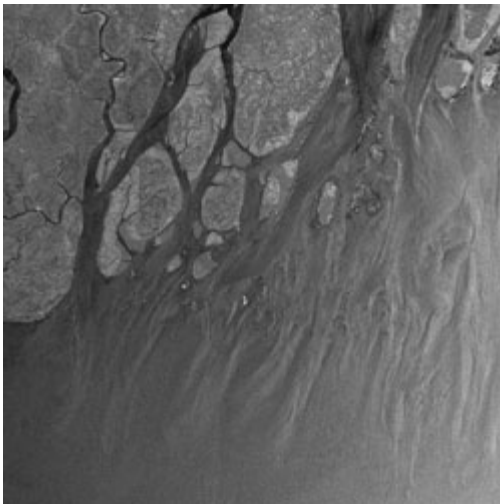


Ganges

Latitude: 21° 45' N - Longitude: 89° 49' E

Composite of two ERS-2 SAR scenes (200 km x 100 km) of the western part of the Bangladesh section of the Mouths of the Ganges. The two large rivers visible in the left-hand section of the image are the Pussar River and the Haringhata River.

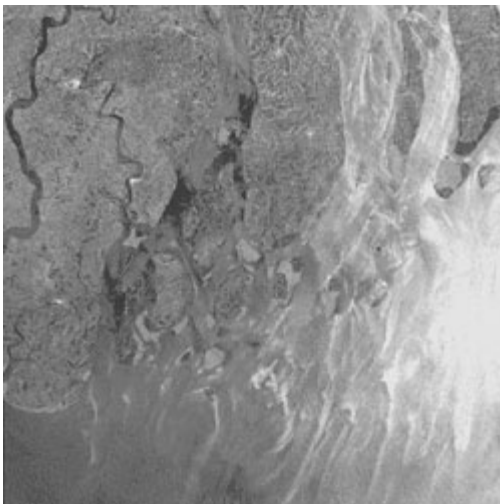
The reason why the land area between these two rivers has a darker grey level tone is not known. It could be that this region was flooded recently leaving a high moisture content in the soil which causes a reduction in the backscattered radar power. Also faintly visible are in the lower section of the image sea surface manifestations of internal wave packets.



Ganges

Latitude: 21° 45' N - Longitude: 90° 32' E

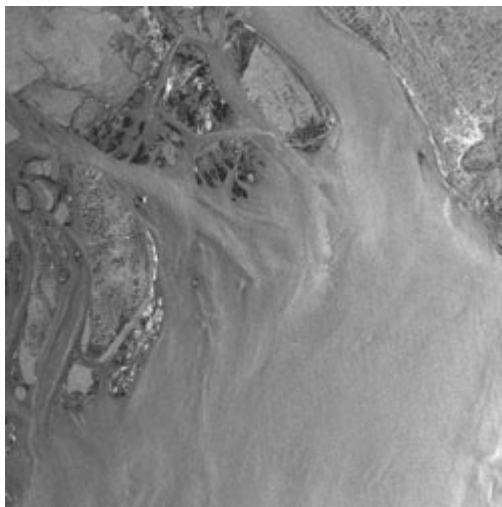
On this ERS-2 SAR image, a section of the Mouths of the Ganges is visible. This area is located further west than the area seen in the previous ERS-2 SAR image. The two large river systems are (from left to right) the Tetulia River and the Meghna River in Bangladesh. In the lower section of the image, sea surface manifestations of internal waves are also visible.



Ganges

Latitude: 21° 45' N - Longitude: 90° 32' E

This ERS-2 SAR image shows the same area in the Bangladesh section of the Mouths of Ganges as the previous ERS-2 SAR image, but at a different time. Note the difference in the sea surface manifestations of the underwater sandbanks visible on these two images. In the lower section of the image, two internal wave packets are also visible.



Ganges

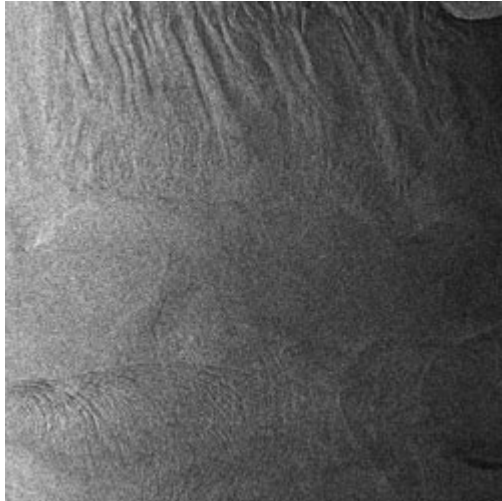
Latitude: 21° 45' N - Longitude: 91° 16' E

This ERS-2 SAR image shows the eastern section of the Mouths of the Ganges. In the upper right-hand section of the image the eastern coast of Bangladesh is visible. The bright area on the coast consisting of a cluster of bright spots is the town Chittagong.

The large island in the center of the upper section of the image is Sandwip Island. The dark areas surrounding this island as well as the other dark areas in this region are sandbanks that have fallen dry.

A comparison of this SAR image with a sea map published in 1990 reveals that the positions and shapes of the sandbanks and the shapes of the islands have changed considerably in the last 7 years.

The streaky features on the water surface result from underwater sandbanks that modify the current flow. The water depth in this region is everywhere less 10m.



Ganges

Latitude: 21° 19' N - Longitude: 90° 27' E

This ERS-2 SAR image shows an area in the Bay of Bengal south of the coast of Bangladesh. In the upper section sea surface manifestations of underwater sandbanks are visible while the lower section contains signatures associated with sea surface manifestations of oceanic internal waves.

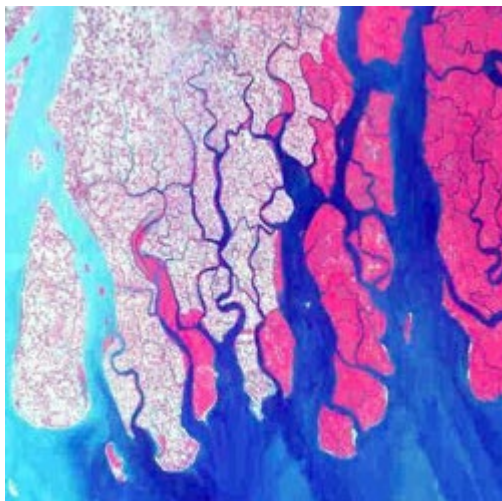


Ganges

Latitude: 22° 00' N - Longitude: 91° 30' E

Panchromatic SPOT 2 image of the eastern section of the Mouths of Ganges belonging to Bangladesh. In the upper section Sandwip Island and the east coast of Bangladesh are visible. Note the different gray tones visible in the sea area.

© CNES 2000 - Spot Image distribution <http://www.spotimage.fr/>



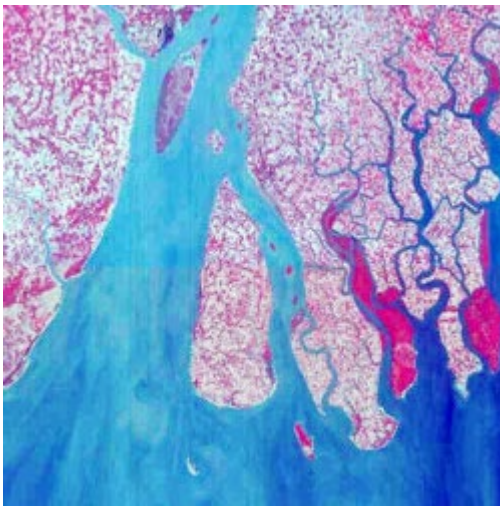
Ganges

Latitude: 21° 30' N - Longitude: 88° 21' E

SPOT 2 image of the Indian section of the Mouths of Ganges. The two broad waterways visible in the upper left-hand and right-hand section of the image are the Hugli River and the Matla River, respectively.

The red-colored areas are probably areas that have been flooded recently. Note the different blue tones visible in the sea area. They are very likely caused by underwater sandbanks and by suspended particles in the water.

© CNES 2000 - Spot Image distribution <http://www.spotimage.fr/>



Ganges

Latitude: 21° 30' N - Longitude: 88° 05' E

The imaged area visible on this SPOT 1 image is approximately the same as in the previous Spot 2 image. The previous image was acquired on January 30, 1999, and this one on March 2, 1999. Note that in the period of 31 days between the two data acquisitions the red area east of the Hugli River has decreased.

© CNES 2000 - Spot Image distribution <http://www.spotimage.fr/>

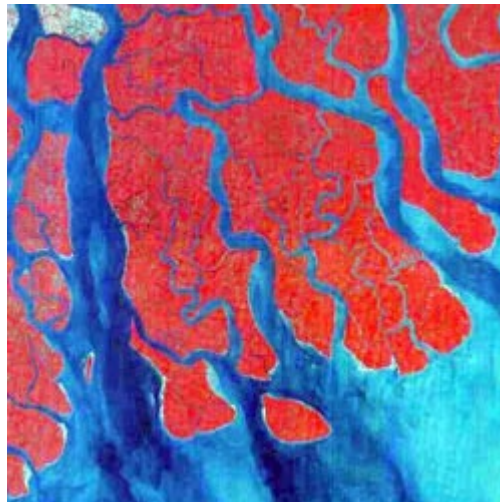


Ganges

Latitude: 21° 30' N - Longitude: 89° 09' E

SPOT-1 image of a section of the Mouths of Ganges belonging to India. The red land areas visible in the upper section of the image are very likely areas that have been flooded recently. Note that the SPOT image contains information on underwater sandbanks and/or suspended matter.

© CNES 2000 - Spot Image distribution <http://www.spotimage.fr/>

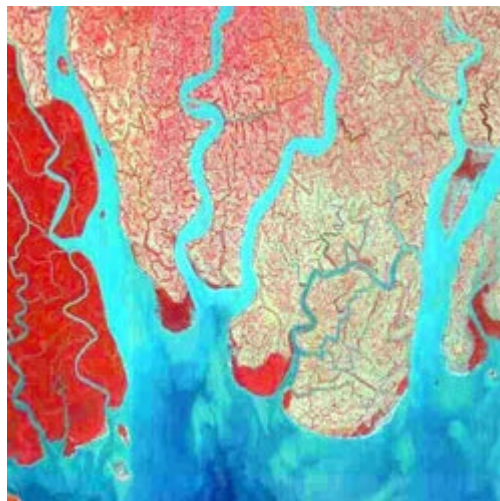


Ganges

Latitude: 21° 30' N - Longitude: 88° 47' E

SPOT 1 image of the Indian section of the Mouths of Ganges. Comparison of this image of the Ganges estuary with a sea map published in 1996 shows that the coastline has changed considerably between 1996 and 1999.

© CNES 2000 - Spot Image distribution <http://www.spotimage.fr/>

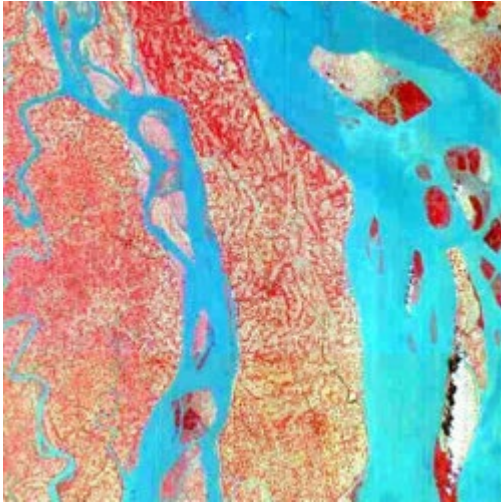


Ganges

Latitude: 22° 00' N - Longitude: 90° 37' E

SPOT 1 image of a section of the Mouths of Ganges belonging to Bangladesh which is located east of the area shown in the previous image.

© CNES 2000 - Spot Image distribution <http://www.spotimage.fr/>

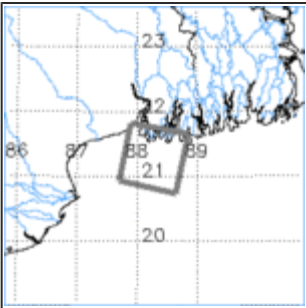
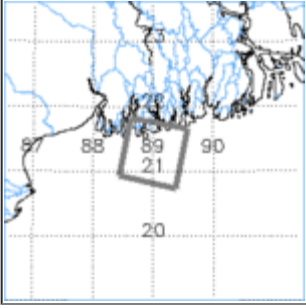
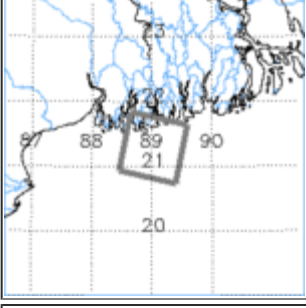
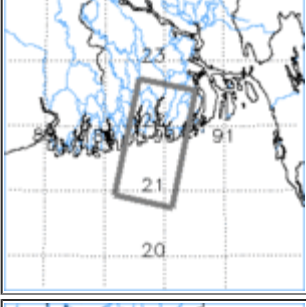
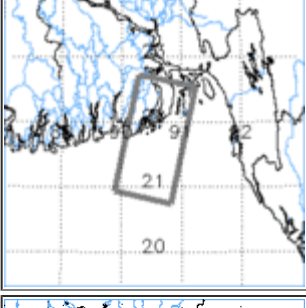
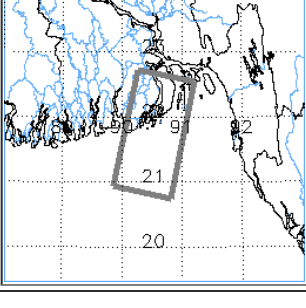


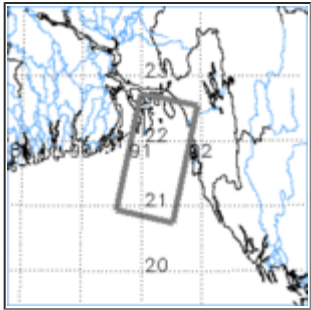
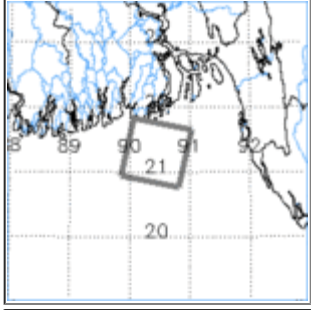
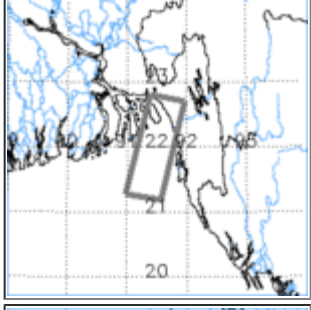
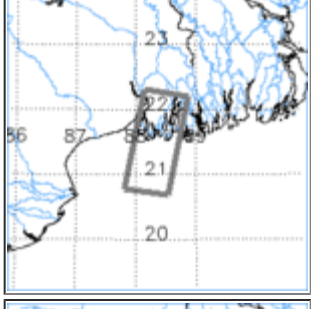
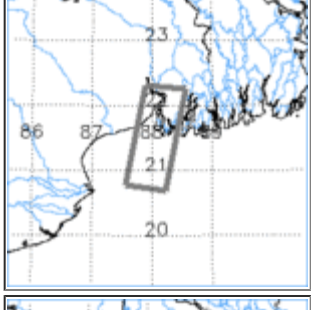
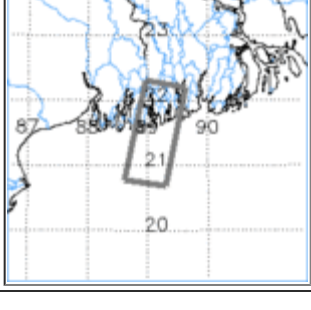
Ganges

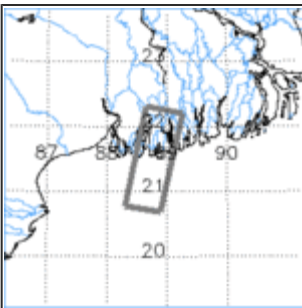
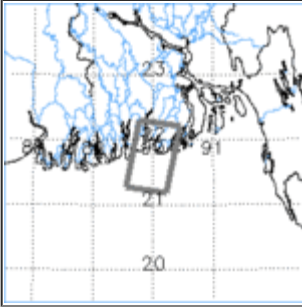
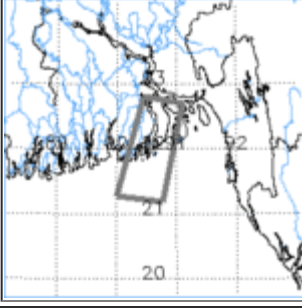
Latitude: 22° 00' N - Longitude: 90° 37' E

SPOT 1 image of a section of the Mouths of Ganges belonging to Bangladesh which is located east of the area shown in the previous image.

© CNES 2000 - Spot Image distribution <http://www.spotimage.fr/>

#	Orbit	Frame(s)	Satellite	Date	Time	Location
1	05541	3177	ERS-2	12-May-1996	04:39	
2	09234	3159-3177	ERS-2	25-Jan-1997	04:30	
3	16291	3177	ERS-2	02-Jun-1998	04:36	
4	09005	3159-3177	ERS-2	09-Jan-1997	04:33	
5	09234	3159-3177	ERS-2	25-Jan-1997	04:30	
6	17250	3159-3177	ERS-2	08-Aug-1998	04:30	

#	Orbit	Frame(s)	Satellite	Date	Time	Location
7	10966	3159-3177	ERS-2	26-May-1997	04:27	
8	13242	3177	ERS-2	01-Nov-1997	04:30	
9	305-306-307-308	Path: 240	SPOT 2	12-Oct-1997	04:38	
10	306-307-308	Path: 233	SPOT 2	30-Jan-1999	04:35	
11	306-307-308	Path: 233	SPOT 1	02-Mar-1999	04:39	
12	306-307-308	Path: 233	SPOT 1	30-Jan-1999	04:35	

#	Orbit	Frame(s)	Satellite	Date	Time	Location
13	306-307-308	Path: 234	SPOT 2	01-Jan-2000	04:42	
14	306-307-308	Path: 237	SPOT 1	03-Dec-1999	04:42	
15	305-306-307	Path: 238	SPOT 1	03-Dec-1999	04:30	

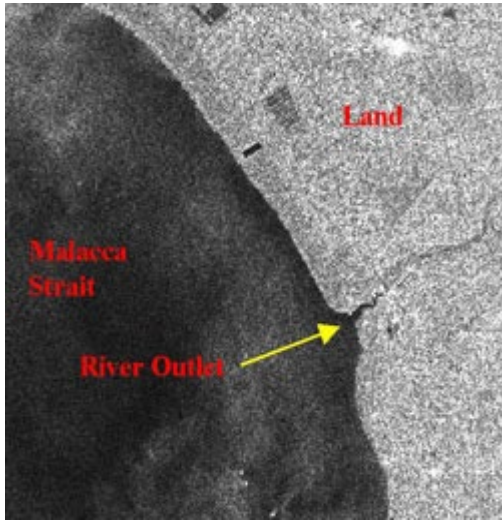
References

- Beardsley, R.C., Limeburner, R., Yu, H. & Cannon, G.A., Discharge of the Changjiang (Yangtze River) into the East China Sea. *Cont. Shelf Res.*, **4**, 57-76 (1985).
- De Castro, B. & de Miranda, L.B., Physical oceanography of the Western Atlantic continental shelf located between 4 ° N and 34 ° S. In: *The Sea*, edited by A.R. Robinson and K.H. Brink, John Wiley & Sons, Inc., **11** Chapter 8, 209-252 (1998).
- Dwivedi, R.S., Rao, B.R.M. & Bhattacharya, S., Mapping wetlands of Sundaban Delta and its environs using ERS SAR data. *Int. J. Remote Sensing*, **20**, 11, 2235-2247 (1999).
- Garvine, R.W., & Monk, J.D., Frontal structure of a river plume. *J. Geophys. Res.*, **79**, 2551-2259 (1974).
- Hessner, K., Rubino, A., Brandt, P. & Alpers, W., Rhine River Plume, submitted to *J. Geophys. Res.*, 2000.
- Geyer, W.R. & Beardsley, R.C., Introduction to special section on physical oceanography of the Amazon shelf. *J. Geophys. Res.*, **100**, No.C2, 2281-2282 (1995).
- Geyer, W.R. & Kineke, G.C., Observations of currents and water properties in the Amazon frontal zone. *J. Geophys. Res.*, **100**, No.C2, 2321-2339 (1995).
- Mooers, C.N.K. & Maul, G.A., Intra-Americas sea circulation. In: *The Sea*, edited by A.R. Robinson and K.H. Brink, John Wiley & Sons, Inc., **11** Chapter 7, 183-208 (1998).
- Rao, B.R.M., Dwivedi, R.S., Kushwaha, S.P.S., Bhattacharya, S.N., Anand, J.B. & Dasgupta, S., Monitoring the spatial extent of coastal wetlands using ERS SAR data. *Int. J. Remote Sensing*, **20**, 2509-2517 (1999).
- Shetye, R.S. & Gouveia, A.D., Coastal circulation in the North Indian Ocean. In: *The Sea*, edited by A.R. Robinson and K.H. Brink, John Wiley & Sons, Inc., **11** Chapter 18, 523-556 (1998).
- Su, J. Circulation dynamics of the China seas north of 18 ° N. In: *The Sea*, edited by A.R. Robinson and K.H. Brink, John Wiley & Sons, Inc., **11** Chapter 16, 483-505 (1998).
- Vogelzang, J., Ruddick, K.G. & Moens, J.B., On the signatures of river outflow fronts in radar imagery. *Int. J. Remote Sensing*, **18**, 3479-3505 (1997).
- Wang, Y. & Ren, M.-E., Sediment transport and terrigenous fluxes. In: *The Sea*, edited by A.R. Robinson and K.H. Brink, John Wiley & Sons, Inc., **11**, Chapter 10, 253-292 (1998).

Intertidal Zone

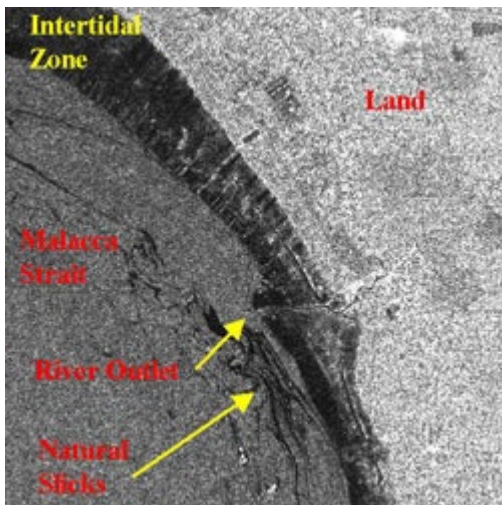
Satellite observation of an intertidal zone

The two images below show an intertidal zone observed in high and low tidal conditions by the synthetic aperture radar (SAR) on-board the ERS-1 satellite. The area is located at about 25 km north of Port Klang, Malaysia.



High Tide Image (ERS SAR)

Acquisition date: 10 May 1996
Time of acquisition: 11:34:58 am (Local Time)
High water time: 10:58 am
© ESA 1996



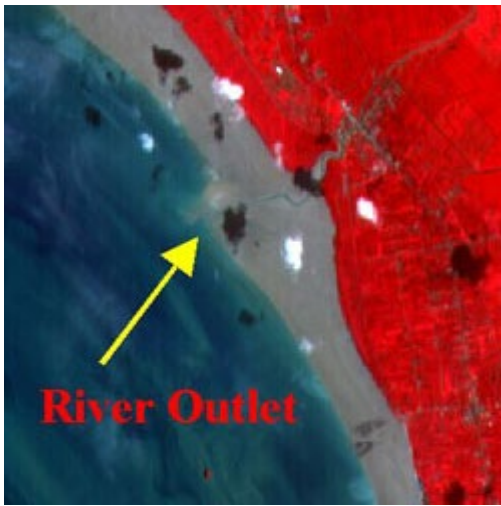
Low Tide Image (ERS SAR)

Acquisition date: 17 October 1997
Time of acquisition: 11:34:45 am (Local time)
Low water time: 1:01 pm
© ESA 1997

High Tide Image (ERS SAR) shows the land distinctly demarcated from the sea during high tide. Low Tide Image (ERS SAR) shows that a strip of intertidal mud or sand flat along the coast is exposed during low tide. This intertidal zone of more than 20 km long extends as far as two kilometers away from the high tide coastline.

The mud or sand flat appears dark in the synthetic aperture radar image due to its generally smooth surface. The brighter structures observed near the river mouth are probably the sand ridges or rocks exposed during low tide.

The river in the middle of the image cuts its course through the mud flat before discharging into the sea. This feature is submerged and not observable in the high tide image. Strips of natural slicks are observed in the low tide image. These natural slicks are probably associated with biological activities in the intertidal zone.



Low Tide Image (SPOT Multispectral)

Acquisition date: 20 January 1999

Time of acquisition: 12:01:54 (local time)

© CNES 1999 Reproduced by CRISP (Singapore) under license from SPOT IMAGE

© Centre for Remote Imaging, Sensing and Processing (CRISP) National University of Singapore

This is a multispectral image of the same area around the river outlet acquired by the SPOT satellite during low tide. The red area is vegetated land while the mud or sand flat appears as a grey strip along the coast. The small white patches in the image are clouds, and the adjacent dark patches are the shadows cast by the clouds.

Oceanic Eddies

Introduction

Since high-resolution images taken from satellites and space shuttles became available, oceanographers were quite surprised to learn that meso-scale and small-scale eddies or vortices are ubiquitous phenomena in coastal regions and at current fronts. Very spectacular images of small-scale eddies in coastal regions were acquired with a hand-held camera by the oceanographer-astronaut Scully-Power from the space shuttle Challenger during the Space Transportation System (STS) 41G mission in October 1984 (Scully-Power, 1986).

However, such optical images can only be acquired during the day when there are no clouds and when the ocean is viewed at a favourable angle which is a function of the elevation and azimuth angle of the sun.

On the other hand, SAR can image eddies day and night and independent of cloud cover. Oceanic eddies become visible on optical and SAR images because the current field associated with the eddy modifies the sea surface roughness. The eddies become best visible on optical and radar images when the ocean surface is partially covered with surface films.

These films are entrained by the flow associated with the eddy and accumulate in convergent regions where they reduce the sea surface roughness. Thus the surface films act as tracers for the flow field associated with the eddy. However, when the sea surface is completely covered with surface films, they lose their ability to trace the current field and the eddy becomes invisible.

Oceanic eddies can be generated by a variety of mechanism, e.g., (1) by local winds that are channeled by coastal geometry and topography, (2) by abrupt changes in wind speed and direction at atmospheric fronts, (3) by instabilities at oceanic current fronts, (4) by oceanic currents that interact with a headland, and (5) by water exchange through straits.



Vortex street generated in the laboratory

- [Kuroshio](#)
- [Pacific Mexican Coast](#)
- [Caspian Sea](#)
- [Mediterranean Sea](#)
- [Pacific Ocean](#)

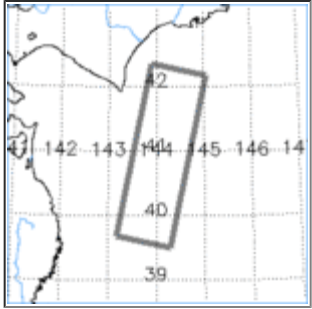
Kuroshio Japan

Japan

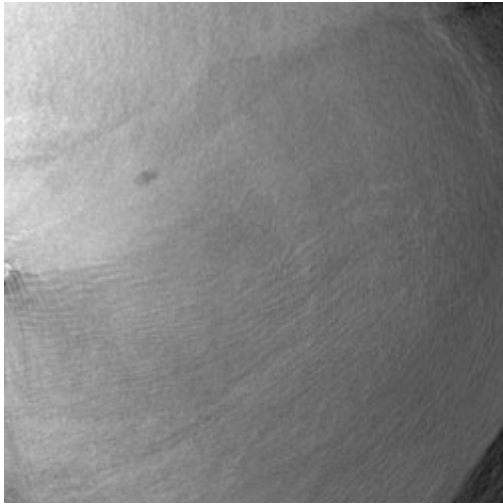
Latitude: 40° 56' N - Longitude: 144° 01' E

Oceanic eddies in the Pacific Ocean generated by the Kuroshio Current. The imaged area lies just east of the strait separating the Japanese islands Honshu and Hokkaido. The Kuroshio Current is the equivalent to the Gulf Stream in the Far East.

The Gulf Stream is the western boundary current of the North Atlantic Ocean, and the Kuroshio Current is the western boundary current of the North Pacific Ocean. Both currents exhibit strong meso-scale variability. This variability in the current system manifests itself in mesoscale meanders and eddies, which are generated in the frontal zone by instabilities.

Orbit	Frame(s)	Satellite	Date	Time	Location
17980	2763-2781-2799	ERS-1	23Dec-1994	01:08	

Pacific Mexican Coast



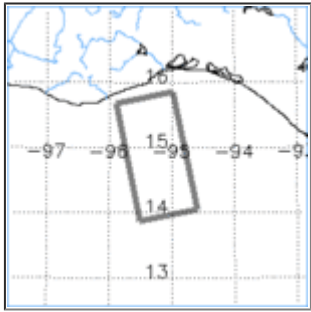
Gulf of Tehuantepec

Latitude: 14° 51' N - Longitude: 95° 14' W

The bright area in the image is caused by an anticyclonic warm eddy in the Gulf of Tehuantepec, which is located on the Pacific coast of Mexico. Here the water temperature is several degrees higher than in the surrounding area (black area in the image).

This interpretation is supported by AVHRR images that were acquired on 12 and 14 March 1996, which show a warm core eddy in the same area.

Such eddies, which typically have a diameter of about 200 km, are generated by strong winds which originate in the Gulf of Mexico and blow through a narrow gap in the mountain range in the Isthmus of Tehuantepec onto the eastern tropical Pacific Ocean (Stumpf,1975; Travina et al,1995; Martinez-Diaz de Leon and Robinson,1997; Martinez-Diaz de Leon et al.,1999).

Orbit	Frame(s)	Satellite	Date	Time	Location
04697	0279-0297	ERS-2	14-Mar-1996	04:52	

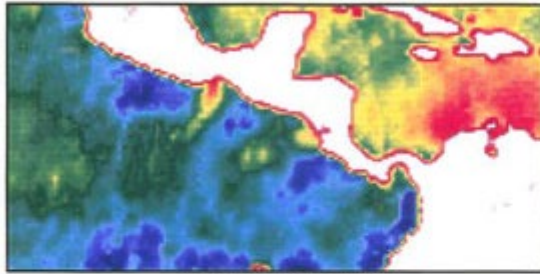
Ancillary information to this image

ERS-1 SCATTEROMETER

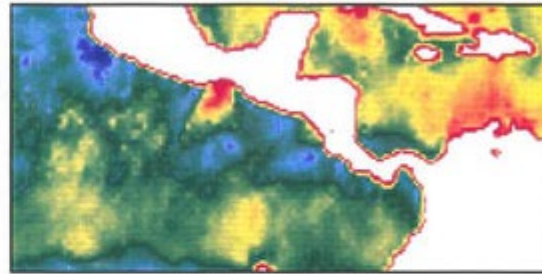
Institute of Oceanography, University of Hamburg

Gulf of Tehuantepec

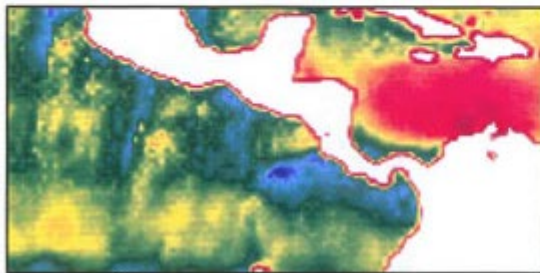
averaged σ_0 values



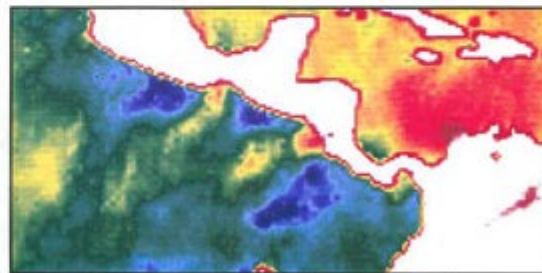
March, April, Mai, 1992



June, July, August, 1992



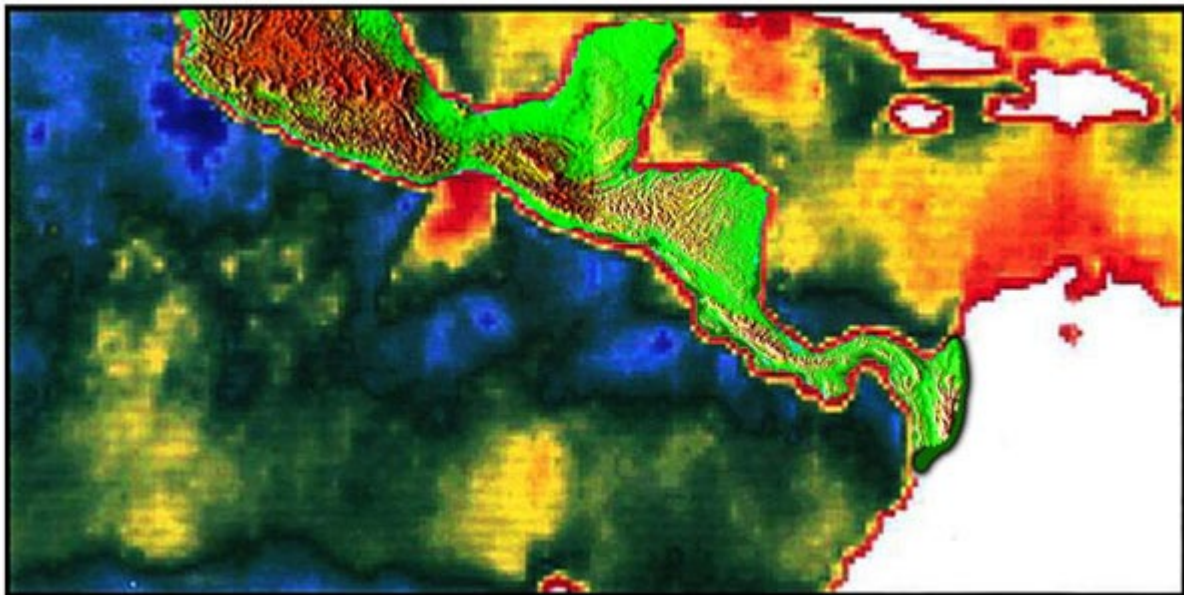
September, October, November, 1992



December, 1992, January, February, 1993



Seasonally averaged wind fields - These maps were generated by Kai Boehnke (formerly at the Institute of Oceanography of the University of Hamburg).



Merge of topography with wind stress for Pacific coast of Mexico

Caspian Sea



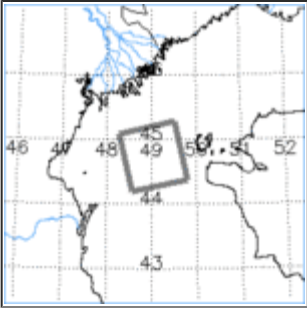
Caspian Sea

Latitude: 44° 45' N - Longitude: 49° 03' E

Eddies in the Caspian Sea south of the Volga estuary. This river carries a heavy load of pollutants originating from fertilisers washed out from agricultural fields and from industrial and municipal plants.

These serve as nutrients for the marine organisms which experience a rapid growth and then generate biogenic surface slicks. They are advected by the current field associated with the eddies and thus act as tracers.

The eddies are very likely wind-induced. The most remarkable features on this image is the mushroom-like feature consisting of two counter-rotating eddies.

Orbit	Frame(s)	Satellite	Date	Time	Location
11724	0891	ERS-1	12-Oct-1993	18:54	 A map of the Caspian Sea region showing the location of the eddies. The map includes a grid with latitude and longitude coordinates. A rectangular box highlights the area where the eddies were observed, centered around 49° 03' E and 44° 45' N. The map also shows the Volga River estuary and the surrounding landmasses.

Mediterranean Sea



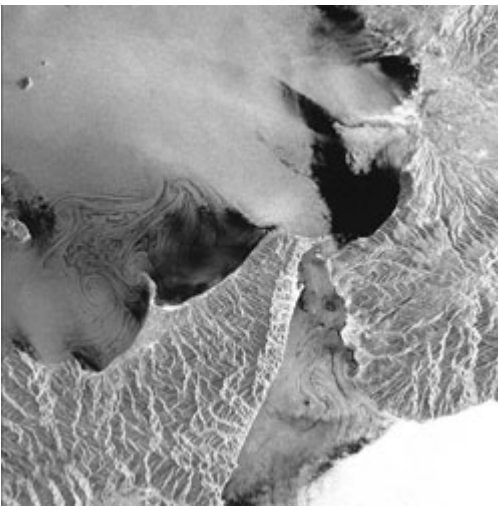
North of Sicily

Latitude: 38° 58' N - Longitude: 15° 28' E

This ERS-1 SAR image which is a composite of the two standard frames shows in the centre a large (diameter appr. 30 km cyclonic eddy. The eddy becomes visible because the associated surface current has entrained natural surface slicks. The dark area in the left-hand section of the image is an area almost completely covered with natural surface slicks.

Note that this image was taken in June when the biological activity is high and much surface active material is produced. The bright patches in the dark areas are slick-free areas where the wind can generate short-scale surface waves. (Note, however, that two bright patches southwest of the large eddy are the islands of Stromboli and Panaria.

The bright tongue like pattern in the lower right-hand section of the image is due to a katabatic wind blowing in the evenings from the mountains onto the sea (see the section: Atmospheric phenomena, Katabatic winds. The wave pattern to the right of the large eddy is very likely the imprint of an atmospheric lee wave.

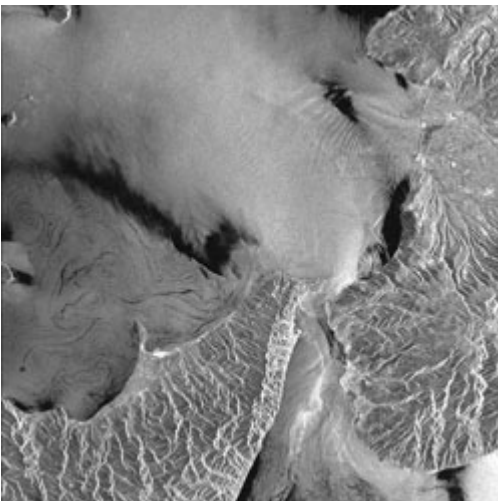


North of Sicily

Latitude: 38° 16' N - Longitude: 15° 30' E

An extraordinary small-scale eddy field is visible on this image at the Sicilian coast. The headland Capo de Milazzo, which projects like a spine from the northern shore of Sicily into the sea, seems to be instrumental in the generation of the eddies. Three cyclonic eddies (i.e., eddies which rotate anti-clockwise and a mushroom-like pattern are visible.

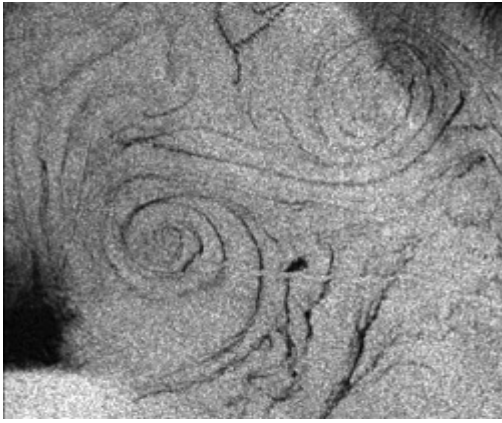
Note that the eddy furthest to the left is only partially visible because in the black area the sea surface is completely covered with surface slicks. Here the current field associated with the eddy cannot redistribute the slick material and thus the surface slick cannot serve as a tracer for this eddy.



North of Sicily

Latitude: 38° 16' N - Longitude: 15° 29' E

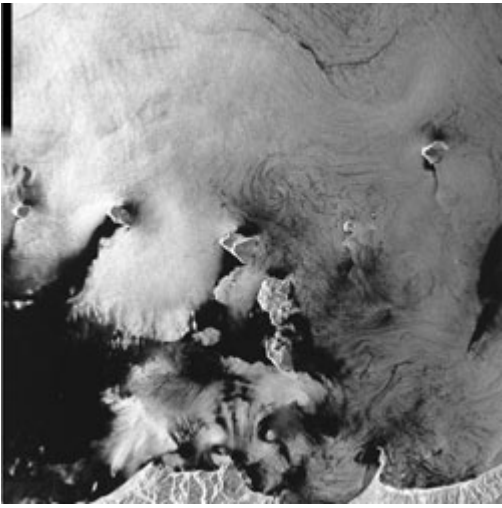
Like the previous image, several eddies are visible on this image north of the Sicilian coast. Noteworthy are two interconnected counter-rotating eddies (vortex pair. A [magnified view](#) of this vortex pair is also available, which has image dimensions of 15 km x 13 km.



North of Sicily

Latitude: 38° 16' N - Longitude: 15° 29' E

Blow-up of the section of the previous image with the vortex pair. The image dimensions are 15 km x 13 km.



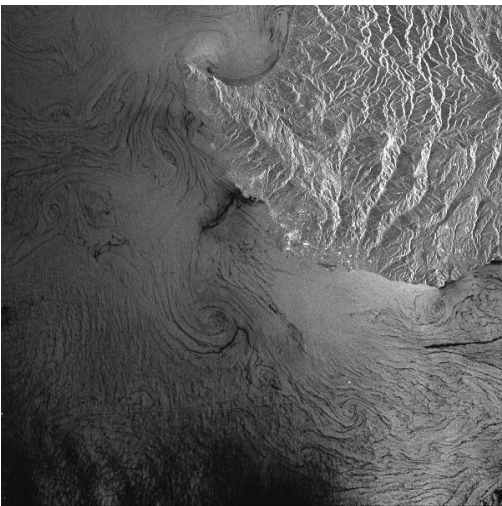
North of Sicily

Latitude: 38° 32' N - Longitude: 14° 53' E

Coastal waters of the northern coast of the Italian island of Sicily. The Italian volcanic islands (from left to right) Alicudi, Filicudi, Salina, Lipari, Volcano, and Panarea are visible north of the Sicilian coast (lower part of the image).

A northeasterly wind gives rise to pronounced wind shadow patterns behind the islands of Alicudi, Filicudi, and Salina. The small-scale eddy located north of the islands of Salina and Panarea becomes visible because (natural) surface slicks are entrained by the spiral surface current field associated with the eddy.

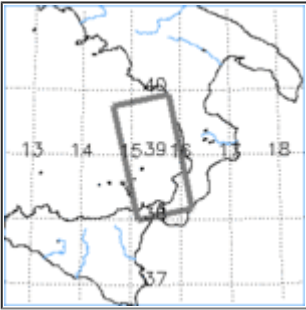
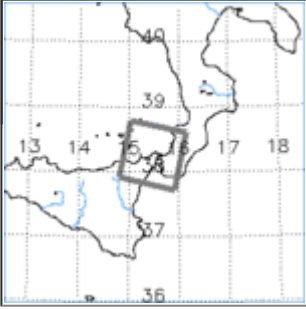
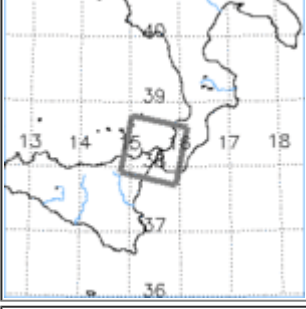
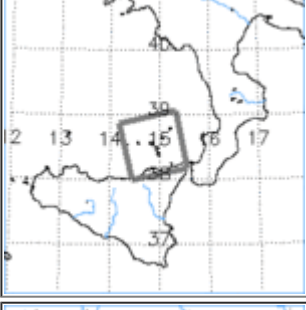
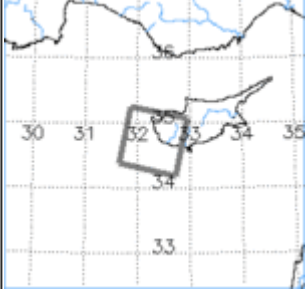
A headland eddy is also faintly visible west of the thorn-shaped peninsula Milazzo (lower right-hand section of the image). The dark areas in the image are very likely caused by surface slicks.



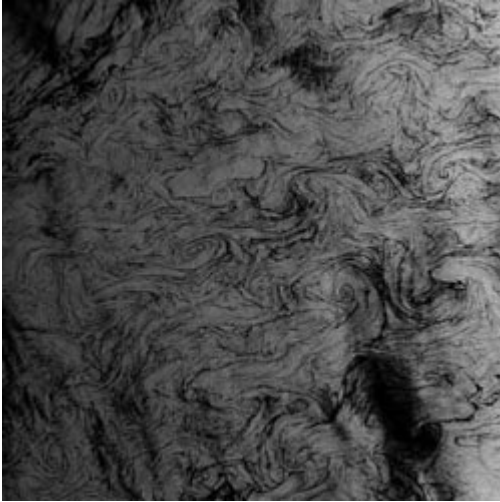
Cyprus

Latitude: 34° 44' N - Longitude: 32° 19' E

Small-scale eddies off the southwestern coast of Cyprus. The eddies become visible because they entrain surface slicks.

#	Orbit	Frame(s)	Satellite	Date	Time	Location
1	15079	0765-0783	ERS-1	03-Jun-1994	21:13	
2	22254	2835	ERS-1	17-Oct-1995	09:41	
3	11389	2835	ERS-1	19-Sep-1992	09:41	
4	08971	0765	ERS-1	21-Mar-1993	21:16	
5	16865	2907	ERS-1	06-Oct-1994	08:32	

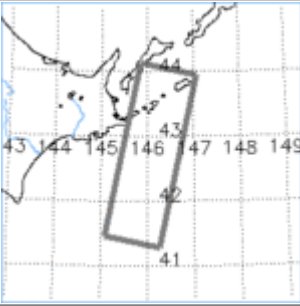
Pacific Ocean



Hokkaido

Latitude: 42° 43' N - Longitude: 146° 04' E

Extensive oceanic eddy field in the Pacific Ocean west of the Japanese island Hokkaido. Here the eddies become visible because the surface currents associated with these eddies entrain (natural) slicks floating on the sea surface.

Orbit	Frame(s)	Satellite	Date	Time	Location
21891	2727-2745-2763	ERS-1	22-Sep-1995	01:03	

References

- Arestegui, J., Tett, P. et al., The influence of island-generated eddies on chlorophyll distribution: study of mesoscale variation around Gran Canaria, *Deep-Sea Res.*, **44**, 71-96 (1997).
- Fischer, J., Schott, F. & Stramma, L., Currents and transports of the Great Whirl - Socotra Gyre system during the summer monsoon, August 1993, *J. Geophys. Res.*, **101**, 3573-3587 (1996).
- Grundling, M.L., Tracking eddies in the southeast Atlantic and southwest Indian Oceans with Topex/Poseidon, *J. Geophys. Res.*, **100**, 24977-24986 (1995).
- Hsu, M-K., Mitnik, L.M., Lobanov, V.B., Liu, C.T. & Bulatov, N., Kuroshio front and oceanic phenomena near Taiwan and in the Southern Okhotsk Sea from ERS SAR data, *Proc. 3rd ERS Symp.*, Florence, Italy, 17-21 March 1997, ESA publication SP-414, 1259-1266 (1997).
- Hubert, L.F. & Krueger, A.F., Satellite pictures of mesoscale eddies, *Monthly Weather Rev.*, November, 457-463 (1962).
- Jensen, V.E., Samuel, P. & Johannessen, O.M., Mesoscale studies in the Indian Ocean using altimeter data. *Proc. 3rd ERS Symp.*, Florence, Italy, 17-21 March 1997, ESA publication SP-414, 1279-1285.
- Kirby, D.S., Barton, E.D., Mitchelson-Jacob, E.G. & Trasvina, A., Synthetic aperture radar (SAR) remote sensing of wind-driven circulation in the Gulf of Tehuantepec, Mexico, *Proc. 3rd ERS Symp.*, Florence, Italy, 17-21 March 1997, ESA publication SP-414, 1273-1277 (1997).
- Liu, A.K., Peng, C.Y. & Schumacher, J.D., Wave-current interaction study in the Gulf of Alaska for detection of eddies by synthetic aperture radar, *J. Geophys. Res.*, **99**, 10075-10085 (1994).
- Lyzenga, D. & Wackerman, C., Detection and classification of ocean eddies using ERS-1 and aircraft SAR images, *Proc. 3rd ERS Symp.*, Florence, Italy, 17-21 March 1997, ESA publication SP-414, 1267-1271 (1997).
- Martinez-Diaz de Leon, A. & Robinson, I.S., Fronts and eddy features in coincident ERS-2 SAR and AVHRR-IR images for a case of offshore wind forcing, *Proc. 3rd ERS Symp.*, Florence, Italy, 17-21 March 1997, ESA publication SP-414, 1427-1431.
- Martinez-Diaz de Leon, A., Robinson, I.S. & Ballesteros, D., Wind driven ocean circulation features in the Gulf of Tehuantepec, Mexico, revealed by combined SAR and SST satellite sensor data, *Int. J. Remote Sensing*, **20**, 1661-1668 (1999)
- McWilliams, J.C., Submesoscale, coherent vortices in the ocean, *Rev. of Geophys.*, **23**, 165-182 (1985).
- Mied, R.P., McWilliams, J.C. & Lindemann, G.J., The generation and evolution of mushroom-like vortices, *J. Phys. Ocean.*, **21**, 490-510 (1991).
- Munk, W., Armi, L., Fischer, K. & Zachariasen, F., Spirals on the sea, *Proc. R. Soc. Lond.*, **456**, 1217-1280 (2000).
- Scully-Power, P., Navy oceanographer shuttle observations: *STS 41-G Mission Report*, Naval Underwater Systems Center, Technical Report no. 7611 (1986).
- Stumpf, H.G., Satellite detection of upwelling in the Gulf of Tehuantepec, *J. Phys. Ocean.*, **5**, 383-388 (1975).
- Stumpf, H.G. & Legeckis, R.N., Satellite observations of mesoscale eddy dynamics in the Eastern Tropical Pacific Ocean, *J. Phys. Ocean.*, **7**, 648-658 (1977).
- Swaters, G.E. & Mysak, L.A., Topographically-induced baroclinic eddies near a coastline, with application to the Northeast Pacific, *J. Phys. Ocean.*, **15**, 1470-1485 (1985).
- Trasvina, A., Barton, E.D., Brown, J., Velez, H.S., Kosro, P.M. & Smith, R.L., Offshore wind forcing in the Gulf of Tehuantepec, Mexico: The asymmetric circulation, *J. Geophys. Res.*, **100**, 20649-20663 (1995).

Oceanic internal waves

Introduction

Internal waves are waves in the interior of the ocean. They exist when the water body consists of layers of different density. This difference in water density is mostly due to a difference in water temperature, but can also be due to a difference in salinity. Often the density structure of the ocean can be approximated by two layers. The interface between layers of different densities is called pycnocline. When the density difference is due to temperature it is called thermocline, and when it is due to salinity it is called halocline.

Like the well-known ocean surface waves, which are waves at the interface of two media of different density, i. e., of water and air, the internal waves are waves at the interface between two water layers of different density. In both cases the restoring force is gravity, which is the reason why both waves sometimes are called gravity waves. These waves are generated when the interface is disturbed. In the case of surface waves, this disturbance can be caused by a stone thrown into the water or by wind blowing over the water surface. In the case of internal waves, this disturbance is usually caused by tidal flow pushing the layered water body over shallow underwater obstacles, e. g., over shallow sills or shallow ridges (Maxworthy, 1975, Helfferich et al., 1984, Lamb, 1994).

Internal waves in the ocean typically have wavelengths from hundreds of meters to tens of kilometers and periods from tens of minutes to several hours. Their amplitude (peak-to trough distance) often exceeds 50 m. Associated with internal waves are orbital motions of the water particles as depicted in Fig. 1 (the dashed circular lines). The radius of the circular motion of the water particles is largest at the pycnocline (or thermocline) depth and decreases downwards as well as upwards from this depth. To first order, the internal waves do not give rise to an elevation of the sea surface as the familiar surface waves do, but they do give rise to a variable (horizontal) surface current.

The current velocity at the sea surface varies in magnitude and direction giving rise to convergent and divergent flow regimes at the sea surface as depicted in Fig. 1. The variable surface current interacts with the surface waves and modulates the sea surface roughness (Hughes, 1978, Alpers, 1985). This interaction is the reason why oceanic internal waves become visible on radar images of the sea surface and, in some cases, also on images acquired in the visible ultraviolet or infrared wavelength band (see, e. g., Apel et al., 1975).

Due to the hydrodynamic interaction of the variable surface current with the surface waves, the amplitude of the Bragg waves is increased in convergent flow regions and is decreased in divergent flow regions. As a consequence, the radar signatures of oceanic internal waves consist of alternating bright and dark bands on a uniform background.

But there exist also other radar signatures of internal waves: Sometimes they consist only of bright lines or only of dark bands. When the wind speed is below threshold for Bragg wave generation, only bright bands are encountered and when surface slicks are present, only dark lines are seen (da Silva et al., 1998). However, radar imaging theories capable of explaining these exceptional radar signatures of internal waves quantitatively still do not exist.

The tidally generated internal waves are usually highly nonlinear and occur often in wave packets. The distance between the waves in a wave packet and also the amplitude decrease from the front to the back. The amplitude of large internal waves can exceed 50 m in some cases. Theoretically, these highly nonlinear waves are often described in terms of internal solitons. Thus a wave packet consists of several solitons. Since soliton theory was developed by Korteweg and De Vries (1895), hundreds of papers have been published dealing with this subject.

Soliton theories applicable to the description of the generation and propagation of internal solitary waves predict that, if the depth of the upper water layer is much smaller than the depth of the lower layer, then the internal solitary wave must be a "wave of depression". This means that this soliton is associated with a depression of the pycnocline as depicted schematically in Fig. 2 and as measured in the ocean (see Fig. 3). The leading edge of a soliton of depression is always associated with a convergent surface current region and the trailing edge with a divergent region.

At the front of the soliton the amplitude of the Bragg waves is increased, while at the rear it is decreased. According to Bragg scattering theory, the normalized radar cross section (NRCS) is proportional to the amplitude squared of the Bragg wave (Valenzuela, 1978). This is the reason why on SAR images the front section of a soliton of depression is bright, and the rear section dark (Alpers, 1985). As mentioned before, the radar signatures of internal solitary waves may deviate from this scheme when surface slicks are present or the wind speed is low.

Oceanic internal solitary waves have been observed in many parts of the world's ocean. A very comprehensive list of publications on observation of large internal waves has been compiled by M. Miyata of the University of Hawaii and can be accessed by internet (<http://iprc.soest.hawaii.edu/~miyata/IWavesPublicationList.htm>).

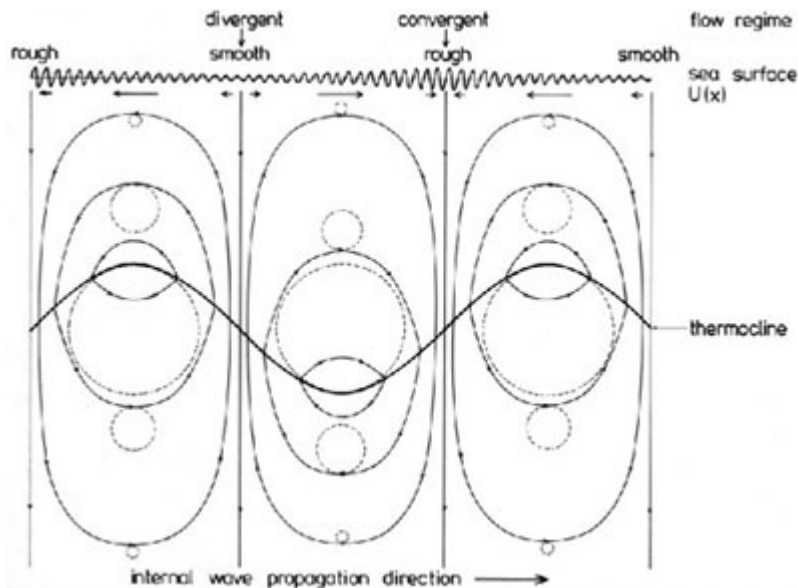


Fig. 1: Schematic plot of processes associated with the passage of a linear oceanic internal wave. Deformation of the thermocline (heavy solid line), orbital motions of the water particles (dashed lines), streamlines of the velocity field (light solid lines), surface current velocity vectors (arrows in the upper part of the image), and variation of the amplitude of the Bragg waves (wavy line at the top).

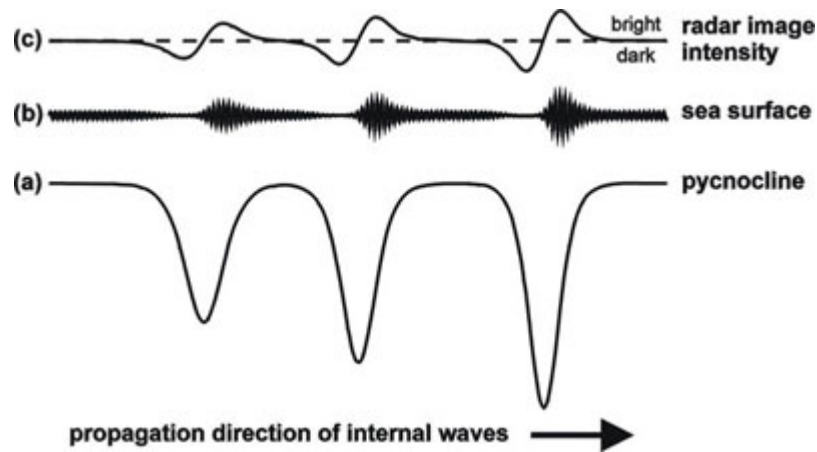


Fig. 2: Shape of the pycnocline (a), sea surface roughness pattern (b), and SAR image intensity (c) associated with an internal solitary wave packet consisting of solitons of depression of decreasing amplitude.

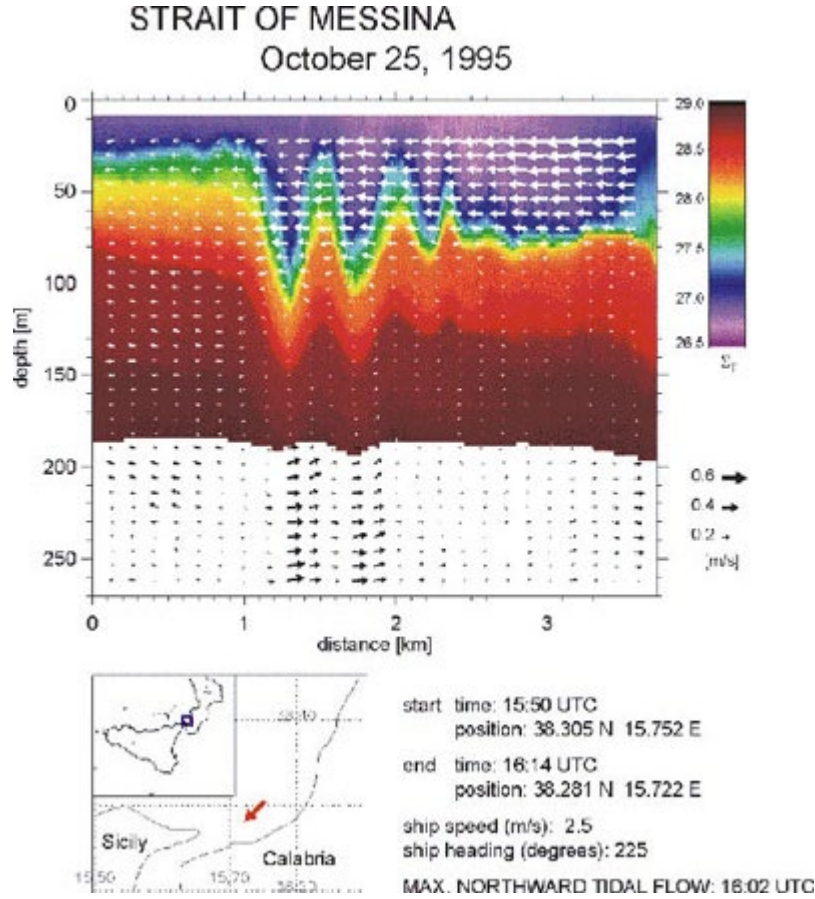
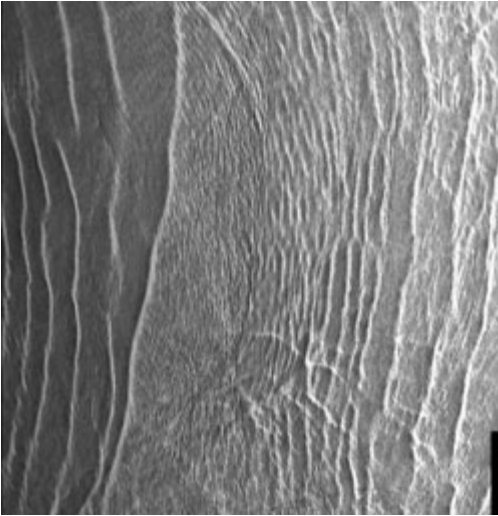


Fig. 3: Density and current distributions measured in the Mediterranean Sea north of the Strait of Messina during the passage of a northward propagating packet of internal solitary waves. The density distribution was measured by a CTD (conductivity temperature, depth) chain (Sellschopp, 1997) and the current distribution by an acoustic Doppler current profiler from the research ship "Alliance" (Figure provided by P. Brandt and A. Rubino, Institute of Oceanography, University of Hamburg).

References

- Alpers, W., Theory of radar imaging of internal waves, *Nature*, **314**, 245-247 (1985).
- Apel, J.R., Byrne, H.M., Proni, J.R. & Charnell, R.L., Observation of oceanic internal and surface waves from the Earth Resources Technology Satellite, *J. Geophys. Res.*, **80**, 865-881 (1975).
- da Silva, J.C.B., Ermakov, S.A., Robinson, I.S., Jeans, D.R.G. & Kijashko, S.V., Role of surface films in ERS SAR signatures of internal waves on the shelf, 1. Short-period internal waves, *J. Geophys. Res.*, 8009-8031 (1998).
- Helfrich, K.R. & Melville, W.K., On long nonlinear internal waves over slope-shelf topography, *J. Fluid Mech.*, **167**, 285-308 (1986).
- Hsu, M.-K., Liu, A.K. & Liu, Ch, A study of internal waves in the China Seas and Yellow Sea using SAR, *Continental Shelf Research*, **20**, 389-410 (2000).
- Hughes, B.A., The effect of internal waves on surface wind waves, 2, Theoretical analysis, *J. Geophys. Res.*, **83**, 455-465 (1978).
- Korteweg, D.J. & de Vries, G., On the change of long waves advancing in a rectangular canal and a new type of long stationary waves, *Phil. Mag.*, **5**, 422 (1895).
- Lamb, K.G., Numerical experiments of internal wave generation by strong tidal flow across a finite amplitude bank edge, *J. Geophys. Res.*, **99**, 843-864 (1994).
- Maxworthy, T., A note on the internal solitary waves produced by tidal flow over a three-dimensional ridge, *J. Geophys. Res.*, **84**, 338-346 (1979).
- Miyata, Motoyasu, URL <http://iprc.soest.hawaii.edu/~miyata/TWavesPublicationList.htm>
- Sellschopp, J., A towed CTD chain for high-resolution hydrography, *Deep-Sea Res.*, **44**, 147-165 (1997).
- Valenzuela, G.R., Theories for the interaction of electromagnetic and ocean waves - A review, *Boundary Layer Meteorol.*, **13**, 61-85 (1978).

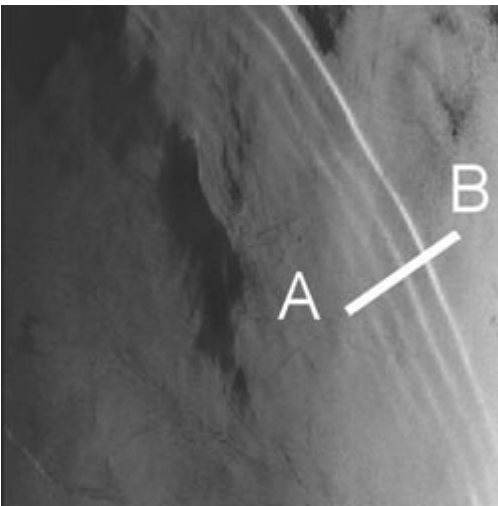
Andaman Sea



Andaman Sea

Latitude: 08° 48' N - Longitude: 96° 22' E

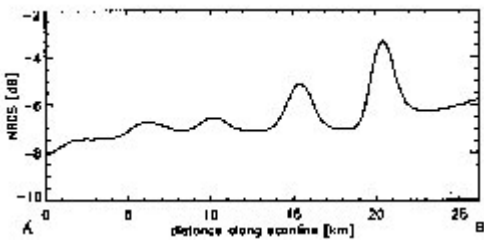
The front of a packet of internal solitary waves (left-hand section of the image) interacting with the tail of another internal solitary wave packet (right-hand section of the image). The leading soliton of the western packet seems to sweep clean the trailing part of the previous packet.



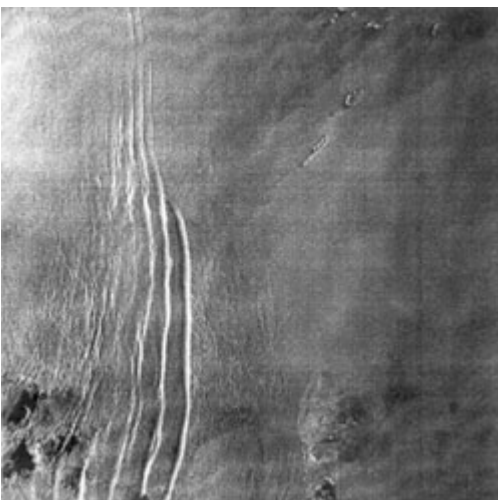
Andaman Sea

Latitude: 07° 01' N - Longitude: 97° 25' E

Sea surface manifestations of two internal wave packets generated at successive semi-diurnal tidal cycles. The variation of the NRCS along the profile AB is shown in the figure below.



Variations of the NRCS in dB along the scan line A-B shown in the ERS image above.

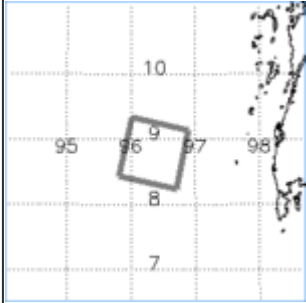
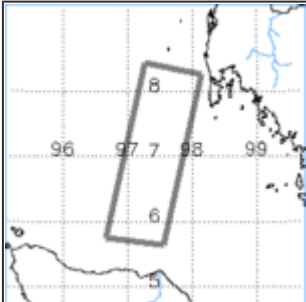
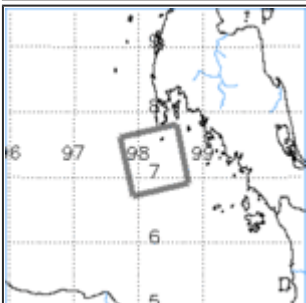


Andaman Sea

Latitude: 07° 17' N - Longitude: 98° 15' E

The irregular shape of the sea surface manifestations of this packet of internal solitary waves result from the interaction with the shallow bottom topography in this region of the Malayan shelf.

The position where the sea surface manifestation of the leading solitary wave suddenly disappears coincides with the 90m depth line. It is suggested that at this position the leading solitary wave breaks. According to theory, wave breaking occurs where the water depth is equal to twice the depth of the upper layer.

#	Orbit	Frame(s)	Satellite	Date	Time	Location
1	9477	3429	ERS-2	11-Feb-1997	03:58	
2	05426	3447-3465-3483	ERS-2	04-May-1996	03:52	
3	07514	0135	ERS-1	22-Dec-1993	16:03	

Internal Solitary Waves in the Andaman Sea

The Andaman Sea of the Indian Ocean is known to be one of the sites in the world's ocean where extraordinarily large internal solitons are encountered.

For centuries seafarers passing through the Strait of Malacca on their journeys between India and the Far East have noticed that in the Andaman Sea bands of strongly increased surface roughness often occur. These have also been referred to as bands of choppy water or riplings and have been found mainly between the Nicobar Islands and the north east coast of Sumatra. A description of such bands of choppy water observed from ships in the western approaches of the Malacca Strait can, e.g., be found in the book of Mauray which was published in 1861 and which is quoted in Osborne and Burch (1980): "The riplings are seen in calm weather approaching from a distance, and in the night their noise is heard a considerable time before they come near.

They beat against the sides of a ship with great violence, and pass on, the spray sometimes coming on deck; and by carrying out oceanographic measurements from a ship, a small boat could not always resist the turbulence of these remarkable riplings".

Perry and Schimke (1965) were the first to show by oceanographic measurements carried out from a ship that these bands of choppy water in the Andaman Sea are associated with large amplitude oceanic internal waves. Later Osborne and Burch (1980) analysed oceanographic data collected by the Exxon Production Research Company in the southern Andaman Sea with the aim to assess the impact of underwater current fluctuations associated with oceanic internal waves on drilling operations carried out from a drill ship. They concluded that the visually observed roughness bands are caused by internal solitons which can be described by the Korteweg - de Vries equation (1885).

The oceanographic measurements of Osborne and Burch (1980) showed that the time interval between the first solitons in the packets was typically 40 minutes and then decreased towards the end. In one event, the amplitude (peak-to-trough distance) of the foremost soliton was estimated to be 60 m, i.e., warm water from above was pushed down by the internal soliton by 60 m. The roughness bands associated with one of the internal soliton packets extended from horizon to horizon and were 600 to 1200 m wide.

The first band of choppy water consisted of breaking waves about 1.8 m high. The background wave field preceding this band had only a waveheight of 0.6m. Behind this band of strongly increased surface roughness, the waveheight gradually decreased and a band of reduced surface roughness followed, which had a waveheight of less than 0.1 m and looked "as smooth as a millpond".

Occasionally, long narrow stripes of rough water have also been identified in the Andaman Sea on satellite images acquired in the visible band, e.g., from the Russian-US space station Apollo-Soyuz (Apel, 1979), the Landsat satellites (Osborne and Burch, 1980), and the SPOT satellites. However, no systematic investigations of internal solitons could be carried out with optical satellite images because they can be acquired only sporadically when there are no clouds present and when the sun elevation angle is favourable.

A large number of spaceborne SAR images of the Andaman Sea have become available after the ERS receiving station in Singapore became operational in Sept. 1995. These ERS SAR images allow for the first time to study systematically the spatial distribution of internal solitons in the Andaman Sea and thus to obtain information on their generation and propagation characteristics.

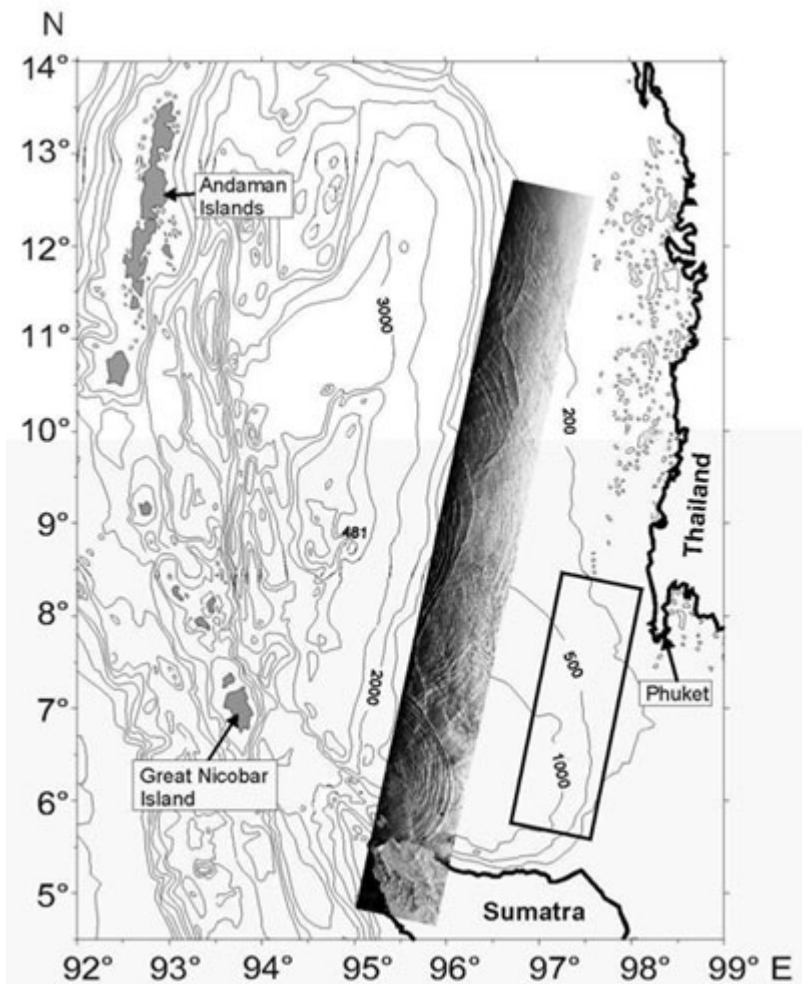
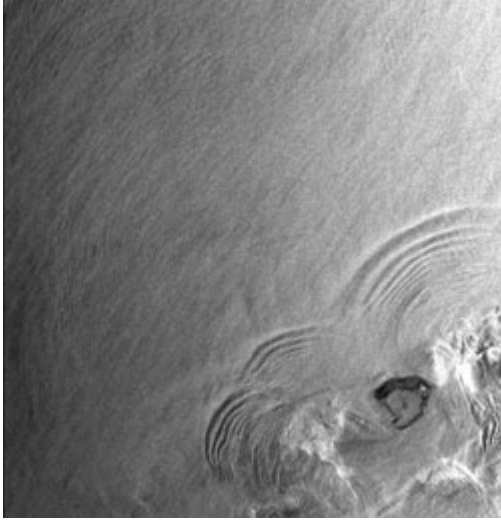


Figure 1: A SAR strip inserted into a map of the Andaman Sea which was acquired on Feb. 11, 1997. The sea surface manifestations of several internal solitary wave packets having their origin in three locations in the shelf region of the Andaman and Nicobar islands are visible. Inserted is also the location of the ERS-2 SAR strip shown in Figure 2.

References

- Alpers, W., Heng, W.-C. & Hock, L., Observation of internal waves in the Andaman Sea by ERS SAR, Proc. 3rd ERS Symp., Florence, Italy, 17-21 March 1997, ESA publication SP-414, 1287-1291 (1997).
- Apel, J.R., Thomson, D.R., Tilley, D.G. & van Dyke, P., Hydrodynamics and radar signatures of internal solitons in the Andaman Sea, John Hopkins APL Technical Digest, Vol.6, 4, 3330-3337 (1985).
- Osborne, A.R. & Burch, T.L., Internal solitons in the Andaman Sea, Science, 1980, 208, 451-460.
- Perry, B.R. & Schimke, G.R., Large-amplitude internal waves observed off the northwest coast of Sumatra, J. Geophys. Res., 70, 2319-2324 (1965).

Sulu Sea



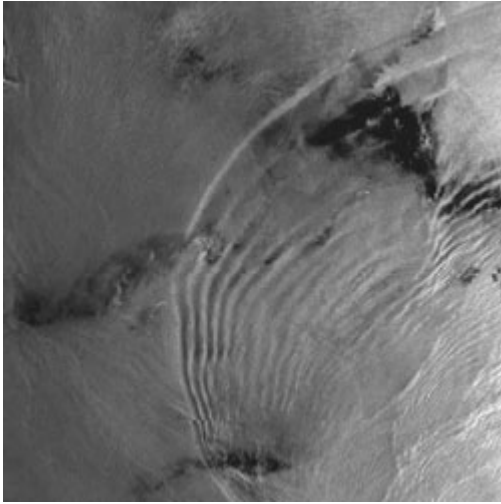
Sulu Sea

Latitude: 06° 07' N - Longitude: 119° 28' E

Sea surface manifestations of three packets of nonlinear internal waves shortly after they were generated by tidal flow over (1) the saddlelike sill spanning the passage between Pearl Bank and Doc Can Island east of Pearl Bank and (2) over topographic features west of Pearl Bank. Pearl Bank is visible in the lower right-hand section of the image as a dark circular feature.

A bathymetric map of the generation region east of Pearl Bank and two depth profiles along and across the sill axis are depicted in the figures below (reproduced from Apel et al., 1985).

The propagation direction of the eastern packet is about 345°, of the central packet 330°, and of the western packet 315°. From the shape of the circular patterns we conclude that the eastern packet was generated earlier than the other ones.

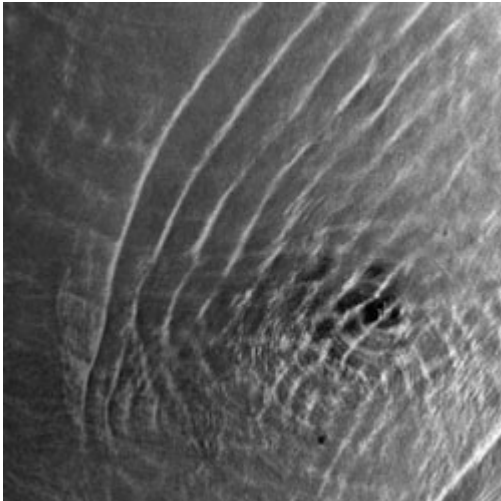


Sulu Sea

Latitude: 06° 38' N - Longitude: 118° 50' E

Sea surface manifestations of a packet of nonlinear internal waves, which, very likely, were generated at a location east of Pearl Bank.

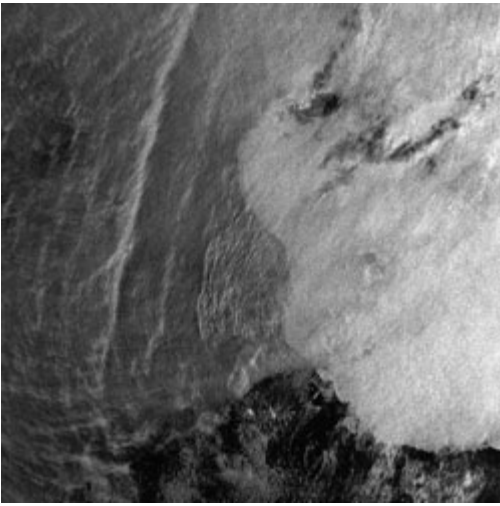
The distance between the first and the second soliton varies from 6.5 km to less than 1 km which may be attributed to the interaction with the sea bottom. Note that the propagation velocity decreases with decreasing depth.



Sulu Sea

Latitude: 08° 21' N - Longitude: 118° 31' E

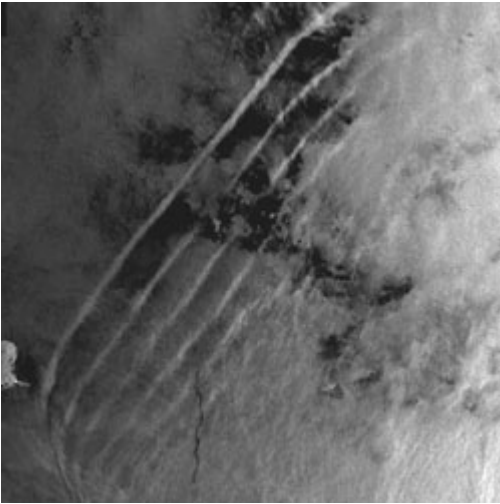
Sea surface manifestations of 3 packets of nonlinear internal waves generated during 3 successive tidal cycles. The distance between the first and the second wave packet is about 100 km, and between the second and the third packet about 90 km. The interruption of the sea surface manifestations in the first packet is due to the interaction with the shallow bottom topography. The dark circular feature in the center of the ERS SAR strip is a coral reef.



Sulu Sea

Latitude: 08° 21' N - Longitude: 118° 32' E

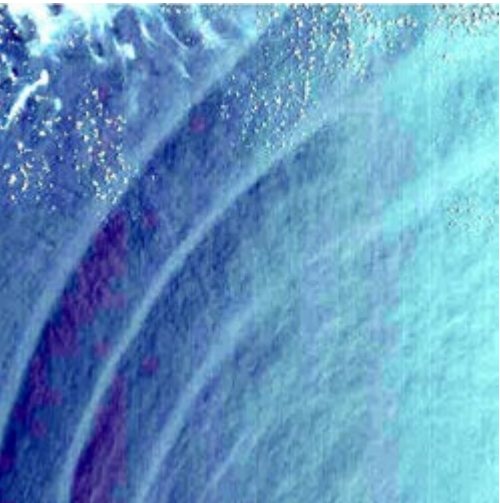
The ocean area visible on this ERS-2 SAR image overlaps partly with the area visible on the previous ERS-1 SAR image of 07-Apr-1996. The comparison of both images shows that the direction of wave propagation, the number of solitons in a wave packet, and the width ("wavelength") of the solitons varies considerably depending on the environmental conditions. The bright features with embedded dark patches visible in the right-hand section of the image are sea surface imprints of tropical rain cells.



Sulu Sea

Latitude: 07° 28' N - Longitude: 119° 02' E

Sea surface manifestations of 6 internal wave packets in an area which is about 185-200 km away from the generation region. The western boundary of the crest of the solitons is determined by the location of an isobath between 50 and 100 m (see bathymetric map). The eastern part of Kagayan-Sulu Island is visible near the first soliton in the lower left-hand section of the image.

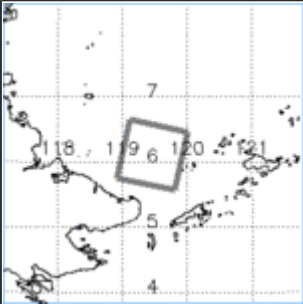
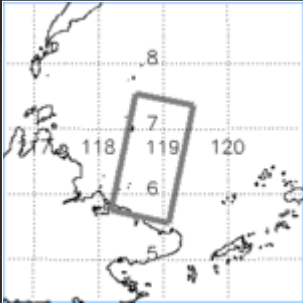
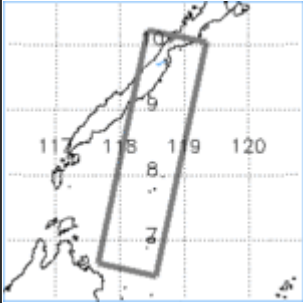
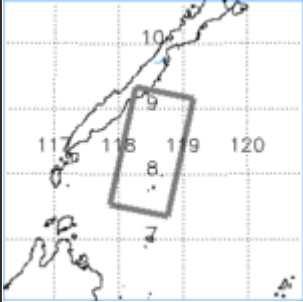
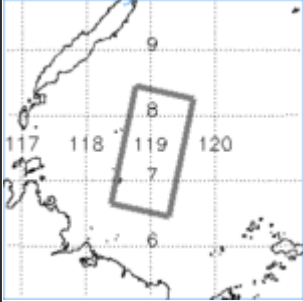
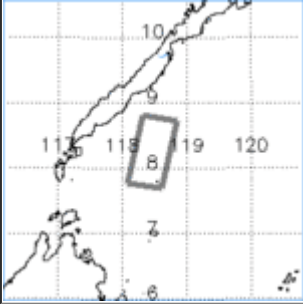


Sulu Sea

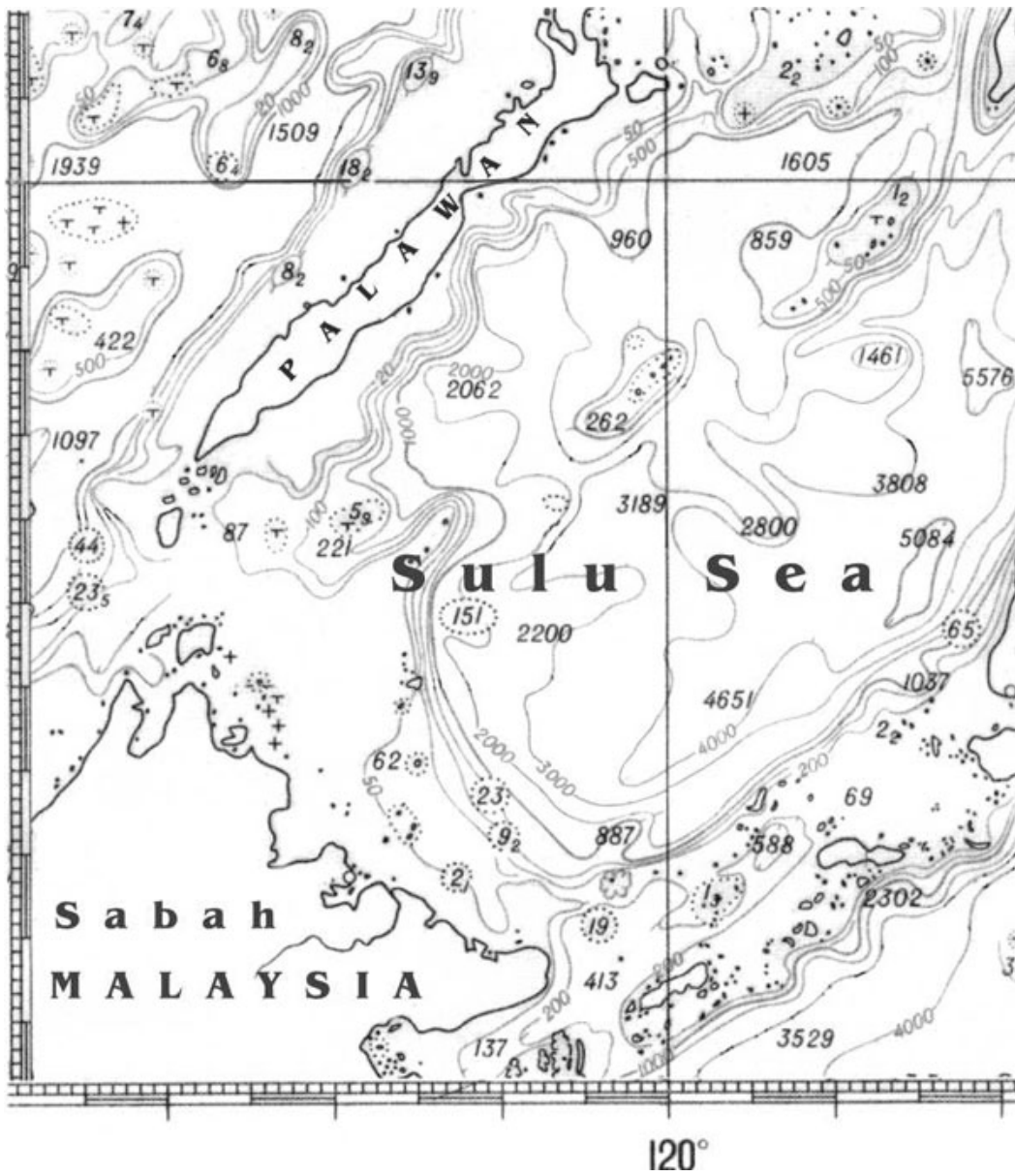
Latitude: 08° 16' N - Longitude: 118° 28' E

SPOT 2 quick-look image (image size: 60 km x 120 km) of partly the same ocean area as visible on the previous ERS SAR images. At the bottom of this image are visible the islands Bankoran and San Migel. The curved bright stripes of 1.5 - 2 km width are sea surface manifestations of internal solitary waves. The imaged area lies outside the sunglint area. Thus bands of increased sea surface roughness (and possibly increased foam coverage) are imaged as bright bands.

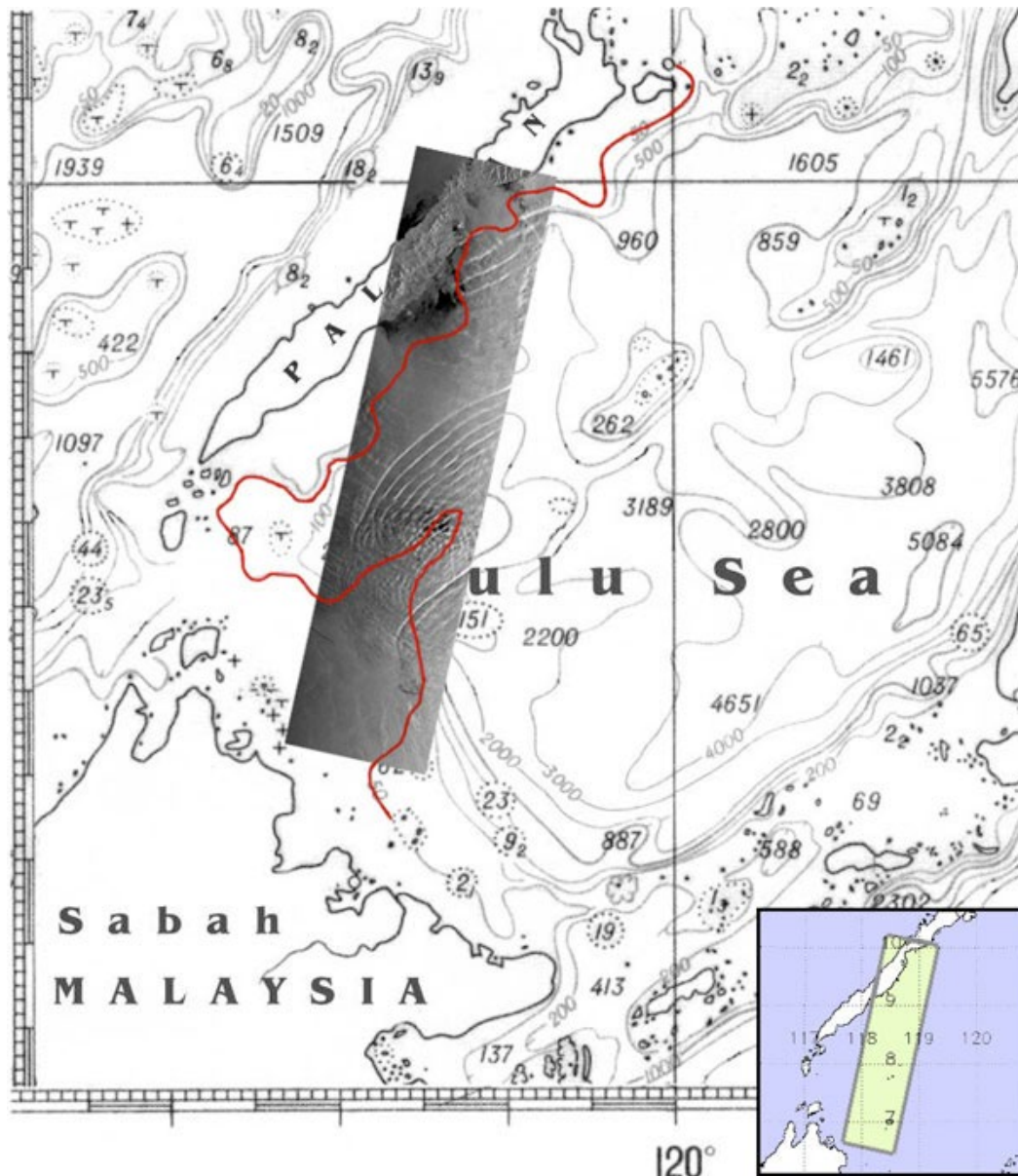
© CNES 2000 - [Spot Image](#) distribution

#	Orbit	Frame(s)	Satellite	Date	Time	Location
1	14529	3483	ERS-2	30-Jan-1998	02:24	
2	06284	3465-3483	ERS-2	03-July-1996	02:27	
3	24726	3411-3429-3447-3465	ERS-1	07-Apr-1996	02:30	
4	24091	3429-3447	ERS-2	29-Nov-1999	02:29	
5	24320	3447-3465	ERS-2	15-Dec-1999	02:27	
6	Path: 302	333-334	SPOT-2	15-Sep-1999	02:42	

Ancillary information to these images



Bathymetric map of the Sulu Sea (the numbers denote water depth in metres)



Bathymetric map showing internal wave breaking

References

- Apel, J.R., Oceanic internal solitons, Backscatter, 10, 2, 20-22, 24-25 (1999).
- Apel, J.P., Holbrook, J.R., Liu, A.K. & Tsai, J.J., The Sulu Sea internal soliton experiment, J. Phys. Oceanogr., 15, 1625-1651 (1985).
- Liu, A.K., Holbrook, J.R. & Apel, J.R., Nonlinear internal wave evolution in the Sulu Sea, J. Phys. Oceanogr., 15, 1613-1624 (1985).
- Porter, D.L. & Thompson, D.R., Continental shelf parameters inferred from SAR internal wave observations, J. Atmos. and Oceanic Tech., 16, 475-487 (1999).

Introduction to Lombok Strait

The Lombok Strait separates the Indonesian islands Bali and Lombok and is one of the most important straits through which water is exchanged between the Pacific Ocean and the Indian Ocean. This strait is one of the Indonesian throughflows that plays an important role in the global oceanic circulation.

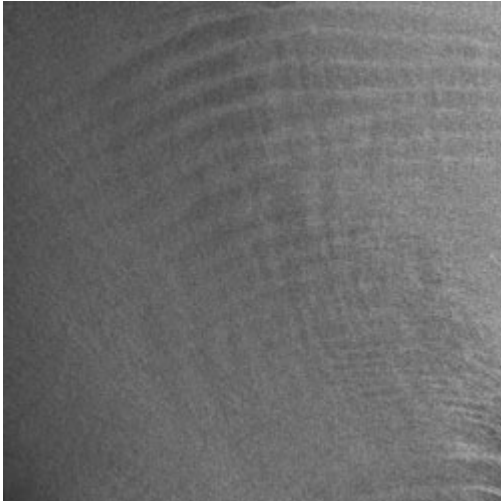
Transport through the Strait exhibits large seasonal variations due to variations in the atmospheric pressure gradient between the Pacific and the Indian Ocean which is a function of the monsoon. As a result, the seasonal currents through the strait are bidirectional. The main topography features inside the Lombok Strait are an island (Nusapenida) and a sill between this island and the smaller Lombok islands in the southern mouth of the strait.

The current pattern consists of the superposition of the main flow and the tidal flow. In the upper 100 meters the current velocity reaches 1.5 m/s at the center of the strait and 3.0 m/s in the sill region. The ERS SAR images of this region reveal that the packets of internal waves propagate both to the north into the Java Sea where they reach the shallow waters surrounding Pulau-Pulau Kangean and to the south into the Indian Ocean.

In the deep waters (deeper than 500 m) south and north of the Lombok Strait the crests of the internal waves have a regular circular shape. The propagation velocity of the internal waves in the Java Sea is about 2 m/s. In the Indian Ocean the internal wave pattern is quite irregular due to the variable currents in this sea area. Sometimes 2-3 systems of internal waves which propagate in different directions are observed in this region.

Available CTD profiles (Murray and Arief, 1990) show a well-mixed surface layer and a salinity maximum at the thermocline depth. South of the sill, in situ hydrological observations detected a well-developed thermal plume with steep thermal gradients near its boundary. The plume intrudes over 30 km into the Indian Ocean. Possibly the curved bright bands which are visible south of the strait in image 4 and 5 are sea surface manifestations of this plume.

Lombok Strait



Lombok Strait

Latitude: 08° 11' N - Longitude: 115° 35' E

The image shows the Kanagan Island and coral reefs (in the upper left-hand section of the image), two northward-propagating packets of solitary waves in the Flores Sea, Bali Island, the Lombok Strait, the small Nusa Penida Island at the south end of the strait and an internal wave packet in the Indian Ocean.

Internal wave packets propagating both to the north and to the south are due to interaction of strong tidal currents (daily maximum speed reaches nearly 3 m/s) with a sill between Nusa Penida and Lombok islands (see bathymetric map). More than 20 crests with monotonically decreasing wavelength can be delineated in the first packet. The leading crest has reached shallow waters where there are coral reefs and small islands.

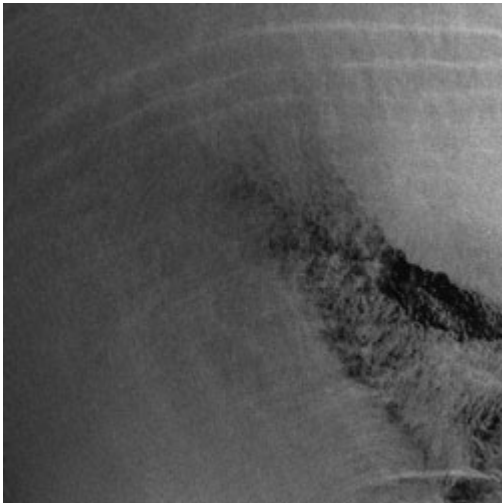
The width of the packet is about 80 km. The leading crest of the second packet is catching up with a rear of the first packet.

Surface manifestations of two phenomena are observed south of the sill: a packet of nonlinear solitary waves and a plume of warmer Pacific waters which intrudes over 25 km into the Indian Ocean (This interpretation is in agreement with the information contained in the temperature and salinity maps shown in the section "Ancillary information to these images").

Lombok Strait

Latitude: 08° 10' N - Longitude: 115° 35' E

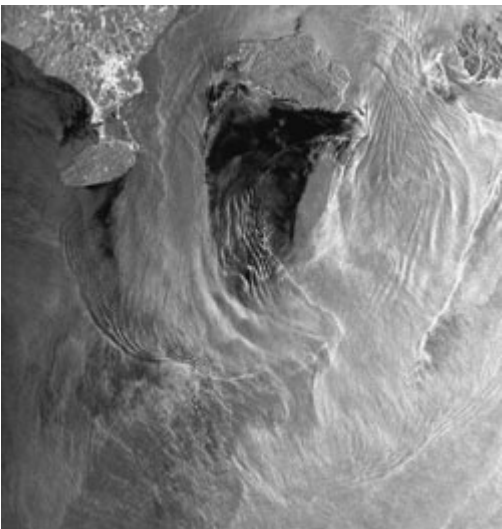
This image was acquired a day later and at an earlier phase of the tidal cycle than the previous one. It shows a solitary wave pattern similar to the pattern visible in the previous image. The distance between the leading solitons in the packet and the coral reefs is about 10 km. The eastern part of the second northward-propagating solitons has the larger radar contrast due to the decreased brightness of the background (area of Lombok Island wake). Solitons in the Indian Ocean also have a weak radar contrast.

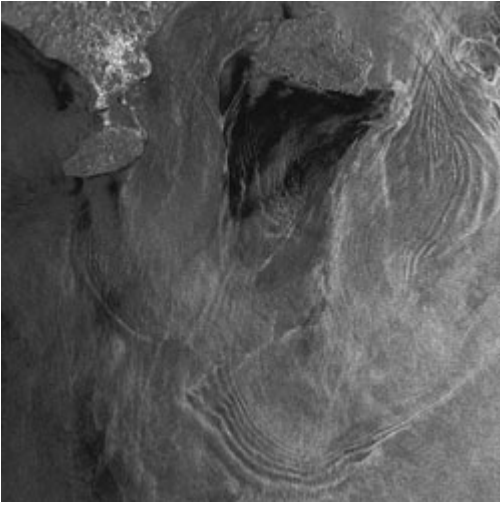


Lombok Strait

Latitude: 09° 05' S - Longitude: 115° 24' E

This ERS-1 SAR image of the southern section of the Lombok Strait shows sea surface manifestations of several internal wave packets. This SAR image should be compared with the next SAR image which was acquired one day later by ERS-2 and which also shows sea surface manifestations of internal wave packets in the southern section of the Strait.





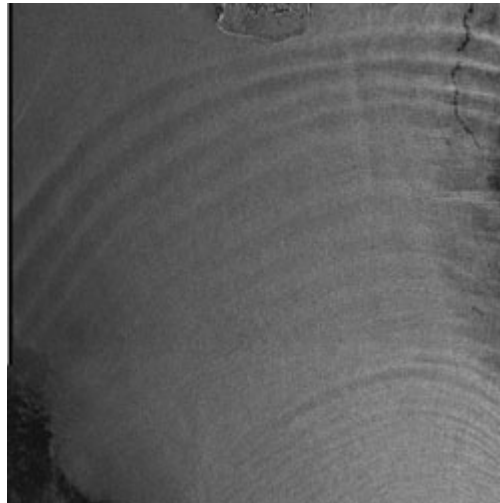
Lombok Strait

Latitude: 09° 06' S - Longitude: 115° 21' E

Sea surface manifestations of several internal wave packets south and north of the sill between the Nusa Penida and Lombok islands. It is very probable that the wave packets were generated during the same tidal cycle.

At least four internal wave packets are clearly visible south of the sill: one southward-propagating packet consisting of 8 solitons, one southwestward propagating packet, and two packets south of the sill propagating in opposite directions.

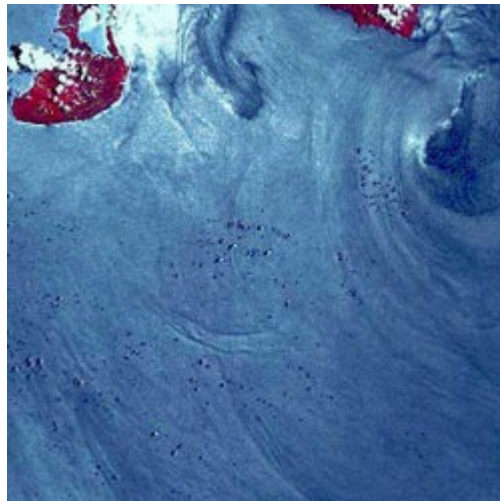
The dark triangle-shape area is very likely an island wake downstream from Nusa Penida island. A wave packet propagating into the Bali Sea has a very weak radar contrast.



Lombok Strait

Latitude: 08° 22' S - Longitude: 115° 18' E

Packets of nonlinear solitary waves propagating both into the Bali Sea and the Indian Ocean. The irregular surface pattern near the sill between the Nusa Penida island and the Lombok Strait and in the area south of the sill is very likely caused by the interaction of internal solitons with a thermal plume.

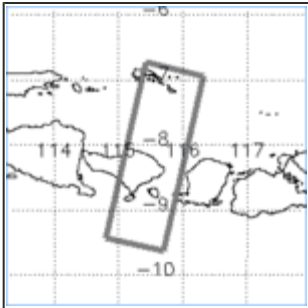
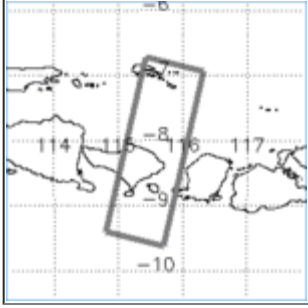
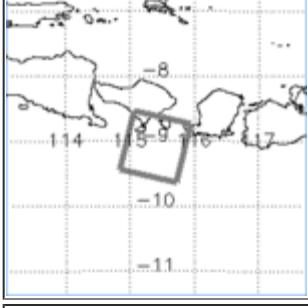
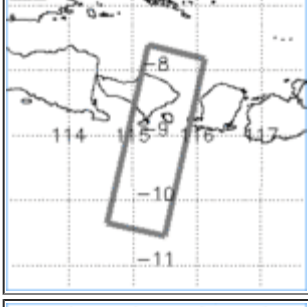
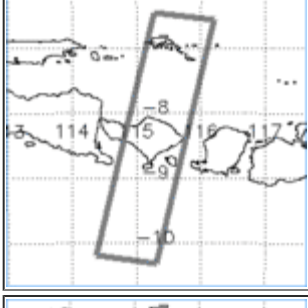
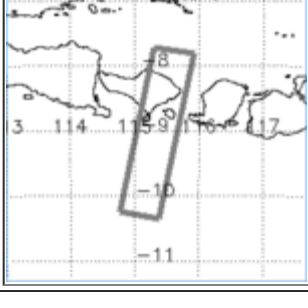


Lombok Strait

Latitude: 09° 01' S - Longitude: 115° 20' E

Quick-look SPOT image of an area of 60 km x 300 km stretching through the Lombok Strait. The white patches in the lower part of the images result from clouds.

© CNES 2000 - [Spot Image](#) distribution

#	Orbit	Frame(s)	Satellite	Date	Time	Location
1	24955	3753-3771-3789	ERS-1	23-April-1996	02:32	
2	05282	3753-3771-3789	ERS-2	24-Apr-1996	02:32	
3	32470	3789	ERS-1	30-Sep-1997	02:32	
4	12797	3771-3789-3807	ERS-2	01-Oct-1997	02:31	
5	13298	3753-3771-3789-3807	ERS-2	05-Nov-1997	02:32	
6	Path: 303	366-367-368-369-370	SPOT-1	18-Oct-1998	02:54	

Ancillary information to these images

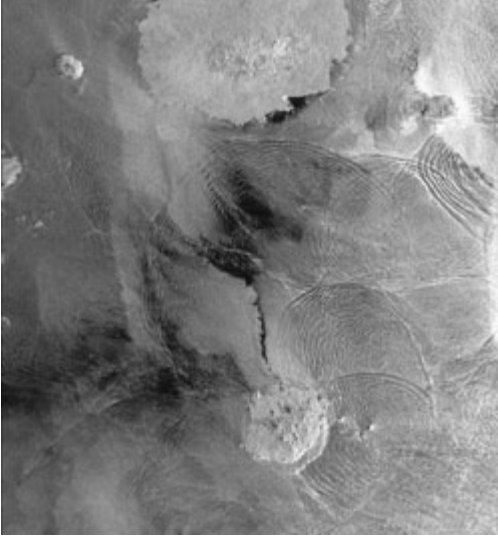
[Bathymetric map of the Sulu Sea \(the numbers denote water depth in metres\)](#)

[Bathymetric map showing internal wave breaking \(Bathymetric map of the Sulu Sea with the ERS-1 SAR image acquired on 07 April 1996 - image #3 in the table - inserted\)](#)

References

- Arief, D. & Murray, S.P., Low-frequency fluctuations in the Indonesian Throughflow through Lombok Strait. *J. Geophys. Res.*, 101, 12455-12464 (1996).
- Arief D. Outer southeast Asia: A region of deep straits, including the Banda Sea (13,S). In: *The Sea*, vol.11, edited by A.R. Robinson and K.H. Brink, John Wiley & Sons, Inc., Chapter 17, 507-522 (1998).
- Coatanoan, C., Metzl, N., Fieux, M. & Coste, B., Seasonal water mass distribution in the Indonesian throughflow entering the Indian Ocean. *J. Geophys. Res.*, 104, 20801-20826 (1999).
- Fieux, M., Andrie, C., Delacluse, P., Ilahude, A.G., Kartavseff, A. et al. Measurements within the Pacific-Indian Oceans Throughflow region. *Deep-Sea Res.*, 41, part 1, 1091-1130 (1994).
- Godfrey, J.S. The effect of the Indonesian throughflow on ocean circulation and heat exchange with the atmosphere: A review. *J. Geophys. Res.*, 101, 12217-12237 (1996).
- Gordon, A.L. & Fine, R.A., Pathways of water between the Pacific and Indian oceans in the Indonesian seas. *Nature*, 379, 146-149 (1996).
- Meyers, G. Variation of Indonesian Throughflow and the El Nino-Southern Oscillation. *J. Geophys. Res.*, 101, 12255-12263 (1996).
- Meyers, G., Bailey, R.J. & Worby, A.P., Geostrophic transport of Indonesian Throughflow. *Deep-Sea Res.*, 42, 1163-1174 (1995).
- Murray, S.P. & Arief, D., Throughflow into the Indian Ocean through the Lombok Strait, January 1985-January 1986, *Nature*, 333, 444-447 (1988).
- Murray, S.P. & Arief, D., Characteristics of circulation in an Indonesian archipelago strait from hydrography, current measurements and modeling results. In: *The Physical Oceanography of Sea Strait*. L.J. Pratt, editor, NATO ASI Series. Vol. 318. Kluwer Academic Publishers, Dordrecht, Boston, London. pp. 3-23 (1990).
- Rodgers, K.B., Cane, M.A. & Naik, N.H., The role of the Indonesian Throughflow in equatorial Pacific thermocline ventilation. *J. Geophys. Res.*, 104, 20551-20570 (1999).

Galapagos Islands



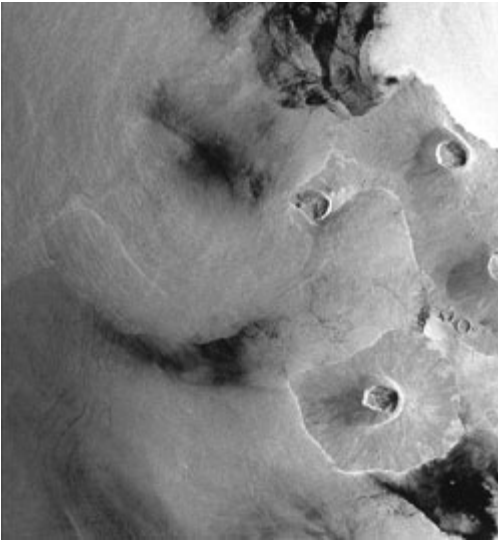
Galapagos Islands

Latitude: $01^{\circ} 07' S$ - Longitude: $90^{\circ} 28' W$

Several tidally generated internal solitary wave packets in the waters surrounding the Galapagos Islands in the Equatorial Pacific Ocean.

The island visible in the upper section of the image is the island Santa Cruz and in the lower section the island Santa Maria. Both islands are covered with small craters. From the spherical shape of the wave patterns one can infer that their generation areas ("birth places") are well-confined shallow sea areas which in this case are very likely underwater volcanic craters.

One likely generation area is the Banca Hancock, which is located 25 km northeast of Santa Maria. Here the ocean is only 18 m deep.



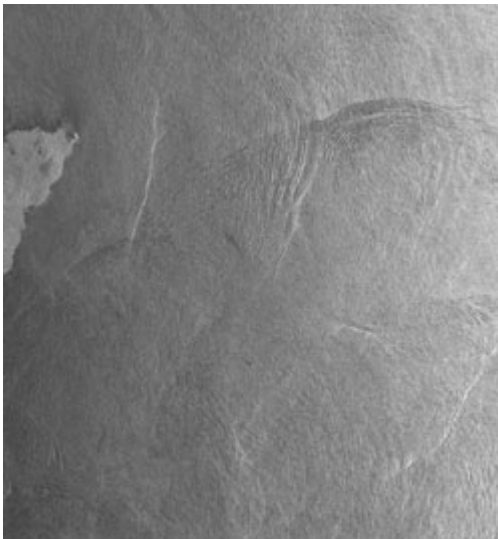
Galapagos Islands

Latitude: $0^{\circ} 04' N$ - Longitude: $91^{\circ} 41' W$

In the upper right-hand section of the image the northeastern part of the island Isabela is visible while the island Fernandina with its large volcanic crater can be seen in the lower right-hand section.

The semi-circular feature in the centre of the image is very likely an atmospheric front (possibly connected with a rain event). We speculate that the wave pattern visible in the waters southeast of the western crater of the island Isabela is the sea surface imprint of oceanic internal waves which are triggered by the atmospheric front.

The dark/bright patterns in the upper right-hand corner of the image seem to be associated with tropical rain cells.



Galapagos Islands

Latitude: $01^{\circ} 01' S$ - Longitude: $89^{\circ} 00' W$

Internal solitary wave packets in the sea area east of the island San Cristobal which is the most eastern island of the Galapagos Islands group in the Pacific Ocean.

#	Orbit	Frame(s)	Satellite	Date	Time	Location
1	07027	3627	ERS-1	18-Nov-1992	16:20	
2	6569	3607	ERS-1	17-Oct-1992	16:26	
3	06984	3627	ERS-1	15-Nov-1992	16:14	

South China Sea

Introduction

The South China Sea, like the Andaman Sea and the Sulu Sea, is another ocean area in the Far East where large amplitude and long-crested internal solitary waves are encountered.

The waves are generated by the interaction of the tidal current with shallow bottom topography in the Luzon Strait (between Taiwan and Luzon). The orientation of the soliton crests is approximately in north-south direction. An interesting phenomenon is the interaction of internal solitons with the coral reef Dongsha which can be studied by ERS SAR images.



Dongsha Island

Latitude: 20° 52' N - Longitude: 120° 33' E

Composite of four standard ERS-1 SAR images (100 km x 400 km) of the Luzon Strait located between Taiwan (visible at the top) and the Indonesian island Luzon (not visible) showing radar signatures of internal solitary waves propagating westward.

The crest length of the leading soliton exceeds 200 km. The wave packets have been generated by the interaction of tidal flow with different shallow underwater ridges.

In situ measurements (CTD casts) carried out by a Taiwanese research ship in this region have shown that the amplitude (crest-to-trough distance) of internal solitary waves in this region can exceed 100 m.

South China Sea

Latitude: 20° 26' N - Longitude: 117° 35' E

Composite of three standard ERS-1 SAR images (100 km x 300 km) showing radar signatures of internal solitary waves in the central northern part of the South China Sea. The single soliton visible in the upper section of the image has a crest length larger than 200 km.

Note that the width of the radar signature (the width of the bright and dark band) of the leading soliton increases from north to south. Sea surface imprints of several tropical rain cells having circular and elliptical shapes are also visible on this image.

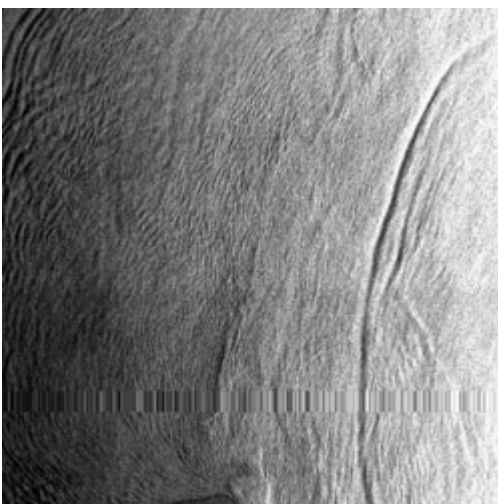
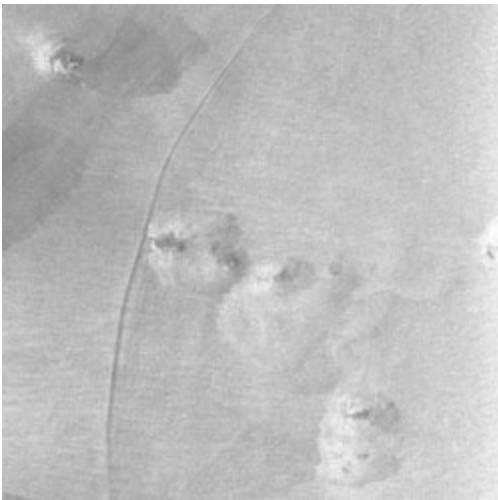
Dongsha Island

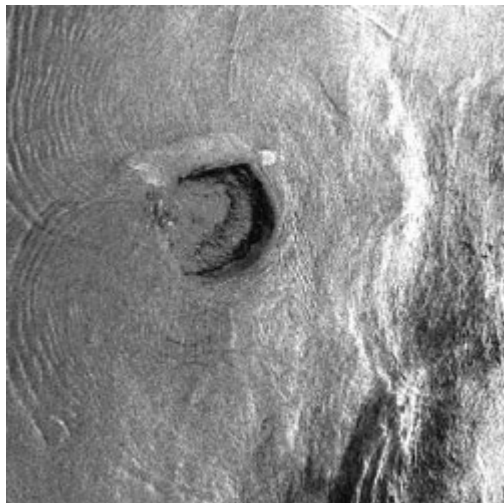
Latitude: 19° 59' N - Longitude: 116° 46' E

Composite of four standard ERS-1 SAR images (100 km x 400 km) of a sea area lying west of the sea area visible on the previous image. On this image the Dongsha atoll (the circular feature in the upper section of the image) is visible.

Its diameter is approximately 25 km. The Dongsha Island is located at the western end of the atoll. Radar signatures of two large-amplitude internal solitary wave packets are clearly visible on this image.

The northern part of the first wave packet has crossed already the atoll and the southern part has almost crossed it. A second wave packet, which was generated during the next tidal cycle, is approaching the Dongsha atoll.

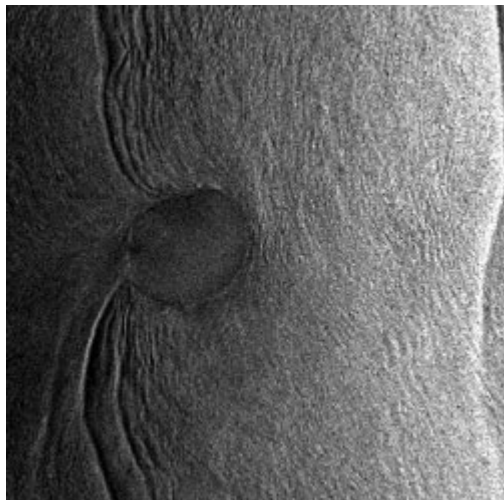




Dongsha Island

Latitude: 19° 95' N - Longitude: 116° 46' E

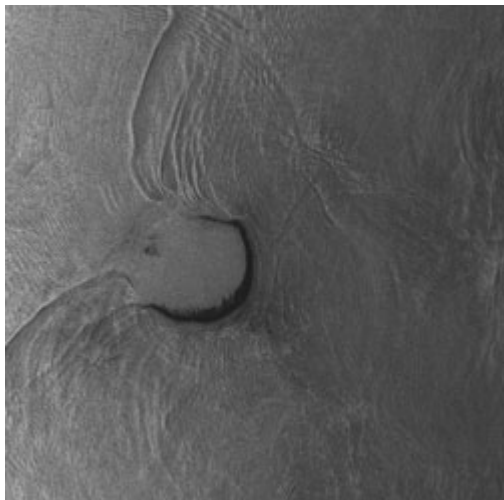
Visible on this ERS-2 SAR image is again the Dongsha atoll. Note that the location, the shape and the strength of the radar signatures of the internal solitary waves visible on this image are quite different from those of the previous image. Visible are two packets of internal waves which result from the interaction of an internal solitary wave packet with the Dongsha atoll.



Dongsha Island

Latitude: 20° 52' N - Longitude: 116° 58' E

On this ERS-2 SAR image two packets of internal solitary waves and the Dongsha atoll are visible. The first packet has almost crossed the atoll. The leading soliton of the second one is visible at the right edge of the image. The distance between these packets is approximately 75-85 km. If we assume that they have been generated at successive semi-diurnal tidal cycles, we obtain as propagation speed 1.7-1.9 m/s.

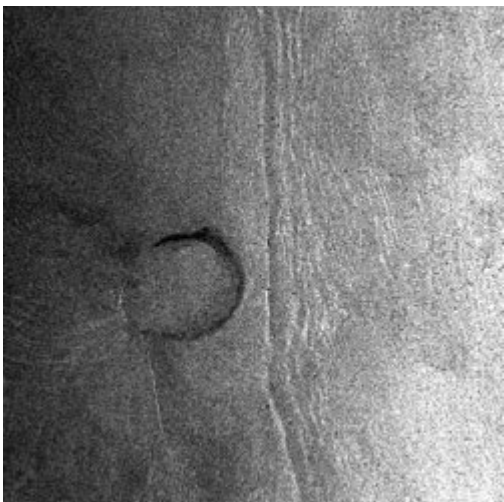


Dongsha Island

Latitude: 20° 31' S - Longitude: 116° 44' E

This ERS-2 SAR image shows large-amplitude internal solitary waves around the Dongsha atoll (the dark horseshoe-shaped area in the center of the image).

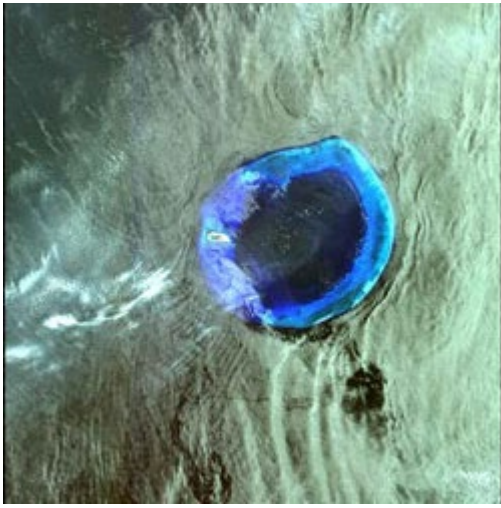
Another packet of nonlinear solitary waves consisting of more than 10 waves propagates northward. It crosses the first wave packet almost at an angle of 90 degrees



Dongsha Island

Latitude: 20° 52' N - Longitude: 116° 52' E

Packet of internal solitons approaching the Dongsha atoll. The leading soliton has a crestlength of more than 200 km. The curvature of the crestline is small indicating that the generation region of the solitons must be far away.



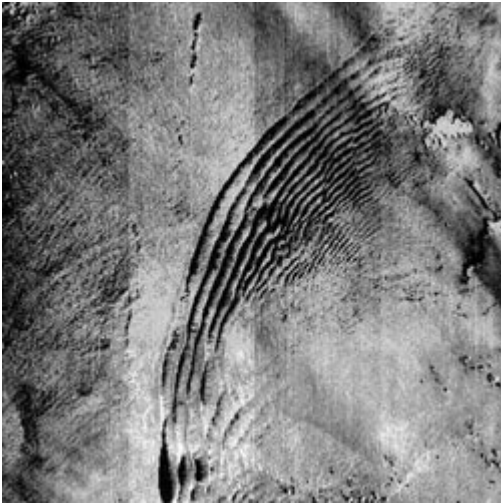
Dongsha Island

Latitude: 20° 15' N - Longitude: 116° 36' E

This SPOT 3 image shows in colour the Dongsha atoll with the Dongsha island (the bright elliptic spot in the left-hand section of the blue ring).

Also sea surface manifestations of internal solitary waves are visible. The image was acquired outside the sunglint area: the viewing angle was 2.0°, the sun elevation angle 70°, and the sun azimuth angle 116°.

© CNES 2000 - [Spot Image](#) distribution



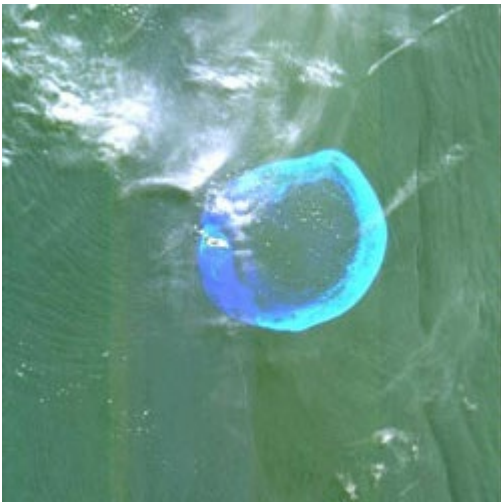
Dongsha Island

Latitude: 21° 00' N - Longitude: 116° 51' E

Visible on this SPOT 1 image is a packet of nonlinear solitary waves north of the Dongsha atoll. The image was acquired outside the sunglint area: the viewing angle was 15.0°, the sun elevation angle 68°, and the sun azimuth angle 128°.

The narrow dark line crossing the coral reef area is the shadow of a contrail, i.e. of a trail of condensed water vapour that sometimes forms in the wake of an aircraft.

© CNES 2000 - [Spot Image](#) distribution

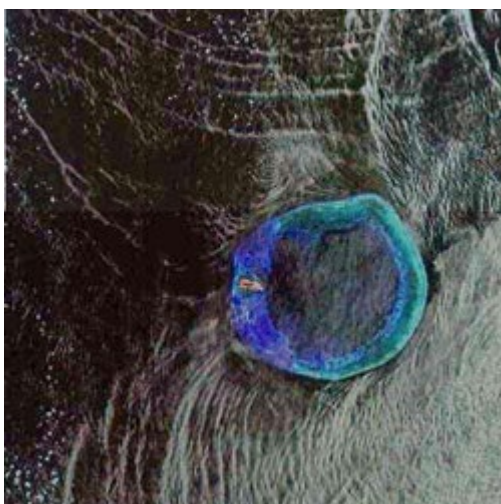


Dongsha Island

Latitude: 20° 30' N - Longitude: 116° 54' E

This SPOT 1 image (size 60 km x 180 km) was acquired 5 min later than the ERS-2 SAR image shown in Fig. 7. The image was acquired outside the sunglint area: the viewing angle was -11.5°, the sun elevation 70.3° and the sun azimuth 78°. In this case the rough bands are imaged as bright bands.

© CNES 2000 - [Spot Image](#) distribution



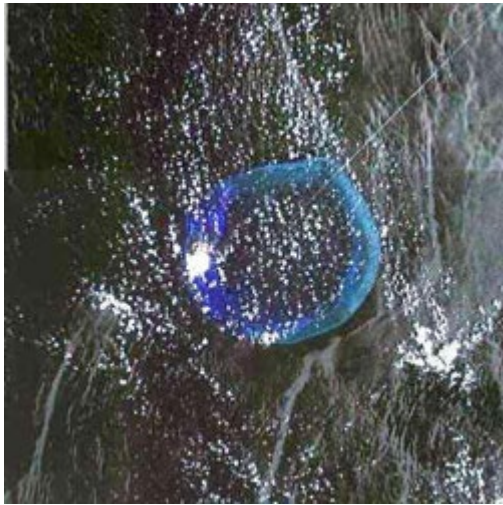
Dongsha Island

Latitude: 20° 56' N - Longitude: 116° 54' E

This SPOT 2 image shows radar signatures of nonlinear solitary waves to the north and south of the Dongsha atoll. A new feature is the packet of southward propagating internal solitary waves with circular crests visible north of the Dongsha coral reefs.

The image was acquired outside the sunglint area: the viewing angle was 2.0°, the sun elevation 70° and the sun azimuth 110°.

© CNES 2000 - [Spot Image](#) distribution



Dongsha Island

Latitude: 20° 13' N - Longitude: 116° 36' E

SPOT 1 image of Dongsha atoll surrounded by internal waves (incidence angle: 2.5°; sun elevation angle: 68.4°). The white splotches are clouds. The straight white crossing the Dongsha atoll is the contrail of an aircraft.

© CNES 2000 - [Spot Image](#) distribution



Dongsha Island

Latitude: 21° 46' N - Longitude: 116° 27' E

ERS-1 SAR image of an ocean area located north-northwest of Dongsha. The bended shape of some sea surface manifestations of internal solitary waves results from the interaction of the solitary waves with shallow bottom topography. In this sea area around the Lufeng Terminal, in which oil fields are located, the water depth is in some locations less than 10 m.



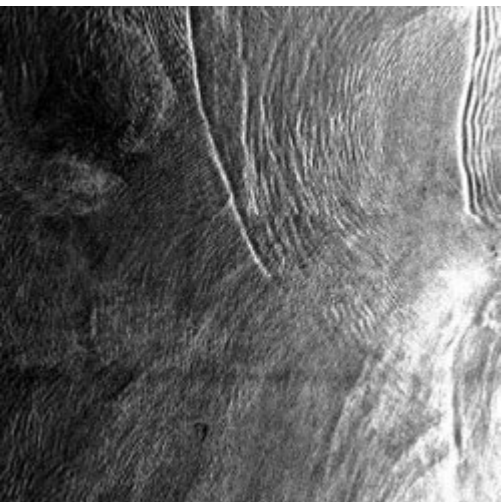
Dongsha Island

Latitude: 21° 33' N - Longitude: 116° 23' E

This SPOT 3 image shows packets of internal solitary waves in the South China Sea northwest of the Dongsha atoll. Visible in the central right-hand section of the image are clouds with their shadows.

In the lower left-hand section two internal solitary wave packets are visible which interact. Note that the interaction of internal solitons is associated with a phase shift (incidence angle: 24.2°; sun elevation angle: 74.6°).

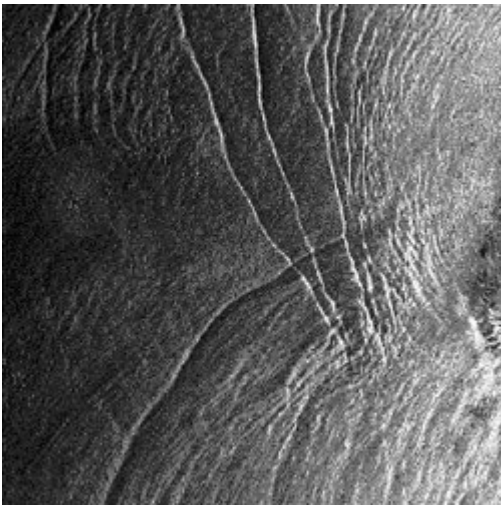
© CNES 2000 - [Spot Image](#) distribution



Dongsha Island

Latitude: 20° 53' N - Longitude: 116° 15' E

ERS-1 SAR image of the ocean area west of Dongsha. Visible are packets of internal solitary waves which have interacted with the coral reef Dongsha.



Dongsha Island

Latitude: 20° 26' N - Longitude: 116° 09' E

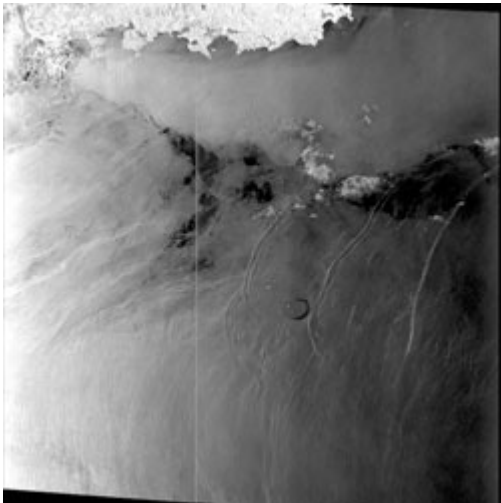
ERS-2 SAR image of an ocean area west of Dongsha Island. Visible are packets of internal solitary waves which have interacted with the Dongsha coral reef.



Dongsha Island

Latitude: 19° 59' N - Longitude: 115° 20' E

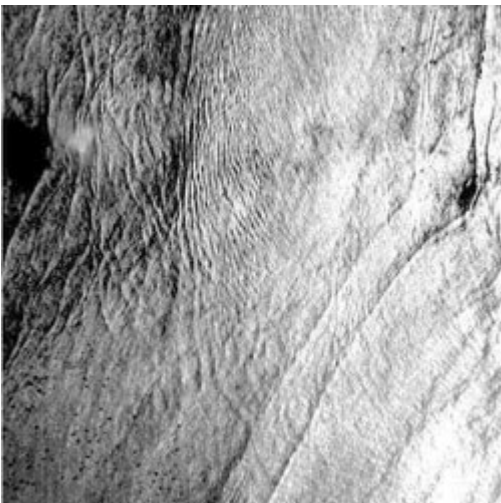
ERS-1 SAR image of an ocean area southwest of Dongsha. Visible are again sea surface manifestations of several internal solitary waves.



Dongsha Island

Latitude: 21° 15' N - Longitude: 114° 56' E

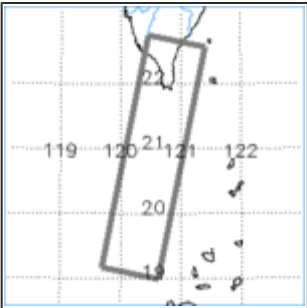
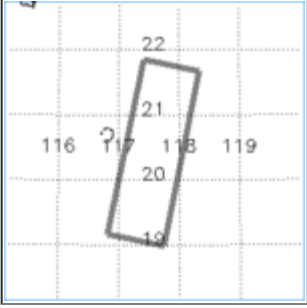
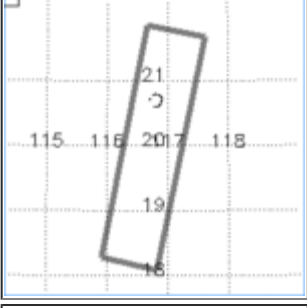
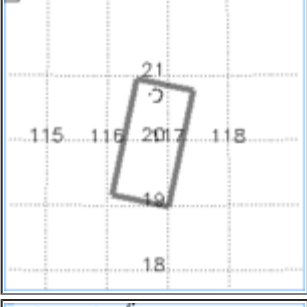
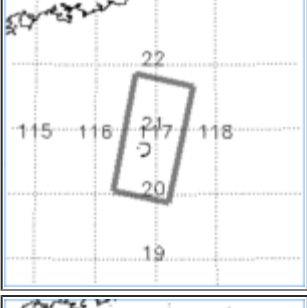
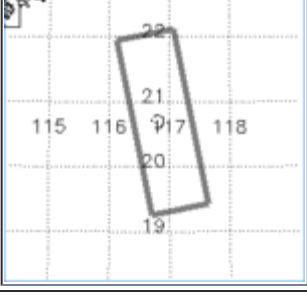
SPOT 3 image of the South China Sea west of Dongsha Island showing several packets of internal waves (incidence angle: 14.6°; sun elevation angle: 74.1°). © CNES 2000 - [Spot Image](#) distribution



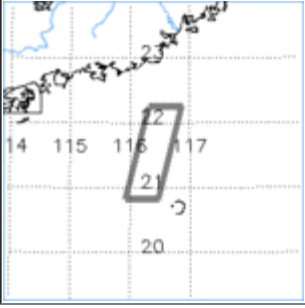
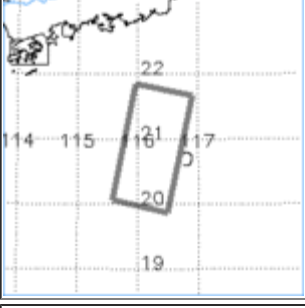
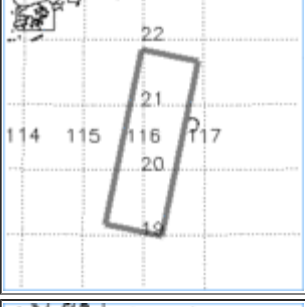
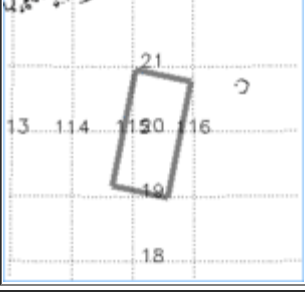
South China Sea

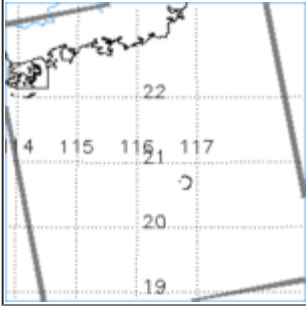
Latitude: 21° 09' N - Longitude: 116° 18' E

On this RADARSAT ScanSAR image four westward-propagating packets of internal waves are visible: two east and two west of the Dongsha coral reef. The coral reef is the horseshoe-like feature in the centre. The imaged area is 528 km x 478 km.

#	Orbit	Frame(s)	Satellite	Date	Time	Location
1	20489	31559-3177-3195-3213	ERS-1	16-Jun-1995	02:29	
2	21076	3177-3195-3213	ERS-1	27-Jul-1995	02:40	
3	20346	3177-3195-3213-3231	ERS-1	06-Jun-1995	02:43	
4	15703	3195-3213	ERS-2	22-Apr-1998	02:44	
5	16204	3177-3195	ERS-2	27-May-1998	02:43	
6	16598	0387-0423	ERS-2	23-Jun-1998	14:41	

#	Orbit	Frame(s)	Satellite	Date	Time	Location
7	16705	3177-3195	ERS-2	01-Jul-1998	02:43	
8	Path: 292	M1_307-308-309-310-311	SPOT 3	19-Apr-1995	02:56	
9	Path: 292	M1_307-308-309	SPOT 1	08-Apr-1998	03:02	
10	Path: 292	308-309-310	SPOT 1	01-Jul-1998	02:49	
11	Path: 292	306X1-307X1-308X1-309X1-310PX	SPOT 2	19-Aug-1999	02:58	
12	Path: 292	307X1-308X1-309X1-310X1-311X1-312X2	SPOT 1	31-Aug-1999	02:57	

#	Orbit	Frame(s)	Satellite	Date	Time	Location
13	21119	3159-3177	ERS-1	30-Jul-1995	02:46	
14	Path: 291	M1_306-307-308-309	SPOT 3	24-Jul-1996	03:11	
15	20618	3177-3195	ERS-1	25-Jun-1995	02:46	
16	16476	3177-3213	ERS-2	15-Jun-1998	02:46	
17	20890	3195-3213	ERS-1	14-Jul-1995	02:49	
18	Path: 2922	M1_305-306-307-308-309-310-311	SPOT 3	30-Jun-1995	03:12	

#	Orbit	Frame(s)	Satellite	Date	Time	Location
19	12918		RADARSAT	26-Apr-1998	unknown	

Ancillary information to these images

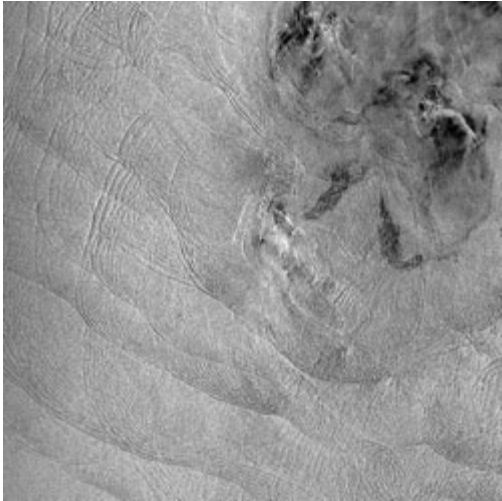
[Optical image of Dongsha Island](#)

[Optical image of Dongsha coral reef](#)

References

- Hsu, M.-K., Liu, A.K. & Liang, N.K.. Evolution of nonlinear internal waves northeast of Taiwan. Proc. Eighth Int. Offshore and Polar Eng. Conf., Montreal, Canada, May 24-29, 18-24 (1998).
- Hsu, M.-K., Liu, A.K. & Liu, C.. A study of internal waves in the China Seas and Yellow Sea using SAR. Cont. Shelf Res. ,20, 389-410 (2000).
- Liu, A.K., Chang, Y.S., Hsu, M.-K. & Liang, N.K.. Evolution of nonlinear internal waves in the East and South China Seas. J. Geophys. Res., 103, No. C4, 7995-8008 (1998).
- Mitnik, L., Alpers, W., Chen, K.S. & Chen, A.J., Manifestation of internal solitary waves on ERS SAR and SPOT images: Similarities and Differences, Proc. IGARSS 2000, Hawaii, 5, 1857-1862 (2000).

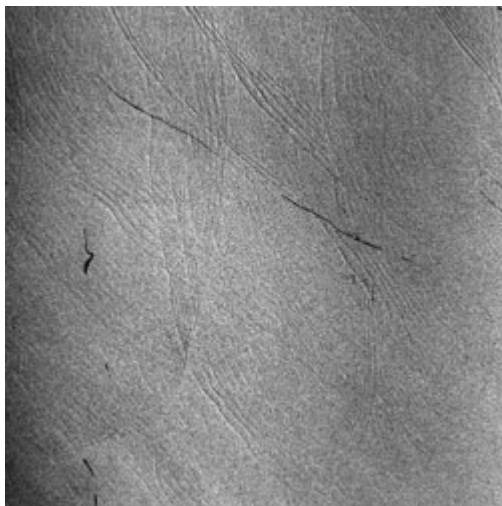
Yellow Sea



Yellow Sea

Latitude: 36° 03' N - Longitude: 125° 35' E

Several packets of internal solitary waves are visible on this ERS-2 SAR image of dimension 200km x 100km. In the upper right-hand section several Korean islands are visible which are located southwest of Korean Peninsula.

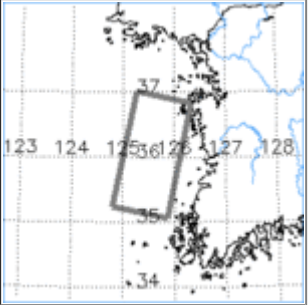
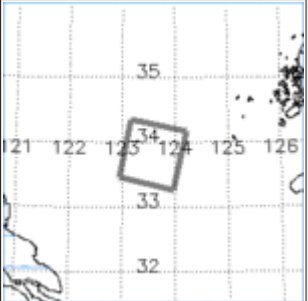


Yellow Sea

Latitude: 33° 49' N - Longitude: 123° 35' E

Internal wave packets in the Yellow Sea southwest of the Korean coast. Oil spills discharged from ships (dark lines) are also visible. The internal waves are generated by the interaction of the semi-diurnal tidal current with shallow underwater features near the Korean coast.

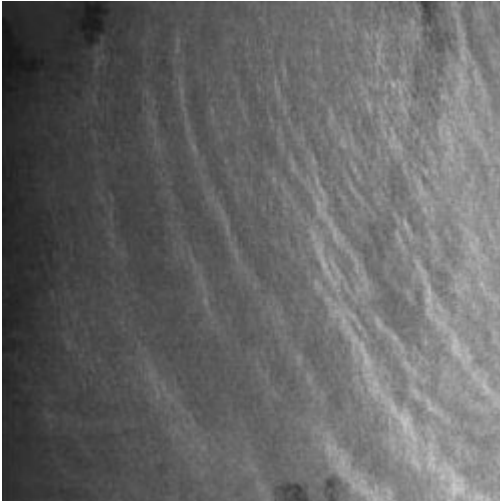
The interaction patterns of the solitary wave packets observed on this image are very interesting. According to soliton theory, the solitons experience a phase shift when interacting with another soliton.

#	Orbit	Frame(s)	Satellite	Date	Time	Location
1	11795	2871-2889	ERS-2	23-Jul-1997	02:19	
2	11838	2925	ERS-2	26-Jul-1997	02:25	

References

- Hsu, M.-K., Liu, A.K. & Liang, N.K., Evolution of nonlinear internal waves northeast of Taiwan, Proc. Eighth Int. Offshore and Polar Eng. Conf. 1998, Montreal, Canada, May 24-29, 18-24 (1998).
- Hsu, M.-K., Liu, A.K. & Liu, C., A study of internal waves in the China Seas and Yellow Sea using SAR, Cont. Shelf Res., 20, 389-410 (2000).
- Liu, A.K., Chang, Y.S., Hsu, M.-K. & Liang, N.K., Evolution of nonlinear internal waves in the East and South China Seas, J. Geophys. Res., 103, 7995-8008 (1998).

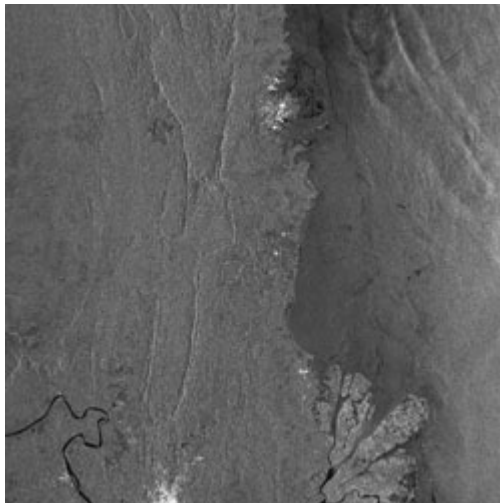
Makassar Strait



Makassar Strait

Latitude: 0° 37' N - Longitude: 118° 13' E

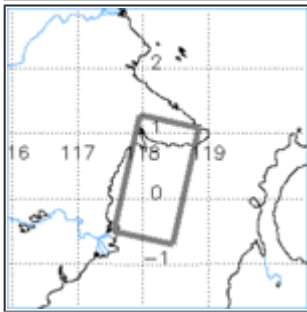
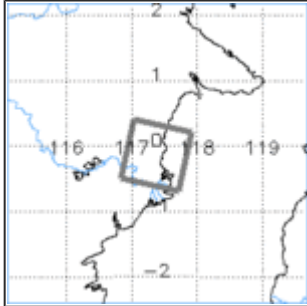
On this ERS-2 SAR image sea surface manifestations of internal solitary waves propagating in southwest direction are visible in the Makassar Strait which separates the island of Borneo and the island of Sulawesi (Celebes).



Makassar Strait

Latitude: 0° 07' N - Longitude: 117° 23' E

Sea surface manifestations of internal waves are visible on this ERS-2 SAR image in the upper right-hand section. The river visible on the lower section is the Kutai river in Borneo.

#	Orbit	Frame(s)	Satellite	Date	Time	Location
1	13527	3591-3609	ERS-2	21-Nov-1997	02:26	
2	24320	3609	ERS-2	15-Dec-1999	02:29	

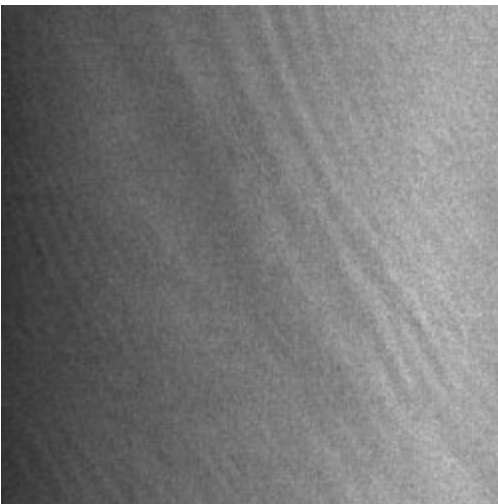
Indian Ocean, Bay of Bengal



Bay of Bengal

Latitude: 18° 38' N - Longitude: 84° 49' E

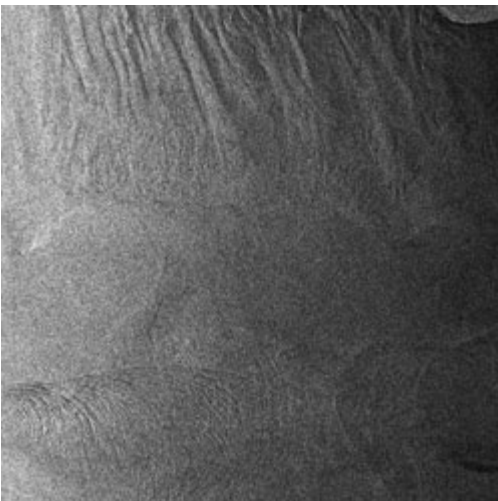
Internal waves in the Bay of Bengal near the shelf break propagating shoreward. The dark streaks in the lower right-hand section of the image are caused by natural surface films.



Indian Ocean

Latitude: 05° 40' N - Longitude: 91° 52' E

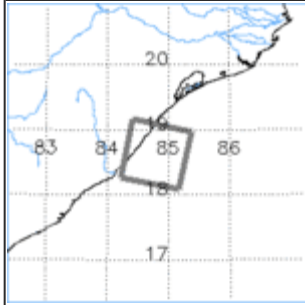
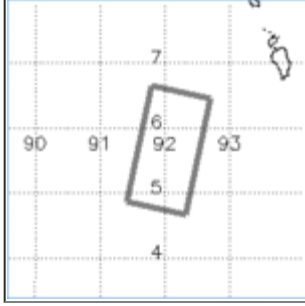
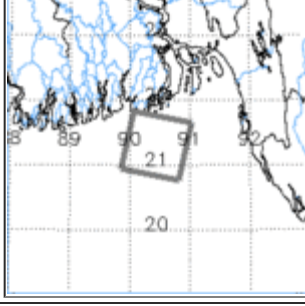
Internal waves in the Indian Ocean southwest of the Nicobar islands propagating westward.



Bay of Bengal

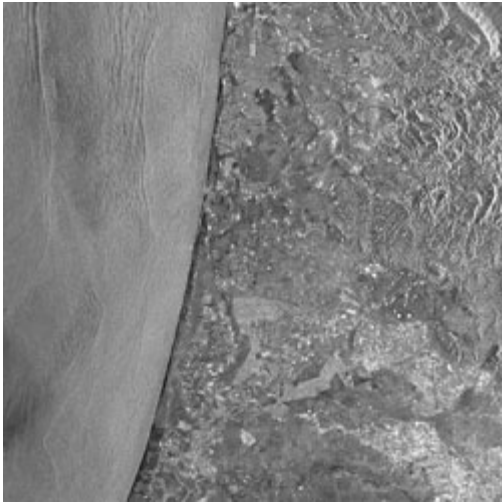
Latitude: 21° 19' N - Longitude: 90° 27' E

Internal waves in the Bay of Bengal south of the Ganges river.

#	Orbit	Frame(s)	Satellite	Date	Time	Location
1	24799	3231	ERS-1	12-Apr-1996	04:50	
2	08833	3483-3501	ERS-2	28-Dec-1996	04:14	
3	13242	3177	ERS-2	01-Nov-1997	04:29	

References

- Zheng, Q., Klemas, V. & Yan, X.-H., Dynamic interpretation of space shuttle photographs: deepwater internal waves in the western equatorial Indian Ocean. *J. Geophys. Res.*, 100, No. C2, 2579-2589 (1995).

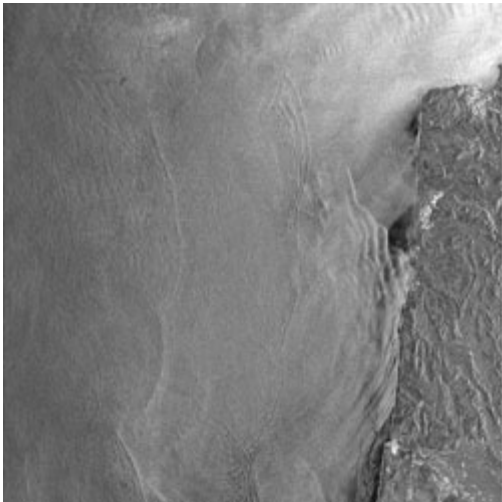


Moroccan West Coast

Latitude: 34° 44' N - Longitude: 06° 15' W

This ERS-1 SAR image shows sea surface manifestations of internal wave packets generated at successive tidal cycles at the shelf break off the Atlantic coast of Morocco.

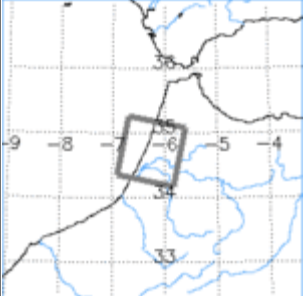
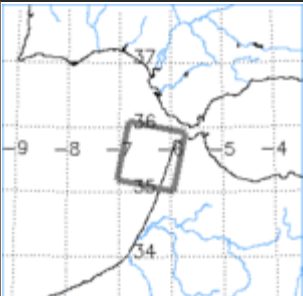
The shape of the patterns is closely related to the bathymetry. Similar internal wave features have been observed at the coast of Portugal.



Moroccan West Coast

Latitude: 35° 34' N - Longitude: 06° 22' W

This ERS-1 SAR image shows similar sea surface manifestations of internal wave packets as the previous image. The wave-like pattern visible in the upper right-hand corner of the image is very likely sea surface manifestations of atmospheric internal waves.

#	Orbit	Frame(s)	Satellite	Date	Time	Location
1	6251	2907	ERS-1	25-Sep-1992	11:05	
2	15618	2889	ERS-1	11-Jul-1994	11:06	

Strait of Gibraltar

Introduction

The Strait of Gibraltar connects the Atlantic Ocean with the Mediterranean Sea. The water body in the Strait of Gibraltar and its approaches consists of a deep layer of salty Mediterranean water (salinity approximately 38 psu) and an upper layer of less salty Atlantic water (salinity approximately 36 psu). The mean flow is composed of two counter-flowing layers: an upper layer of Atlantic water flowing into the Mediterranean Sea and a lower layer of Mediterranean water flowing into the Atlantic Ocean.

The mean depth of the interface between these two layers slopes down from about 80 m at the Mediterranean side of the strait to about 800 m at the Atlantic side. The relative change of density across this interface, which is mainly determined by the salinity difference and is therefore called a halocline, is 0.002. For a comprehensive summary of the oceanography of the Strait of Gibraltar the reader is referred to the paper of Lacombe and Richez (1982).

The Strait of Gibraltar has a complex bottom topography containing several ridges as depicted in the topographic map shown in Fig. 1. The shallowest section in the Strait of Gibraltar is at the Camarinal Sill where the maximum water depth is 290 m. The interaction of the predominantly semidiurnal tidal flow with the sills inside the strait, in particular with the Camarinal Sill, gives rise to periodic deformations of the halocline in the sill regions which then give birth to internal solitary waves.

The ERS SAR images have revealed that the internal solitary waves only propagate eastwards into the Mediterranean Sea and not westwards into the Atlantic. By model calculations Brandt et al. (1996) have shown that this asymmetry of the internal wave field in the Strait of Gibraltar and its adjacent waters results from the east-west asymmetry of the mean flow in the upper and lower layer of the strait.

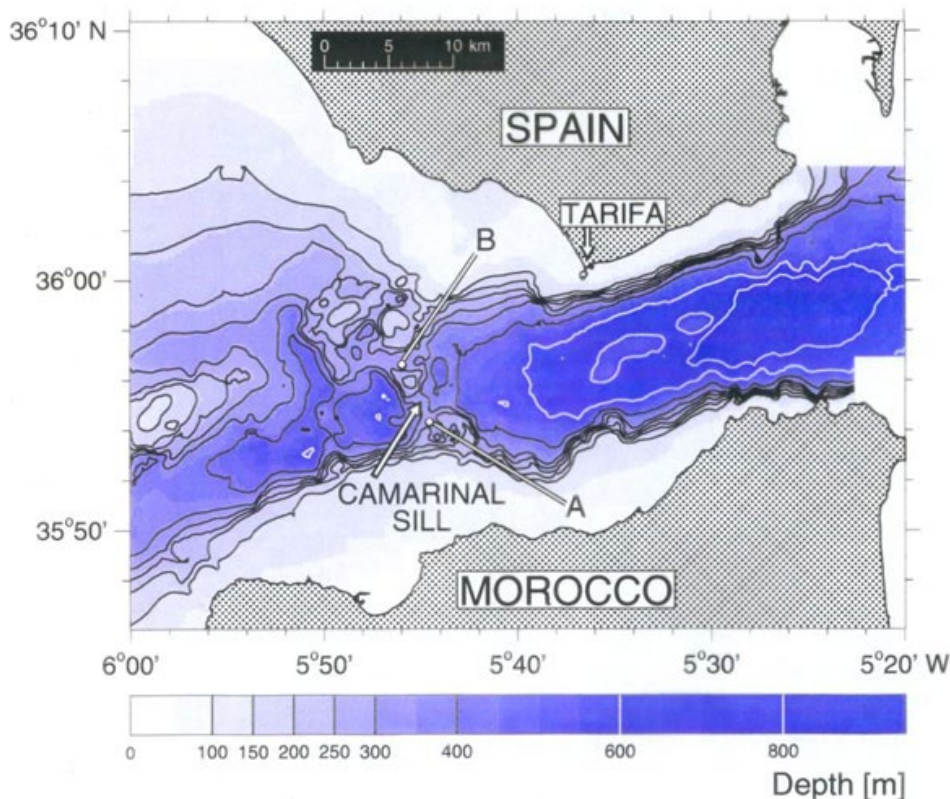
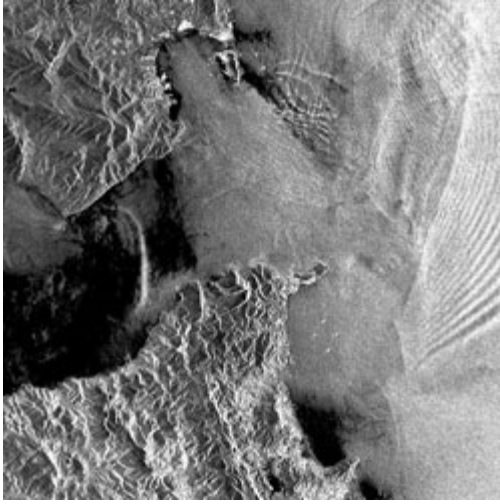


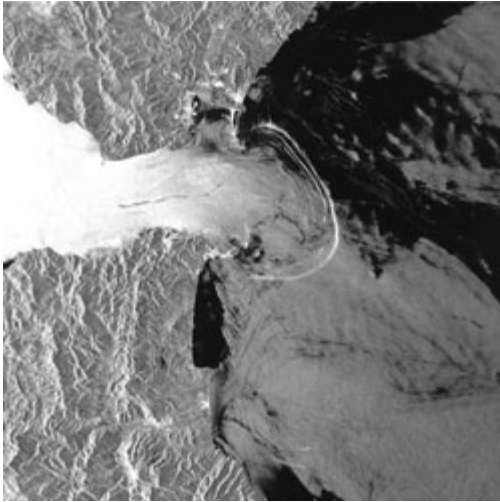
Fig. 1: Bottom topography of the Strait of Gibraltar. The shallowest section is at the Camarinal Sill. (Figure reproduced from Brandt, P., Alpers, W. & Backhaus, J. O., Study of the generation and propagation of internal waves in the Strait of Gibraltar using a numerical model and synthetic aperture radar images of the European ERS 1 satellite, *J. Geophys. Res.*, **101**, 14237-14252 (1996).)



Strait of Gibraltar

Latitude: 36° 08' N - Longitude: 05° 32' W

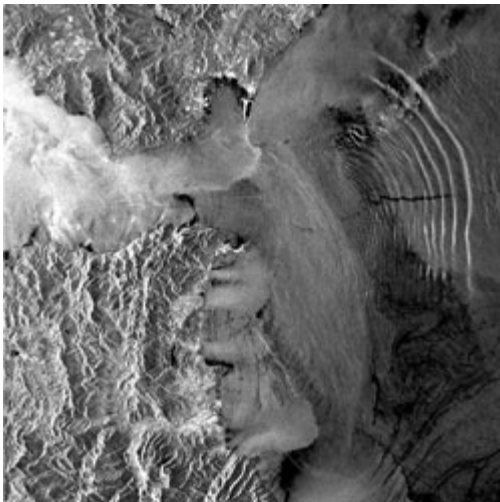
Sea surface manifestations of an internal soliton close to its generation area in the center of the strait (bent bright line in the centre) and an internal wave packet east of the strait which was generated during the previous tidal cycle. The further away the internal wave packet has propagated from its source, the more solitons are in the packet.



Strait of Gibraltar

Latitude: 35° 53' N - Longitude: 05° 13' W

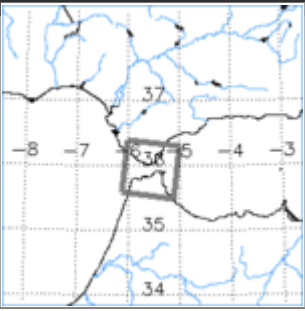
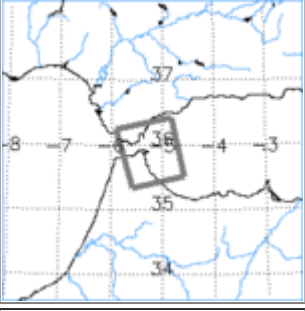
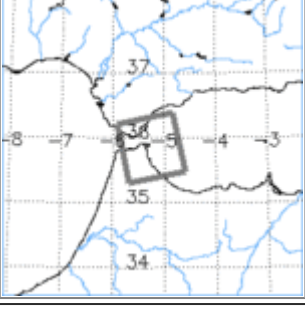
Sea surface manifestations of an internal wave packet which has just passed the eastern exit of the strait. Note that the number of solitons in this wave packet is smaller than the number in the packet visible on the right-hand section of the previous image because its position is closer to the source. Model calculations confirm this observation (see the space-time diagram in the ancillary information).



Strait of Gibraltar

Latitude: 35° 52' N - Longitude: 05° 14' W

Sea surface manifestations of an internal wave packet that has propagated further east than the one visible on the previous ERS SAR image. This results in a larger number of solitons in the packet (more than 10). The dark line intersecting the internal wave packet originates from a ship which has discharged oil en route.

#	Orbit	Frame(s)	Satellite	Date	Time	Location
1	13151	2871-2889	ERS-1	20-Jan-1994	11:03	
2	21532	0711	ERS-1	27-Aug-1995	22:39	
3	7661	0711	ERS-1	01-Jan-1993	22:39	

Strait of Messina

Introduction

The Strait of Messina is a narrow channel in the Mediterranean Sea which separates the Italian peninsula from the island of Sicily and connects the Tyrrhenian Sea north of the strait with the Ionian Sea south of it. A topographic map of the Strait of Messina is shown in Fig. 1. In the shallowest section of the strait, called the sill region, the maximum water depth is 90 m. While in the southern part of the strait the bottom slopes down very steeply to a depth of more than 800 m approximately 15 km south of the sill, the northern region has a more gentle slope. Here the 400 m isobath is located approximately 15 km north of the sill.

Throughout the year, two different water masses are encountered in the Strait of Messina: the Tyrrhenian Surface Water and the colder and saltier Levantine Intermediate Water. In the vicinity of the strait these water masses are separated at a depth of approximately 150 m (Vercelli, 1925). During most of the year, a seasonal thermocline is also present in the strait which overlies this weak stratification.

Although tidal displacements are very small in the Mediterranean Sea (of order of 10 cm), large gradients of tidal displacements are encountered in the Strait of Messina, because the predominantly semidiurnal tides north and south of the strait are approximately in phase opposition. Due to this phase opposition and due to topographic constrictions, the current velocities can attain values as high as 3.0 m/s in the sill region (Vercelli, 1925; Defant, 1961).

These hydrological peculiarities of the Strait of Messina may explain why this site has attracted the attention of many ancient writers and philosophers. Homer (800 B.C.) makes two monsters, Scylla and Charybdis, responsible for the violent currents in the strait (Homer, *Odyssey*, 12th song, line 80-114). Aristotle (384-322 B.C.) argues that hollows in the sea floor and the interaction of two opposing wind-generated currents could produce such intensive currents (Aristotle, *Problema Physica*, chap. 23) and in the poetry of ancient times, allegories alluding to the danger of sailing in the Strait of Messina can often be found ('*Incidis in Scillam cupiens vitare Charybdim*', Ovid, *Metamorphosis*).

The fact that (1) strong tidally induced currents are encountered in the strait, (2) the water body is stratified and (3) there is a shallow sill in the center of the strait which disturbs the tidal flow, suggests that internal waves should be generated in the Strait of Messina. But it was not before 1978 that internal waves were detected in this strait.

The first hint came from a synthetic aperture radar image which was acquired by the American Seasat satellite on September 15, 1978. The three rings visible on the Seasat SAR image of the Tyrrhenian Sea north of the strait were interpreted as sea surface manifestations of a train of internal solitary waves propagating northwards (Alpers and Salusti, 1983).

In the following years internal waves propagating north- as well as southwards have been detected during several oceanographic campaigns by in-situ measurements (Alpers and Salusti, 1983; Griffa et al., 1986; Di Sarra et al., 1987; Sapia and Salusti, 1987; Nicolo and Salusti, 1991). A review of oceanographic investigations carried out in the Strait of Messina up to 1990 can be found in Bignami and Salusti (1990).

Bathymetry of the Strait of Messina

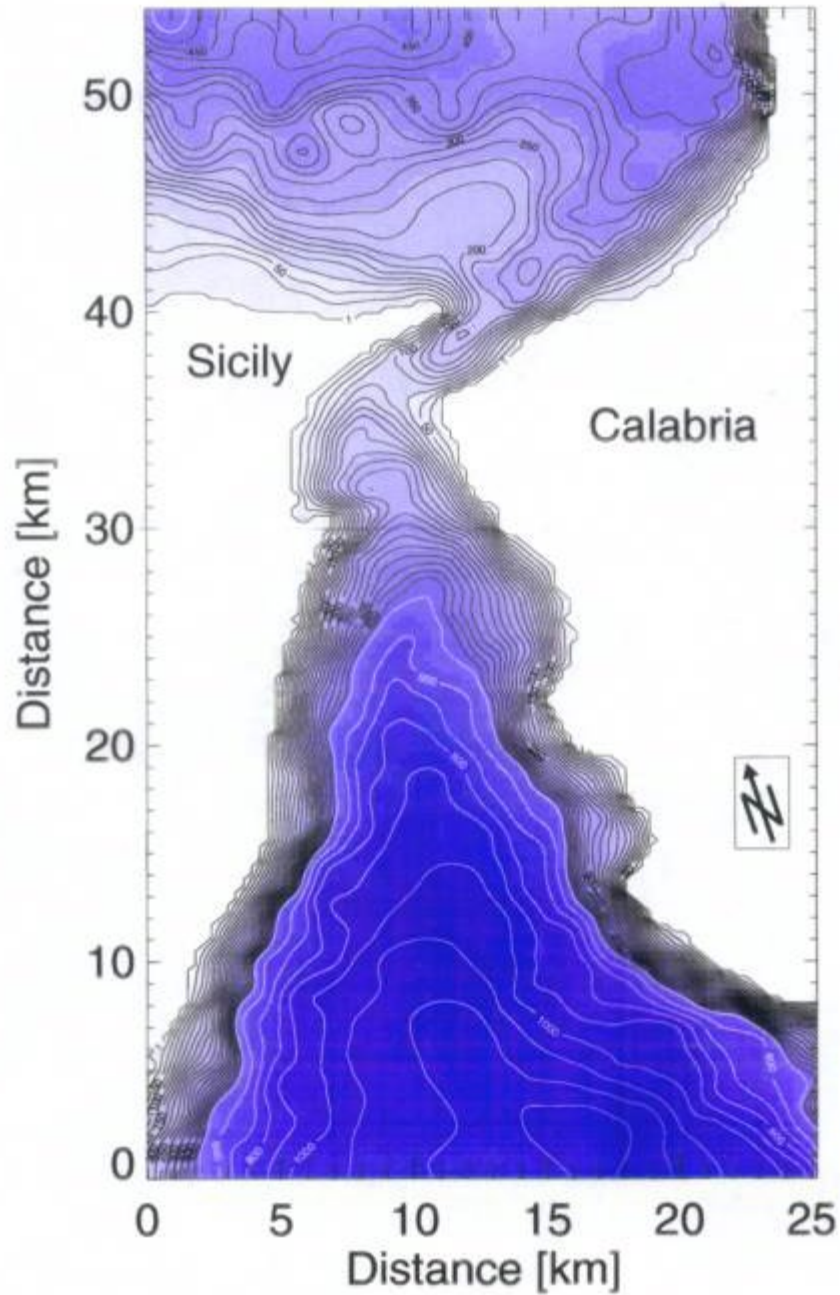
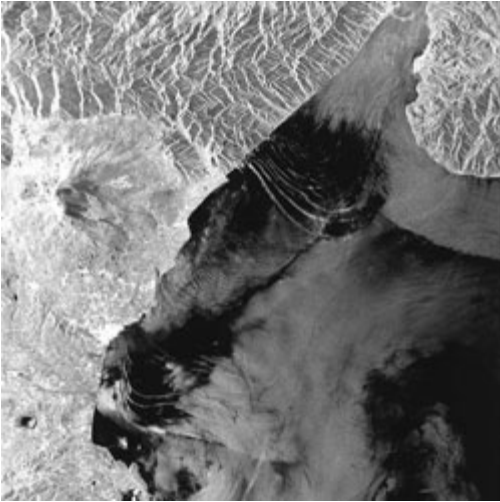


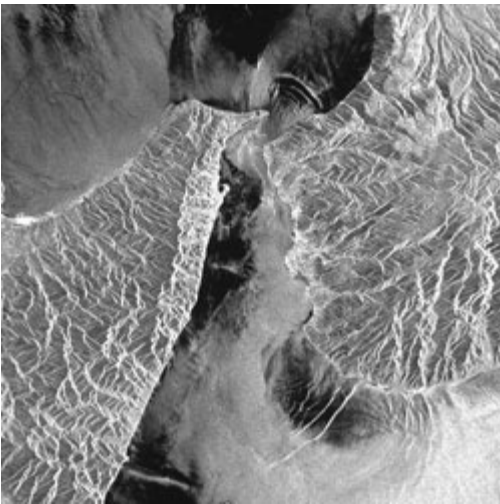
Fig. 1: Bottom topography of the Strait of Messina. The numbers on the depth lines (isobaths) denote depth in meters.



Strait of Messina

Latitude: 37° 38' N - Longitude: 15° 22' E

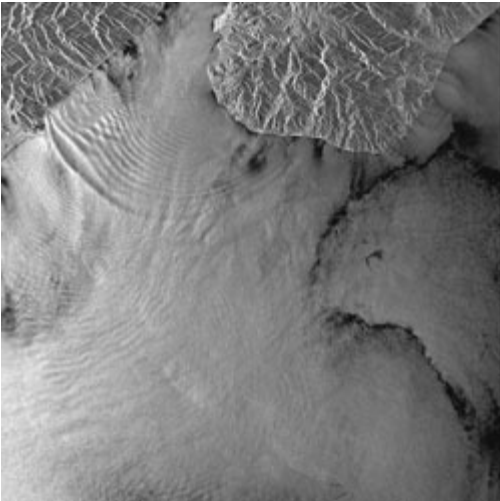
On this ERS-1 SAR image three packets of southward propagating internal solitary waves generated in the Strait of Messina at three successive semi-diurnal tidal cycles are visible. The latest generated packet (closest to the Strait of Messina) consists only of one soliton and the two other packets consist of several solitons. According to soliton theory, the further away the packet has propagated from its source, the more solitons should be in the packet.



Strait of Messina

Latitude: 38° 16' N - Longitude: 15° 29' E

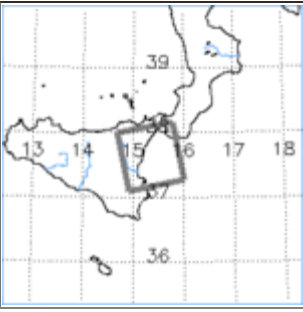
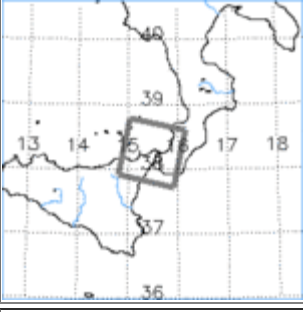
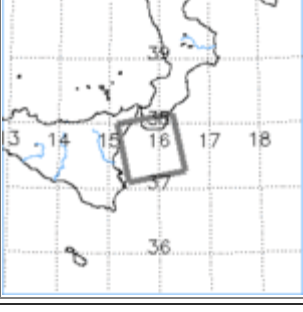
A northward propagating internal solitary wave packet is visible at the northern exit of the Strait of Messina. Northward propagating internal waves are less frequently observed than southward propagating ones. They are only generated when there is a strong seasonal thermocline present, which is usually the case in summer and early autumn.



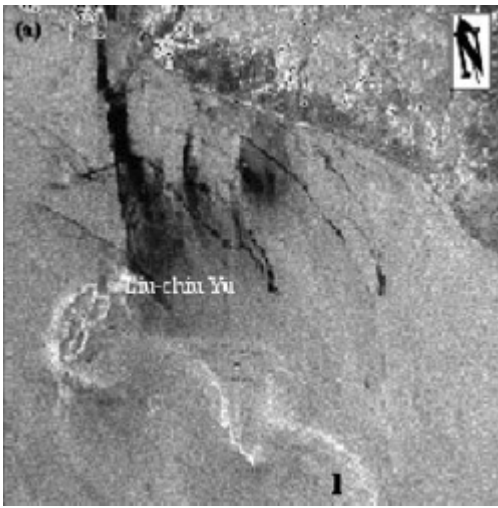
Strait of Messina

Latitude: 37° 39' N - Longitude: 15° 51' E

Visible on this image is a very regular packet of southward propagating internal solitary waves at the southern exit of the Strait of Messina. The dark curved line in the right-hand section of the image seems to be a frontal line in which (natural) surface slicks have accumulated.

#	Orbit	Frame(s)	Satellite	Date	Time	Location
1	16672	0747	ERS-1	22-Sep-1994	21:15	
2	10387	2835	ERS-1	11-Jul-1993	09:41	
3	22390	0747	ERS-1	26-Oct-1995	21:13	

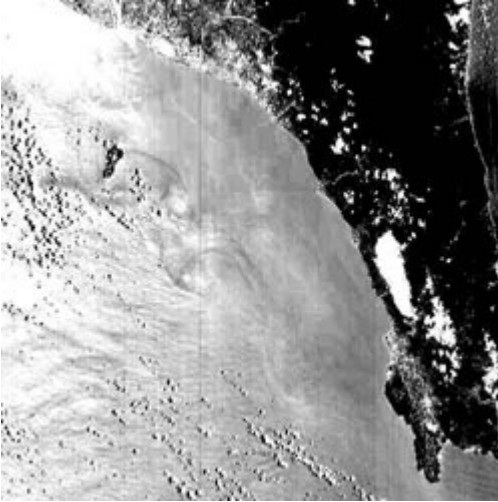
Oceanic Wakes



Taiwan

Latitude: 22° 20' N - Longitude: 120° 24' E

On this ERS-1 SAR image (image size: 28km x 34km) sea surface manifestations of vortex-like features are visible in the wake of the island Liuchiu Yu.

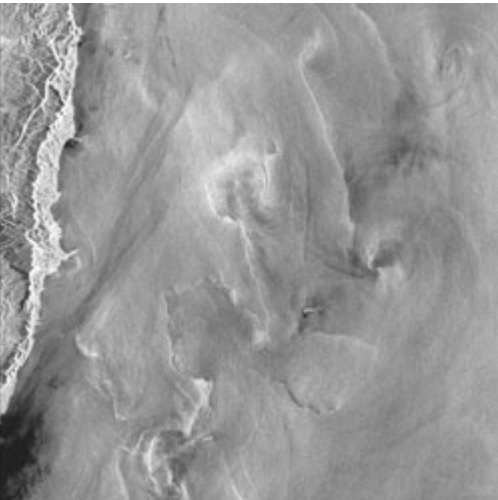


Taiwan

Latitude: 22° 15' N - Longitude: 120° 33' E

On this SPOT-2 image also vortex-like features are visible in the area where similar features were visible on the previous ERS-1 SAR image.

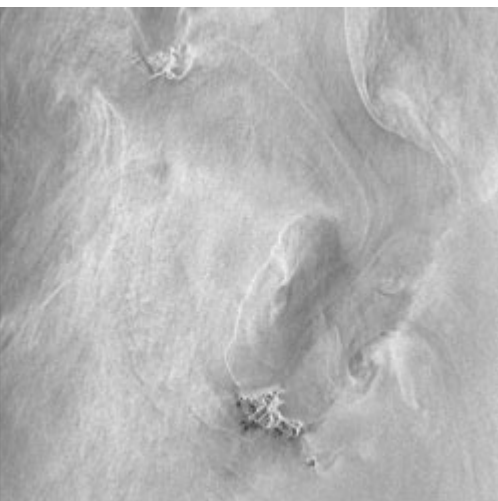
© CNES 2000 - [Spot Image](#) distribution



East of Taiwan

Latitude: 23° 07' S - Longitude: 121° 46' E

A wake pattern is visible in the lower left-hand section of the ERS-2 SAR image behind the island of Lü Tao. It seems to be generated by the interaction of the northward flowing Kuroshio Current with the island. But also other frontal features are visible on this image which are difficult to explain.



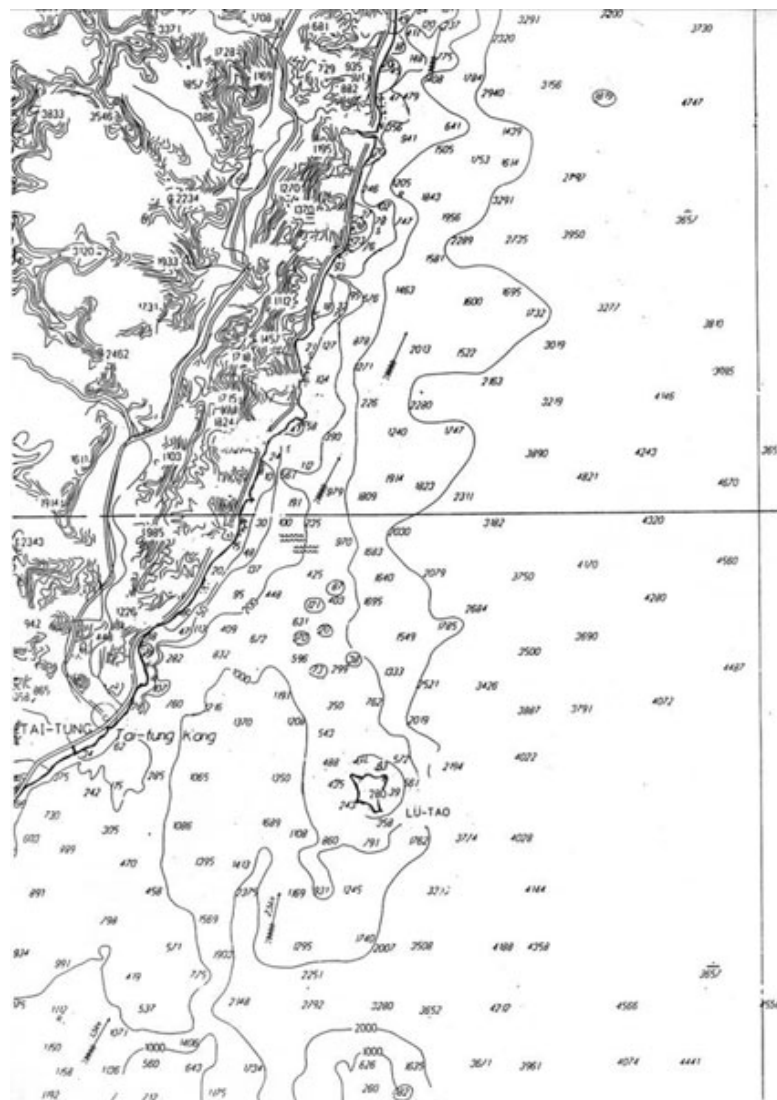
East of Taiwan

Latitude: 22° 40' N - Longitude: 121° 31' E

This is another ERS-2 SAR image showing a wake pattern behind the island Lü Tao (in the centre of the image), which has a different shape than the one visible on the previous ERS-2 SAR image. Also behind the larger island Lan Yü (in the lower section of the image) a wake pattern is visible.

#	Orbit	Frame(s)	Satellite	Date	Time	Location
1	12401	3159	ERS-1	29-Nov-1995	02:32	
2	Path: 299	305P1-306P1	SPOT 2	05-Jun-1996	02:55	
3	18079	3141	ERS-2	05-Oct-1998	02:26	
4	20584	3141-3159	ERS-2	29-Mar-1999	02:26	

Ancillary information to these images



Bathymetric map of the sea area east of Taiwan together with topographic map of the eastern part of Taiwan. The numbers denote the depth in metres.

References

- Arestegui, J., Tett, P. et al. The influence of island-generated eddies on chlorophyll distribution: study of mesoscale variation around Gran Canaria, *Deep-Sea Res.*, 44, 71-96 (1997).
- Davies, P.A. & Mofor, L.A., Observations of flow separation by an isolated island, *Int. J. Remote Sens.*, 11, 767-782 (1990).
- Ferrier, G., Davies, P.A. & Anderson, J.M., Remote sensing observations of a vortex street downstream of an obstacle in an estuarine flow, *Int. J. Remote Sens.*, 17, 1-8 (1996).
- Mitnik, L.M., Hsu, M.-K. & Liu, C.-T., ERS-1 SAR observations of dynamic features in the southern East-China Sea, *La mer*, 34, 215-225 (1996).
- Mitnik, L.M., Atmospheric and oceanic vortex streets: Observations by satellite radars, *J. Atm. Marine Techn.*, 2000, in press (Proc. PORSEC'98).
- Pattiaratchi, C., James, A. & Collins, M., Island wakes and headland eddies: a comparison between remotely sensed data and laboratory experiments, *J. Geophys. Res.*, 92, 783-794 (1987).
- Wolanski, E., Imberger, J. & Heron, M.L., Island wakes in shallow coastal waters, *J. Geophys. Res.*, 89, 10553-10569 (1984).

Oil Pollution

Mineral oil spilled by ships or offshore oil platforms or due to natural oil seepage from subsea deposits becomes visible on SAR images because it damps short surface waves and thus reduces the backscattered radar power over these areas. Such slicks therefore show up as dark areas on SAR images. However, dark patches on SAR images of the ocean surface do not always originate from mineral oil films.

They can originate, e.g., (1) from natural surface films which are produced by plankton or fish and which also strongly damp the surface waves, (2) from low winds which are often encountered in the lee of islands or coastal mountains, and (3) from cold water, as encountered, e.g., in upwelling areas which changes the stability of the air-sea interface and thus the ability of the wind to generate small-scale ocean waves.

But often mineral oil spills released from ships can be identified by their location and by their shape. When released from traveling ships, they form elongated trails.

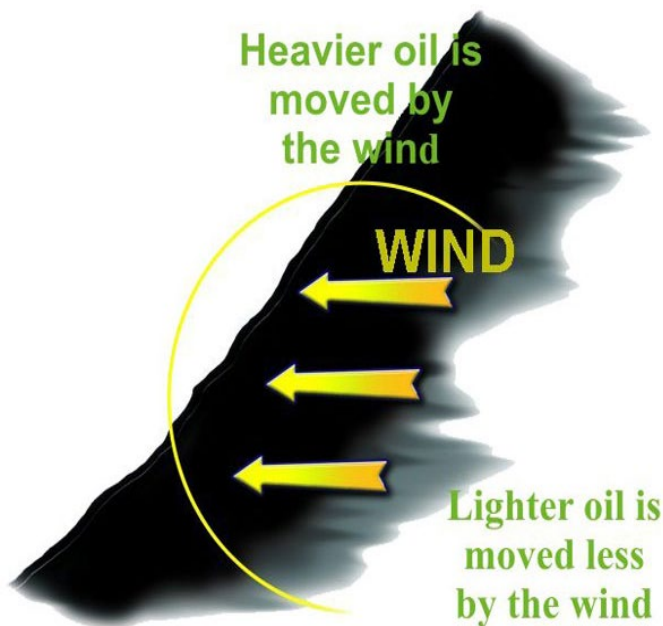


Fig. 1: Ocean currents and winds sometimes deform the shape of the oil trail. The wind often gives rise to a "feathered" structure of the trail. The "feathered" side is always located upwind as depicted in the figure.

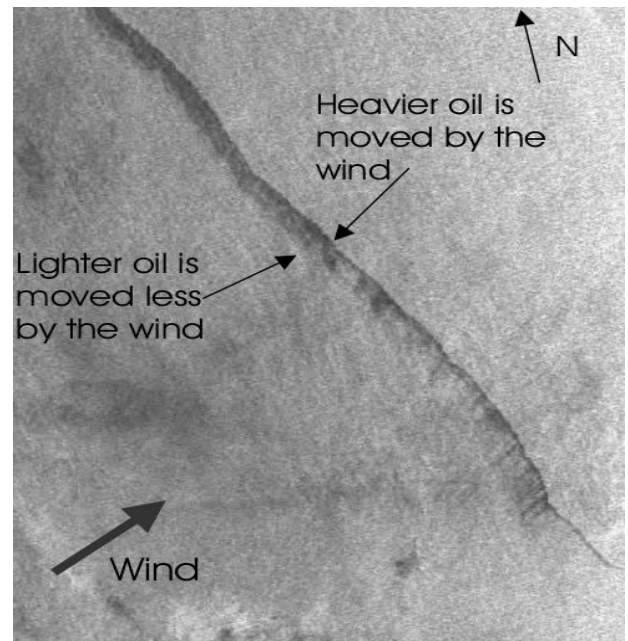
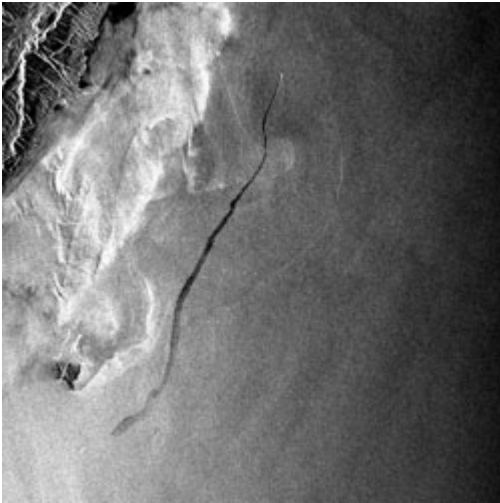


Fig. 2: Section of an ERS-2 SAR image from the Indian Ocean (6 April 1999, 4:58 UTC, orbit: 20700, frame: 3393, frame center: 10° 36'N, 81° 49'E) showing a "feathered" structure of an oil trail. By the action of the wind the heavy components of the mineral oil film accumulate at the downwind side (dark line in the image). The "feathered" side is always located upwind.

Kuroshio East of Japan



Taiwan

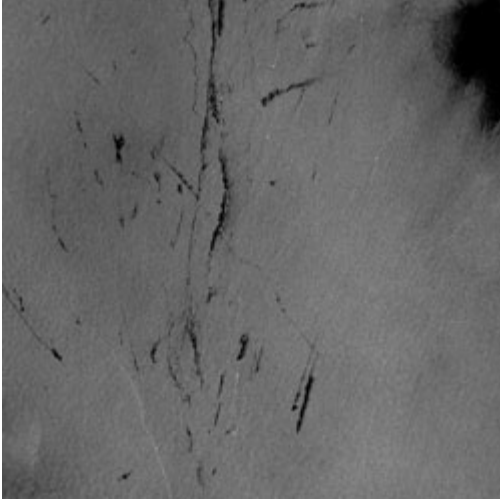
Latitude: 23° 01' N - Longitude: 121° 41' E

A ship travelling northward (bright spot at the front of the black line) discharging oil. The oil disperses with time causing the oil trail to widen. This oil trail is more than 80 km long.

The bright area between the east coast of Taiwan and the oil trail is the Kuroshio current whose water temperature is higher than the temperature of the surrounding waters. Here the air-sea interface is unstable causing a higher wind stress and thus a larger NRCS.

Orbit	Frame(s)	Satellite	Date	Time	Location
14874	2364	ERS-1	20-May-1994	14:20	A map of Taiwan showing its coastline and major cities. A black rectangular box is drawn on the map, centered over the east coast of Taiwan, indicating the location of the satellite frame. The map includes latitude and longitude markings: 120, 121, 123 for longitude and 21, 22, 24 for latitude.

South China Sea



South China Sea

Latitude: 02° 32' N - Longitude: 105° 02' E

Sea area in the South China Sea crossed by the main shipping lane between Singapore and Far East Asian ports.

This sea area northeast of Singapore seems to be a preferred area for discharging oil from ships.

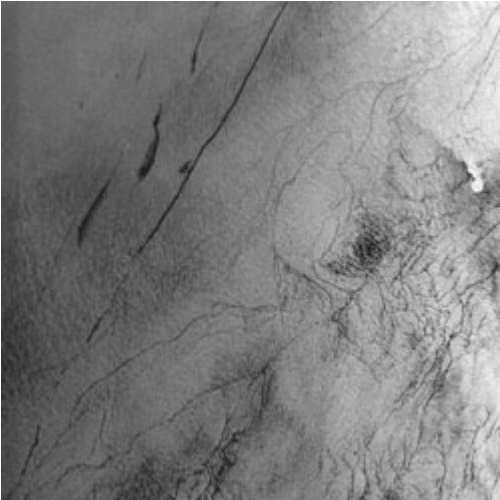
See also the attached map of the spatial distribution of oil slicks in the southeast Asian waters as inferred from ERS SAR images.



South China Sea

Latitude: 04° 20' N - Longitude: 103° 59' E

A sea area off the east coast of Malaysia (near Kuantan) which is heavily polluted by oil discharged from ships.

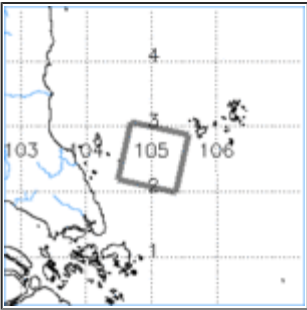
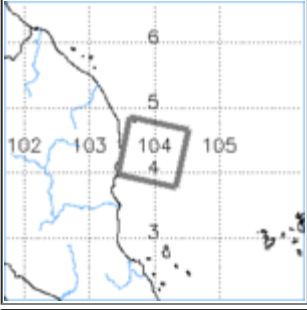
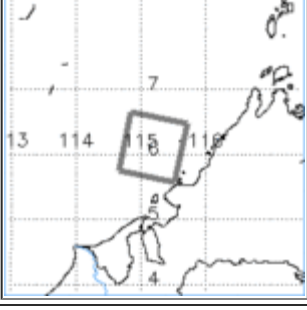


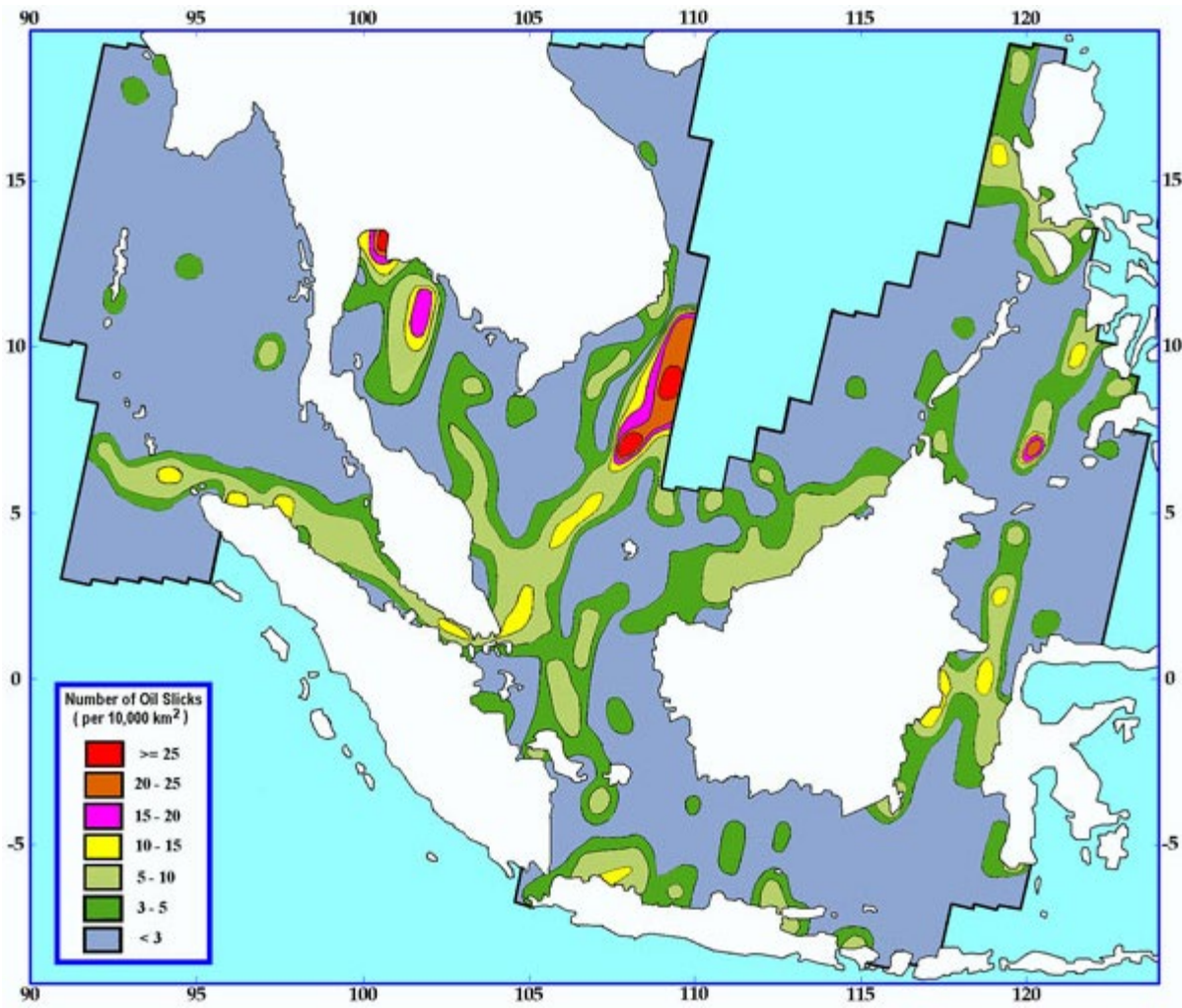
South China Sea

Latitude: 06° 07' N - Longitude: 115° 12' E

Oil pollution in the South China Sea off the west coast of Sabah (Borneo). The dark streaks visible in the left-hand section of the image result from oil discharged from ships.

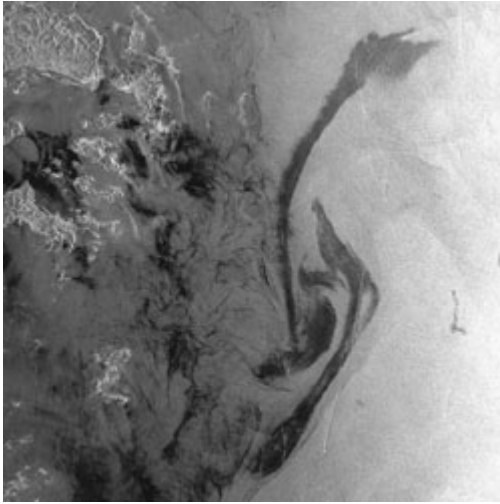
In one case the ship (white spot) is visible at the front of the oil trail. It could be that the dark streaky features visible in the right-hand section of the image originate from oil seeps.

#	Orbit	Frame(s)	Satellite	Date	Time	Location
1	24841	3555	ERS-1	15-Apr-1996	03:20	
2	10221	3519	ERS-2	04-Apr-1997	03:25	
3	11652	3483	ERS-2	13-Jul-1997	02:42	



Spatial distribution map of oil pollution in Southeast Asian waters during the period of September 1995 to September 1998. Figure provided by CRISP.

East China Sea



East China Sea

Latitude: 29° 22' N - Longitude: 122° 31' E

This ERS-2 SAR image (imaged area: 300 km x 100 km) was acquired along the Chinese coast south of Shanghai (Chenkiang province).

The elongated dark patches and the dark streaks visible in the central and right-hand section of this SAR strip are caused by oil discharged from ships.

The dark areas near the coast could be partly caused by pollutants of coastal origin and/or by natural surface films.

Orbit	Frame(s)	Satellite	Date	Time	Location
11838	2997-3015-3033	ERS-2	26-Jul-1997	02:27	A map of the East China Sea region, showing the coastline of China and the surrounding waters. A rectangular box highlights the area covered by the SAR image, which is located south of Shanghai. The map includes latitude and longitude markings, with latitude ranging from 28 to 31 and longitude from 120 to 125.

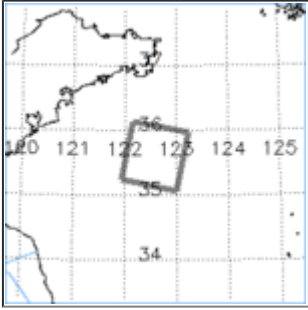
Yellow Sea

Yellow Sea

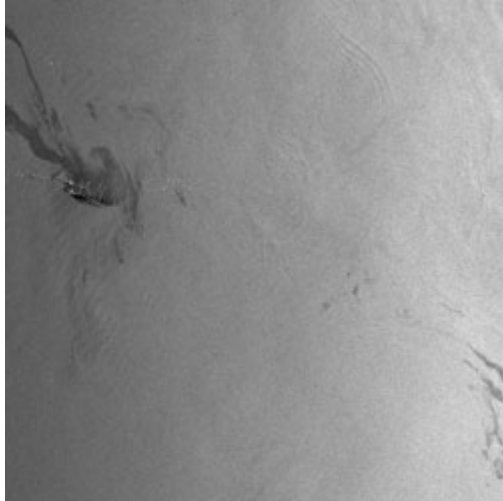
Latitude: 35° 37' N - Longitude: 122° 35' E

Oil slicks in the Yellow Sea of unknown origin. Partly they may originate from natural oil seeps or oil platforms.



Orbit	Frame(s)	Satellite	Date	Time	Location
20532	2889	ERS-1	19-Jun-1995	02:31	

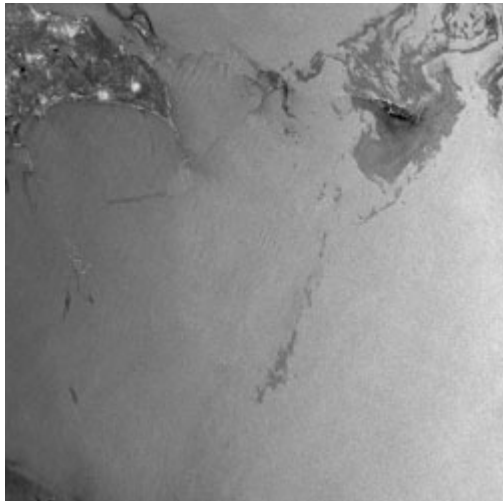
Caspian Sea



Caspian Sea

Latitude: 40° 04' N - Longitude: 51° 11' E

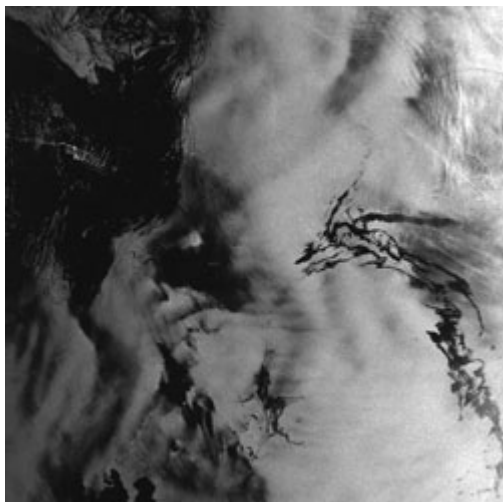
A cluster of oil rigs (bright dots) in the Caspian Sea surrounded by oil slicks are visible in the right-hand side of the image. The imaged area is located east of Baku.



Caspian Sea

Latitude: 40° 04' N - Longitude: 50° 27' E

The same cluster of oil rigs in the Caspian Sea visible on the previous image. Again it is surrounded by oil slicks.

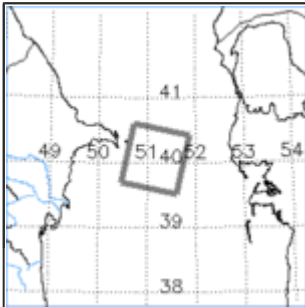
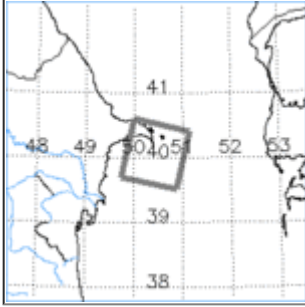
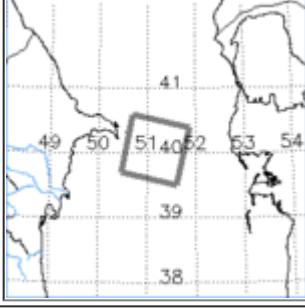


Caspian Sea

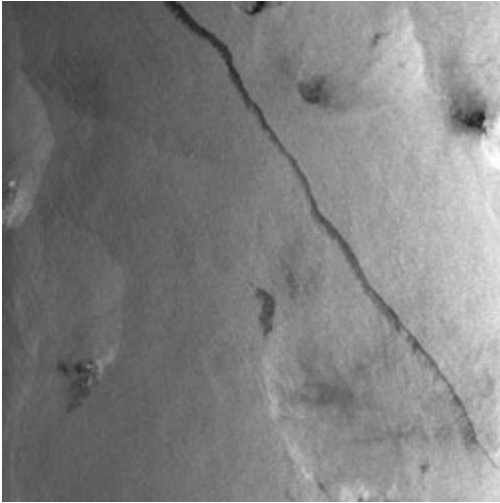
Latitude: 40° 04' N - Longitude: 51° 11' E

Sea area east of Baku with the same cluster of oil rigs which are visible on the two previous images. In the western section the wind speed is very likely below threshold for ripple generation such that the water surface in the oil-covered as well as in the oil-free areas is smooth.

Therefore the oil patches around the oil rigs become undetectable in the SAR image. In the eastern section an oil slick having a very ragged shape is visible.

#	Orbit	Frame(s)	Satellite	Date	Time	Location
1	05786	2799	ERS-2	29-May-1996	07:20	
2	25230	2799	ERS-1	12-May-1996	07:23	
3	25459	2799	ERS-1	28-May-1996	07:20	

Indian Ocean



Indian Ocean

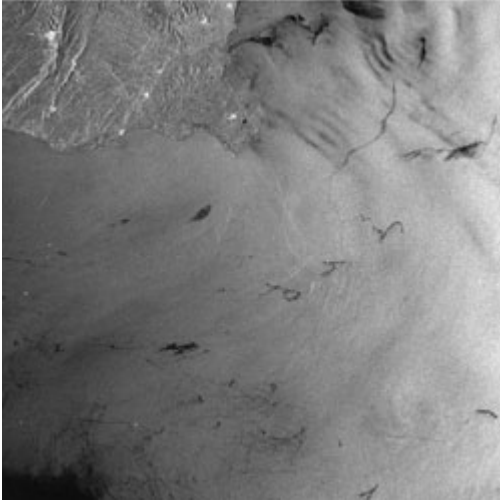
Latitude: 10° 36' N - Longitude: 81° 40' E

Oil trail in the waters south-east of Chennai (Madras), India. Very likely the oil was released from a ship several hours before this image was taken.

The trail has a "feathered" structure caused by the wind blowing from southwest. The small dark patches surrounded by large, slightly bright patches are radar signatures of tropical rain cells.

Orbit	Frame(s)	Satellite	Date	Time	Location
20700	3393	ERS-2	06-Apr-1999	04:58	A map of the Indian Ocean region showing the coastline of India. A grid is overlaid on the map with latitude and longitude coordinates. A small rectangular box highlights the location of the oil trail, centered around 10° 36' N and 81° 40' E. The grid lines are labeled with numbers: 12, 11, 10, 9 for latitude and 80, 81, 82, 83 for longitude.

Mediterranean Sea



Strait of Sicily

Latitude: 36° 28' N - Longitude: 15° 04' E

Sea area in the Mediterranean Sea off the south-east coast of Sicily (Italy). Some of the dark patches visible on this image are very likely due to oil slicks produced by natural oil seeps which are known to exist in this sea area.

The oil seeps at the ocean bottom are stationary, but the position of the oil patches on the sea surface varies according to the oceanic and meteorological conditions. Thus by taking repeatedly SAR images over the same ocean area and taking into account the advection of the oil slicks by ocean currents and by wind drift, the position of oil seeps can be determined.

This method is widely used by oil companies in off-shore oil prospecting.



North of Sicily

Latitude: 38° 32' N - Longitude: 14° 53' E

On this image two straight black lines originating from oil released from traveling ships are visible. Extrapolating along these black lines, leads to two bright spots being hit. Presumably they represent the ships that have released the oil.

#	Orbit	Frame(s)	Satellite	Date	Time	Location
1	14957	2871	ERS-1	26-May-1994	09:41	
2	11797	0765	ERS-1	17-Oct-1993	21:16	

References

- Alpers, W. & Huhnerfuss, H., The damping of ocean waves by surface films: A new look at an old problem. *J. Geophys. Res.*, **94**, 6251-6265 (1989).
- Clemente-Colon, P., Pitchel, W. & Yan, X.-H., Evolution of oil slick patterns as observed by SAR off the coast of Wales. *Proc. 3rd ERS Symp.*, Florence, Italy, 17-21 March 1997, ESA publication SP-414, 565-568 (1997).
- Ermakov, S.A., Salashin, S.G. & Panchenko, A.R., Film slicks on the sea surface and some mechanisms of their formation. *Dynamics of Atm. and Oceans*, **16**, 279-304 (1992).
- Espedal, H.A., Johannessen, O.M. & Knulst, J., Satellite detection of natural films on the ocean surface. *Geophys. Res. Lett.*, **23**, 3151-3154 (1996).
- Gade, M. & Alpers, W., Using ERS-2 SAR images for routine observation of marine pollution in European waters, *The Science of the Total Environment*, **237/238**, 441-448 (1999).
- Gade, M., Alpers, W., Huhnerfuss, H., Masuko, H. & Kobayashi, T., Imaging of biogenic and antropogenic ocean surface films by the multifrequency/multipolarization SIR-C/X-SAR, *J. Geophys. Res.*, **103**, 18851-18866.
- Gade, M., Alpers, W., Huhnerfuss, H., Wismann, V. & Lange, Ph., On the reduction of the radar backscatter by oceanic surface films: Helicopter measurements and their theoretical interpretation, *Remote Sensing of Environment*, **66**, 52-70 (1998).
- Lu, J., Kwoh, L.K., Lim, H., Liew, S.C. & Bao, M., Mapping oil pollution from space, *Backscatter*, 23-26, (February 2000)
- O Chadlick, A.R., Cho, P. & Evans-Morgis, J., Synthetic aperture radar observations of current colocated with slicks. *J. Geophys. Res.*, **97**, 5325-5333 (1992).
- Peltzer, R.D., Griffin, O.M., Barger, W.R. & Kaiser, J.A.C., High-resolution measurements of surface-active film redistribution in ship wakes. *J. Geophys. Res.*, **97**, 5231-5252 (1992).
- Romano, J.-C. Sea-surface slick occurrence in the open sea (Mediterranean, Red Sea, Indian Ocean) in relation to wind speed. *Deep-Sea Res.*, Part I, **43**, 411-423 (1996).
- Trivero, P., Fiscella, B., Gomez, F. & Pavese, P., SAR detection and characterization of sea surface slicks. *Int. J. Remote Sens.*, **19**, 543-548 (1998).
- Yan, X.-H. & Breaker, L.C., Surface circulation estimation using image processing and computer vision methods applied to sequential satellite imagery. *Photogramm. Eng. Remote Sens.*, **59**, 407-413 (1993).

Ship Wakes

Introduction

Ships often become visible on SAR images because the large backscattered radar power from the metal structure of the ship gives rise to a bright spot in the radar image. Travelling ships also become visible on SAR images by their wake. Often the wake of a ship can be delineated on a SAR image, but not the ship itself.

The wake of a ship consists of the turbulent or vortex wake and the Kelvin wake. The turbulent wake trails the ship in the direction of the ship's heading while the Kelvin wake, which consists of two arms (Kelvin arms), trails the ship in the form of a V-shaped pattern. On ERS SAR images, most often the turbulent wake is visible but not the Kelvin wake.

At distances larger than a few shiplengths, the turbulent wake is usually imaged as a black line. This is because the turbulence (generated by the propeller of the ship) damps the surface waves and thus causes a reduction of the backscattered radar power. However, sometimes the turbulent wake is imaged as a bright line.

This can occur when the sea surface is covered by (natural) surface slicks. In this case the two counter rotating vortices within the turbulent wake (see Fig. 1) push aside the slick material. In the slick-free area and sufficiently far from the ship where the turbulence has weakened, the wind can generate short surface waves.

The Kelvin wake is formed by cusp waves which typically have wavelengths between 10 and 40 m and amplitudes between 0.2 and 1.0 m (see Fig. 2). Thus they cannot be resolved by the ERS SAR. The visibility of the Kelvin arms on SAR images depends strongly on the radar look direction (azimuth angle) relative to the ship's heading as discussed in detail in the paper by Hennings et al. (1999).

The radar signatures of Kelvin arms are strongest when the look direction of the radar is normal to the direction of the crests of the cusp waves, and weakest when it is parallel to this direction. This is the reason why on ERS SAR images often only one Kelvin arm is visible while the other is only faintly or not at all visible.

Furthermore, the radar signature (i.e., the change of the NRCS relative to the background) of Kelvin arms depends strongly on wind speed: The larger the wind speed, the smaller is the radar signature. But there are also other factors contributing to the magnitude of the radar signature of Kelvin arms: the size, form and speed of the ship, the radar frequency and polarization, and the incidence angle.

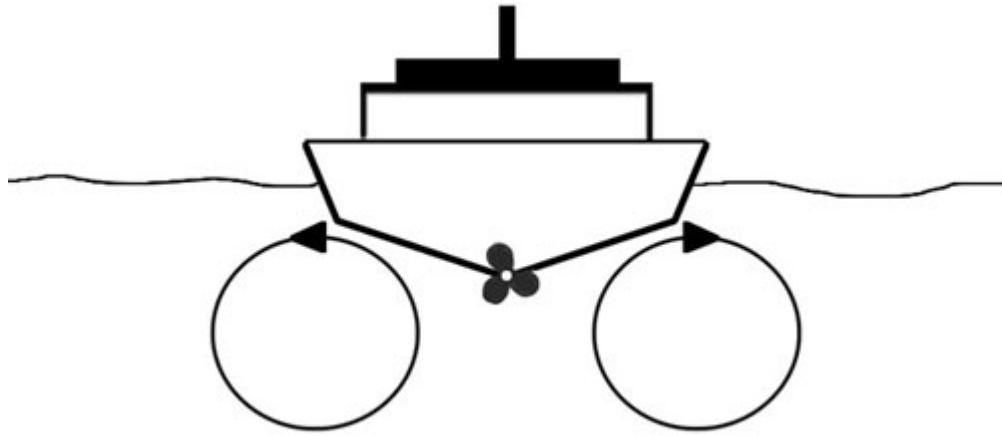


Fig. 1: Schematic drawing of two counter-rotating vortices generated by the propeller of a ship. They persist in the turbulent wake and give rise to convergent flow regimes at both sides of the wake. This is the reason why the radar signature of a ship's turbulent often comprises of two lines at the rim.

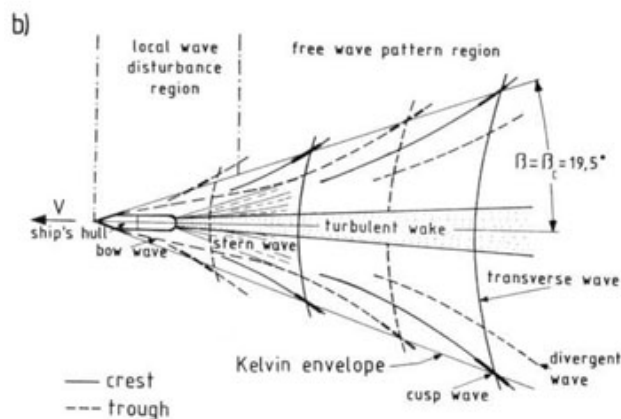
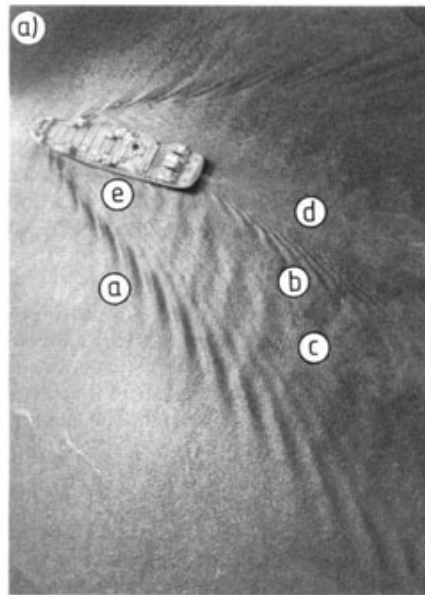
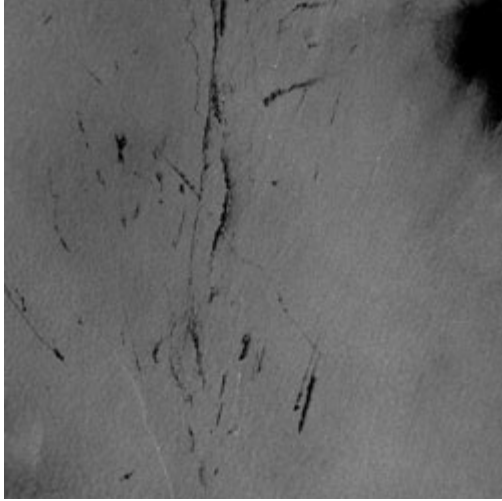


Fig. 2: (a) Aerial photograph showing the components of a ship wake pattern: a, bow wave; b, stern wave; c, transverse wave; d, turbulent wake, and e, turbulence region adjacent to the ship's hull. This photograph was taken by a camera with a fisheye lens aboard a low-flying aircraft (courtesy of R. Doerffer, GKSS). (b) Sketch of the different components of the ship wake pattern shown in (a).

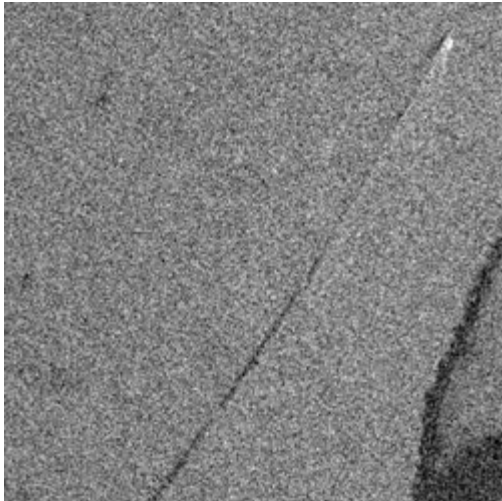
South China Sea



South China Sea

Latitude: 2° 32' N - Longitude: 105° 02' E

ERS-1 SAR image of a sea area in the South China Sea crossed by the main shipping lane between the Strait of Malacca (Singapore) with the Far East sea ports. A large number of ships are visible as bright spots followed by wakes. Note also the numerous dark patches which result from oil discharged from ships.

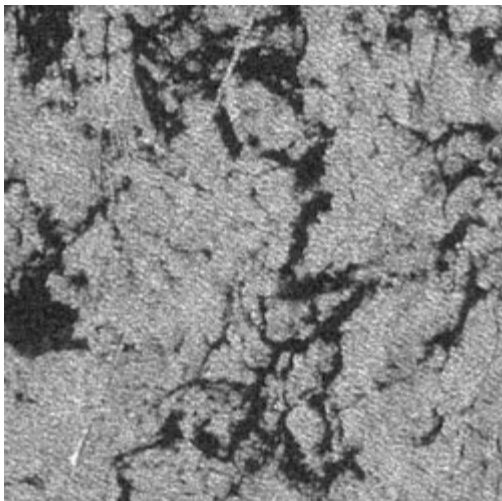


South China Sea

Latitude: 6° 07' N - Longitude: 107° 15' E

The sea area shown in this ERS-2 SAR image has an extent of 14.5 km x 9.7 km and lies in the frame shown above. In the upper right-hand corner a ship followed by a long turbulent wake is visible.

At a distance of 1-3 shiplengths behind the ship the wake is associated with increased sea surface roughness. Further away from the ship the turbulence causes damping of the short wind waves (Bragg waves) and thus a reduction of the backscattered radar power. This is a typical SAR image of a ship's turbulent wake.



South China Sea

Latitude: 7° 54' N - Longitude: 109° 04' E

The sea area shown in this ERS-1 SAR image has an extent of 18.1 km x 8.6 km and lies in the frame shown above. In the lower left-hand corner a ship followed by a long turbulent wake is visible.

This turbulent wake is best visible in the dark areas which are very likely areas covered with (natural) surface slicks. In the turbulent wake the sea surface is slick-free such that the wind can generate there Bragg waves. Thus the turbulent wake is imaged in this area as a bright line.

#	Orbit	Frame(s)	Satellite	Date	Time	Location
1	24841	3555	ERS-1	15-Apr-1996	03:20	
2	05125	3483	ERS-2	13-Apr-1996	03:14	
3	24755	3447	ERS-1	09-Apr-1996	03:08	

East China Sea

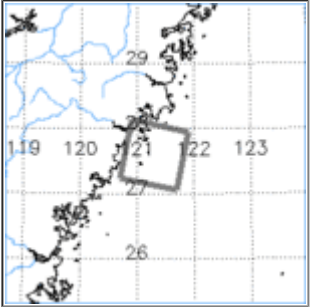


East China Sea

Latitude: 27° 36' N - Longitude: 121° 19' E

The dark area extending almost over the whole image is very likely covered with natural surface slicks.

Such slicks are only one molecular layer thick and are encountered frequently in coastal areas where the biological activity is high. The bright lines are attributed to ship wakes, where the slick has been washed aside enabling the wind to generate Bragg waves.

Orbit	Frame(s)	Satellite	Date	Time	Location
20260	3051	ERS-1	31-May-1995	02:30	

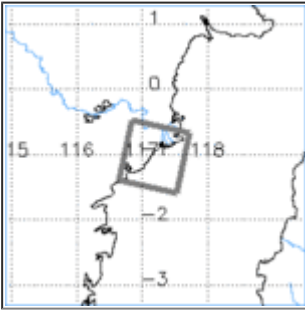
Macassar Strait



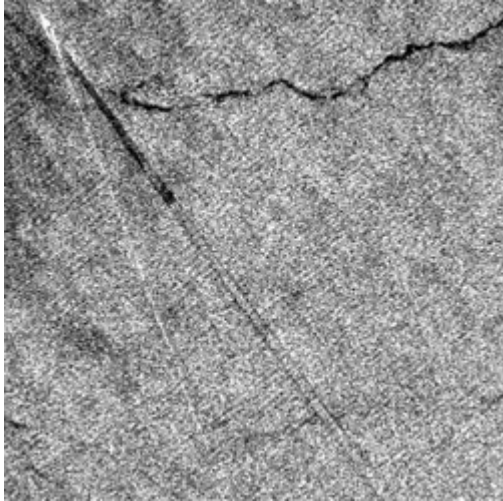
Mahakam

Latitude: 1° 01' N - Longitude: 117° 12' E

This ERS-2 SAR image covers the estuary of the river Kutai in Borneo with its fresh water plume. Inside the plume area are visible several ships (bright spots) together with their turbulent wakes.

Orbit	Frame(s)	Satellite	Date	Time	Location
24320	3627	ERS-2	12-Dec-1999	02:29	

Strait of Malacca



Strait of Malacca

Latitude: 4° 36' N - Longitude: 99° 35' E

This image shows a 10 km x 12.6 km subsection of an ERS-1 SAR scene in the Strait of Malacca. A ship, its turbulent wake (partially dark band) and one arm of its Kelvin wake (bright line) can be seen.

Interestingly, the far-end of the turbulent wake is imaged as two quasi-parallel dark lines. We interpret this as being caused by the accumulation of surface slicks at the convergent lines at both rims of the turbulent wake.

These convergent lines are produced by the orbital motions associated with the two counter-rotating vortices in the wake of a ship (see introduction).

Orbit	Frame(s)	Satellite	Date	Time	Location
25121	0081	ERS-1	04-May-1996	16:00	A map of the Strait of Malacca region, showing the Malay Peninsula and Sumatra. A rectangular box highlights the area covered by the SAR image, centered around 99° 35' E and 4° 36' N. The map includes latitude and longitude markings.

Underwater Bottom Topography

Introduction

Underwater bottom topographic features become visible on radar images of the sea surface when there is a current (usually tidal current) which flows over these features. This causes local perturbations to the current which in turn modulates the sea surface roughness.

Locating underwater sand banks by roughness variations of the sea surface has been used for several hundred years by mariners to avoid running aground. Since SAR is a very sensitive roughness sensor, it is an ideal instrument for mapping the roughness pattern induced by (tidal) flow over underwater bottom topography.

Theories describing the radar imaging of underwater bottom topography have to account for (1) the modulation of the current by the underwater features, (2) the modulation of the sea surface waves by the variable surface current and (3) the interaction of the microwaves with the surface waves.

The last two parts of the SAR imaging theory of underwater bottom topography are the same as for the SAR imaging theory of internal waves. Papers dealing with the SAR imaging of underwater bottom topography are given in the reference list below, but see also the reference list of the general section on "Oceanic phenomena".

These theories are the basis of commercial services which generate bathymetry maps by inverting ERS SAR images at a significantly lower cost than conventional survey techniques.

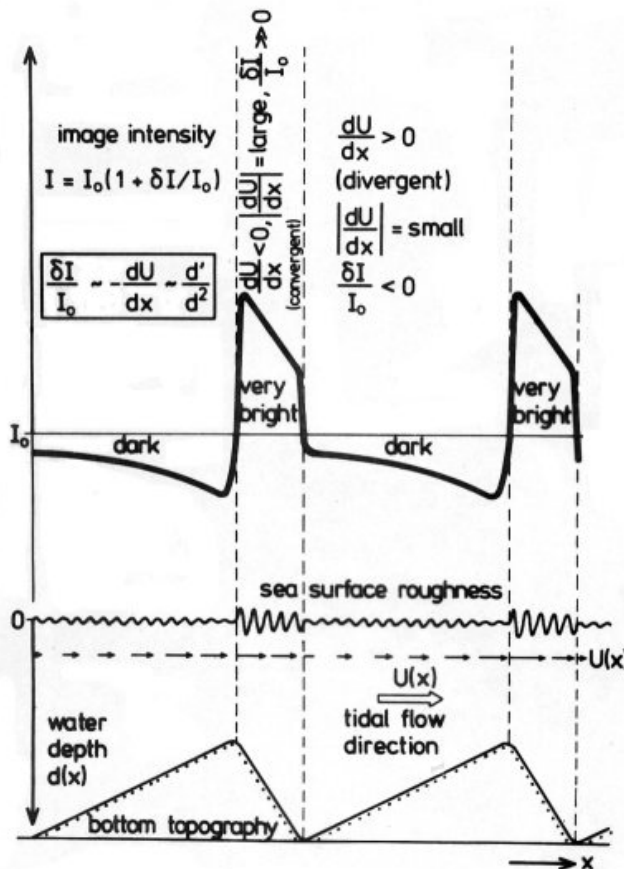


Fig.: Schematic plot of the relationship between an asymmetric sand wave profile and associated variations in tidal current velocity, short-scale surface roughness, and radar image intensity. The steep slopes of the sand waves face the flow direction and are associated with strongly reduced image intensity (dark streaks).



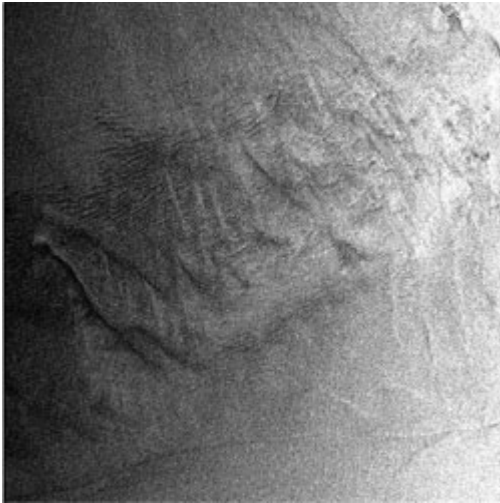
South China Sea

Latitude: 22° 29' N - Longitude: 118° 54' E

ERS-1 SAR image of the central part of the Taiwan Tan Shoals. The exact location is the box marked I in the bathymetric map of this area depicted in the section "Ancillary information to these images".

The water depth in most of the shallow areas (the areas showing wave-like patterns in the image) is between 10 m and 20 m. The Taiwan current is visible in the lower section of the image.

The bright streaks are sea surface manifestations of current fronts which closely follow the depth lines. During the ERS-1 SAR data acquisition a light wind was blowing.



South China Sea

Latitude: 22° 13' N - Longitude: 118° 42' E

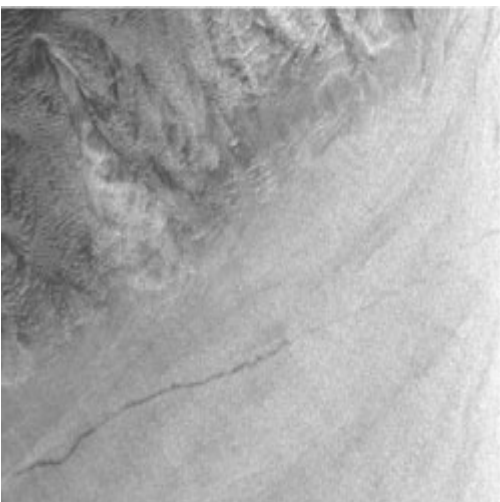
ERS-1 SAR image of the central part of the Taiwan Tan Shoals (approximately the area marked I in the bathymetric map) acquired during another phase of the tidal cycle and under different wind conditions as the first SAR image.



South China Sea

Latitude: 23° 07' N - Longitude: 118° 11' E

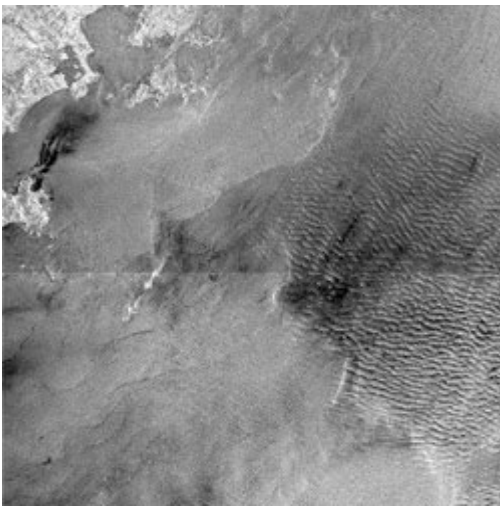
ERS-2 SAR image of the eastern part of the Taiwan Tan Shoals. The imaged area is the box marked III in the bathymetric map.



South China Sea

Latitude: 22° 13' N - Longitude: 118° 42' E

ERS-1 SAR image of the southern part of the Taiwan Tan Shoals. The imaged area is the box marked II in the bathymetric map. Part of the imaged area is the same as in image 1. The wind speed during the ERS-1 SAR data acquisition was between 2 and 5 m/s.



South China Sea

Latitude: 23° 20' N - Longitude: 117° 30' E

ERS-2 SAR image of the north-western part of the Taiwan Tan Shoals. The imaged area is not shown in the bathymetric map. The land area visible in the upper right-hand section of the image is the Chinese coast.

#	Orbit	Frame(s)	Satellite	Date	Time	Location
1	15850	441	ERS-1	27-Jul-1994	14:31	
2	05640	3159	ERS-2	19-May-1996	02:37	
3	13928	3141	ERS-2	19-Dec-1997	02:40	
4	20303	3159	ERS-1	03-Jun-1995	02:37	
5	21715	3123-3141	ERS-2	16-Jun-1999	02:43	

Coast Of China



China

Latitude: 32° 52' N - Longitude: 121° 23' E

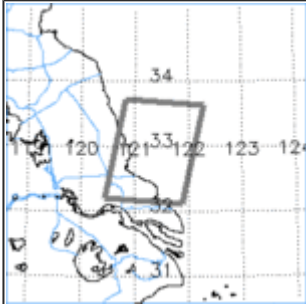
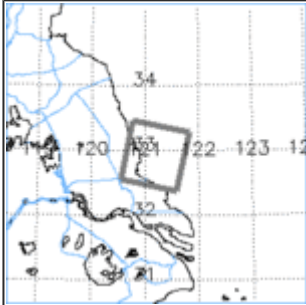
Spot 2 image of the same area as in Fig.1, but slightly shifted to the north. Also the submerged and fallen-dry sand banks can be delineated on this image.



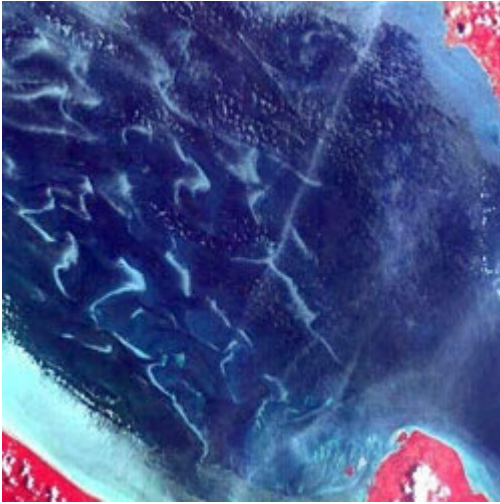
China

Latitude: 32° 56' N - Longitude: 121° 12' E

ERS-1 SAR image of the Xinchuan Gang Shoals at the east coast of China north of Shanghai. Part of the area falls dry during ebb tide (dark areas off the coast).

#	Orbit	Frame(s)	Satellite	Date	Time	Location
1	Path: 294-296	283P1-284P1-285P1-283P2-284P2-285P2	SPOT 2	27-Jul-1997	02:34	
2	20804	2943	ERS-1	08-Jul-1995	02:34	

Strait of Malacca

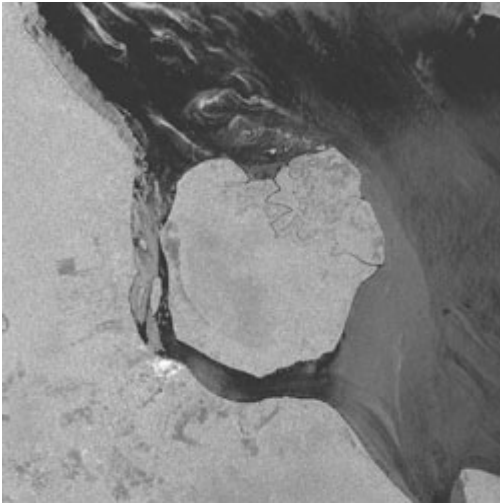


Strait of Malacca

Latitude: 2° 24' N - Longitude: 101° 28' E

Spot image of roughly the same area as visible in the previous ERS-1 SAR image. This image was acquired at an incidence angle of 30.3 degrees. The sun elevation angle was 73.1 degrees.

The sandbanks show up as bright features in this optical image. The bright line crossing the strait is very likely the contrail of an aircraft which consists of condensed water vapor formed in the wake of a jet.



Strait of Malacca

Latitude: 1° 54' N - Longitude: 101° 34' E

This ERS-2 SAR image partly overlaps the area visible in the previous ERS-1 SAR image. Note, however, that on this SAR image the sea surface manifestations of the same sandbanks differ significantly from the ones visible on the previous SAR images. This is due to the fact that the flow and atmospheric conditions were different on both days.



Strait of Malacca

Latitude: 2° 32' N - Longitude: 101° 27' E

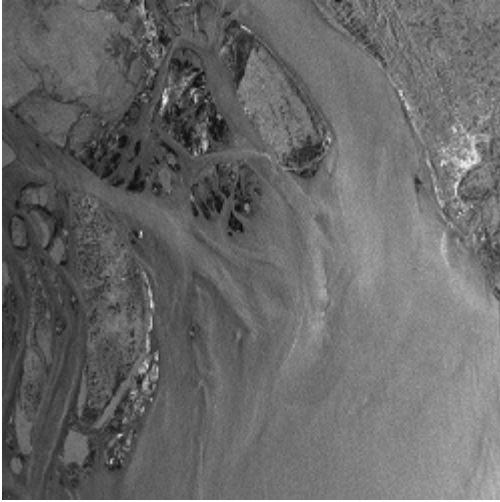
Section of the Strait of Malacca where shallow sandbanks are located. At the bottom of the image the coast of Sumatra is visible and at the top the coast of Malaysia. The irregular features in the lower part of the image are sea surface manifestations of sandbanks.

The tidal flow, which at the time of the SAR data acquisition was directed eastwards, is modified by the sandbanks. This leads to a change in sea surface roughness over the sandbanks which is detectable by SAR.

The sandbanks in this region are only a few meters deep, and some of them even fall dry at low tides. The shipping lane is located north of this area.

#	Orbit	Frame(s)	Satellite	Date	Time	Location
1	Path: 269	345X2	SPOT 2	07-Oct-1999	04:01	
2	21938	0027	ERS-2	01-Jul-1999	15:53	
3	25199	3555	ERS-1	10-May-1996	03:35	

Ganges



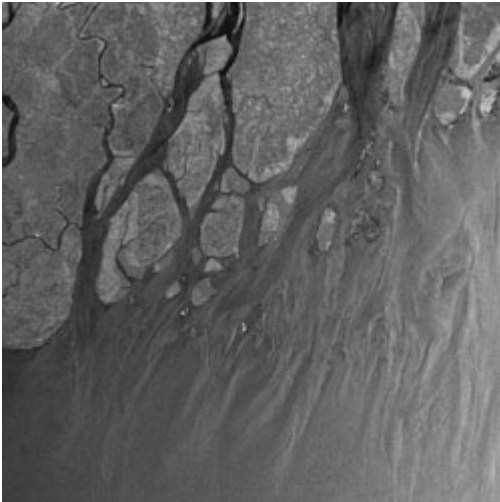
Ganges

Latitude: 21° 45' N - Longitude: 91° 16' E

On this ERS-2 image, the eastern section of the Mouths of the Ganges is visible. In the upper right-hand section of the image the eastern coast of Bangladesh is visible. The bright area on the coast consisting of a cluster of bright spots is the town Chittagong. The large island in the centre of the upper section of the image is Sandwip Island.

The dark areas surrounding this island as well as the other dark areas in this region are sandbanks that have fallen dry. A comparison of this SAR image with a sea map published in 1990 reveals that the positions and shapes of the sandbanks and the shapes of the islands have changed considerably in the last 7 years.

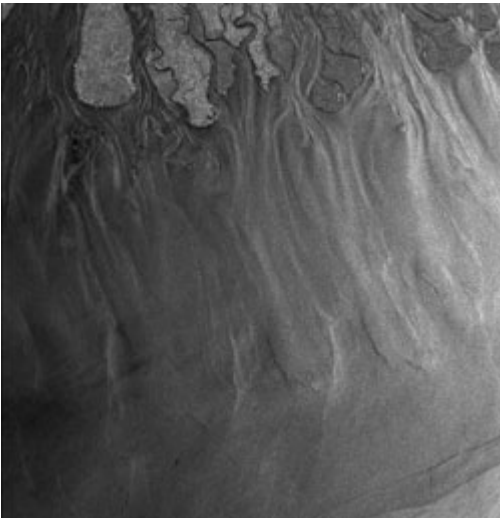
The streaky features on the water surface result from underwater sandbanks that modify the current flow. The water depth throughout this region is less than 10m.



Ganges

Latitude: 21° 45' N - Longitude: 90° 32' E

On this ERS-2 SAR image, a section of the Mouths of the Ganga which is located further west than the section visible on the previous ERS-2 SAR image is visible. The two large river systems are (from left to right) the Tetulia River and the Meghna River in Bangladesh. In the lower section of the image, sea surface manifestations of internal waves are also visible.



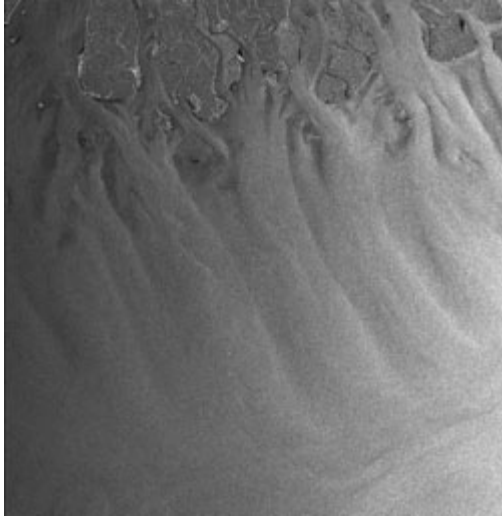
Ganges

Latitude: 21° 18' N - Longitude: 88° 18' E

The area visible on this image is part of the Indian section of the Mouths of the Ganga, which is also called "The Sandheads". Several long-stretched shallow sandbanks protrude from the coast into the Bay of Bengal.

In the upper left-hand corner of the image the estuary of the Hugli River is visible, which connects the harbour of Calcutta in India with the Bay of Bengal.

A comparison of this SAR image with a sea map of "The Sandheads" published in 1996 reveals that the positions and shapes of the sandbanks have varied considerably in the last 4 years.

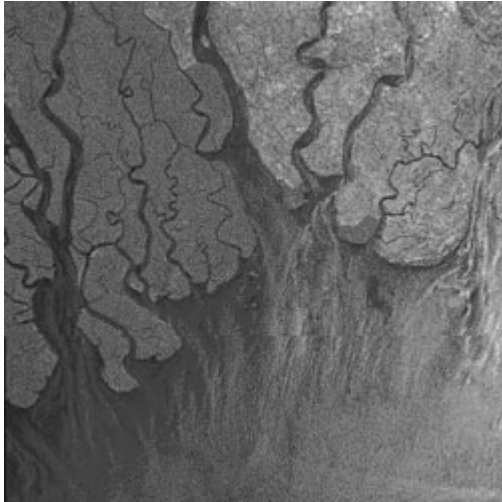


Ganges

Latitude: 21° 18' N - Longitude: 88° 17' E

The area visible on this ERS-2 SAR image is the same as visible on the previous image, however imaged at a different time.

Note the differences in the sea surface manifestations of the underwater sand banks on these two ERS SAR images.



Ganges

Latitude: 21° 45' N - Longitude: 89° 49' E

Composite of two ERS-2 SAR scenes (200 km x 100 km) of the western part of the Bangladesh section of the Mouths of the Ganga. The two large rivers visible in the left-hand section of the image are the Pussar River and the Haringhata River.

The reason why the land area between these two rivers has a darker grey level tone is not known. It could be that this region was flooded recently leaving a high moisture content in the soil which causes a reduction in the backscattered radar power.

Also faintly visible are in the lower section of the image sea surface manifestations of internal wave packets.

#	Orbit	Frame(s)	Satellite	Date	Time	Location
1	10966	3159-3177	ERS-2	26-May-1997	04:27	
2	09234	3159-3177	ERS-2	25-Jan-1997	04:30	
3	09048	3177	ERS-2	12-Jan-1997	04:39	
4	05541	3177	ERS-2	12-May-1996	04:39	
5	09005	3159-3177	ERS-2	09-Jan-1997	04:33	

Upwelling

Introduction

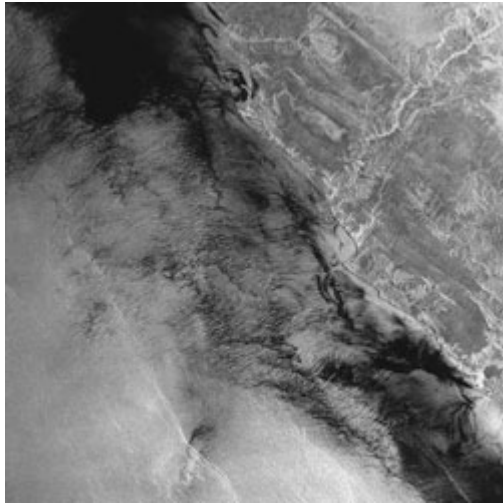
Upwelling areas are often located at the eastern boundary of an ocean. If the wind blows parallel to the coast and toward the equator at the eastern boundary of an ocean, water of the upper layer (the so-called Ekman layer) moves away from the coast in either hemisphere and is replaced by water upwelling from below this layer. The upwelled water is cooler than the original surface water and a band of low temperature surface water develops close to the coast.

Often this band has a patchy structure. Usually it has a larger concentration of nutrients (phosphates, nitrates, silicates, etc.) than the original surface water. Thus upwelling areas are usually areas of high biological productivity with a high fish population.

This implies that in these regions the amount of surface active substances secreted by marine plants and animals, which float to the sea surface and create there a surface film, are greatly enhanced.

Upwelling areas of this kind are found off the northwest and southwest African coast, off the coast of Peru, and off the North American coast from British Columbia to California.

Angola



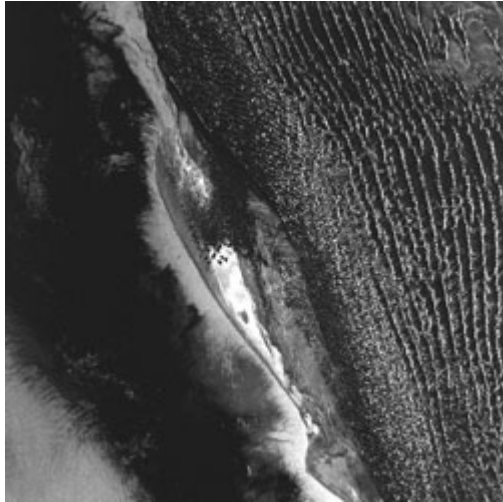
Angola

Latitude: 9° 57' S - Longitude: 13° 09' E

The dark areas adjacent to the coast of Angola are very likely upwelling areas.

Orbit	Frame(s)	Satellite	Date	Time	Location
23499	3807	ERS-1	12-Jan-1996	09:20	A map showing the location of the satellite image. The map displays the coastline of Angola and the surrounding ocean. A grid of latitude and longitude lines is overlaid on the map. The latitude lines are labeled with values 8, 9, 10, 11, and 12, with negative signs indicating south. The longitude lines are labeled with values 11, 12, 13, and 14. A rectangular box is drawn on the map, highlighting the specific area of interest along the coast of Angola, which corresponds to the satellite image shown in the previous block.

Namibia

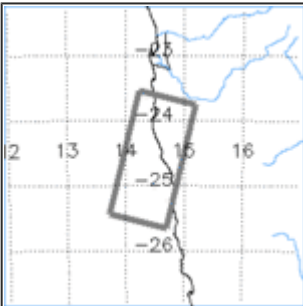


Namibia

Latitude: 24° 33' S - Longitude: 14° 29' E

ERS-2 SAR strip along the coast of Namibia. The wave-like features visible in the right-hand section of the image are sand dunes in the Namibia desert. It is known that at this coast strong upwellings occur.

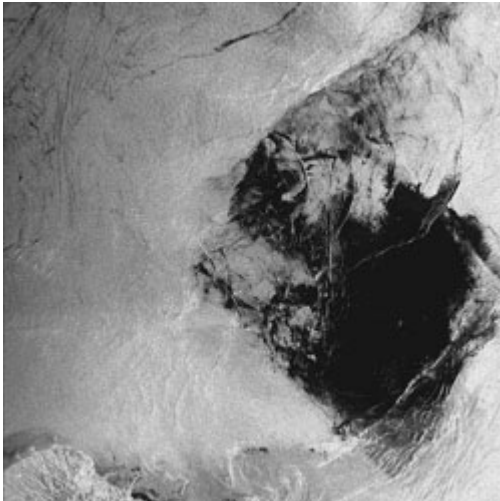
Very likely the dark band stretching along the coast is an upwelling area. Note also the sea surface manifestations of internal wave patterns visible in the lower left-hand corner of the image.

Orbit	Frame(s)	Satellite	Date	Time	Location
3425	4095-4113	ERS-2	16-Dec-1995	09:04	 A map showing the location of the SAR strip in Namibia. The map includes a grid with latitude lines at 24, 25, and 26 degrees South, and longitude lines at 13, 14, 15, and 16 degrees East. A black rectangle highlights the area covered by the SAR strip, which is centered around 24.5 degrees South and 14.5 degrees East.

Thailand

Upwelling is a phenomena that is often encountered in coastal areas. In upwelling areas cold water is convected from larger depths to the surface where it changes the stability of the air-sea interface. As a consequence the wind stress is reduced in this area and thus also the sea surface roughness.

Furthermore, the cold upwelling water is rich in nutrients which enhances the biological productivity. The increased plankton and fish population leads to a higher concentration in natural surface films which damp the Bragg waves. Both effects cause a reduction of the NRCS in upwelling regions. In general it is not known which effect is the dominant one.

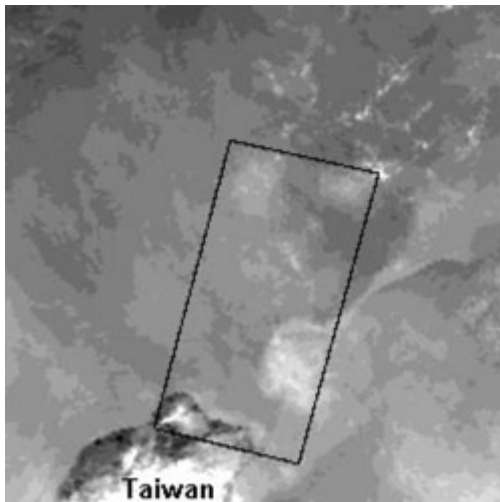


Taiwan Strait

Latitude: 25° 20' N - Longitude: 121° 56' E

Upwelling area northeast of Taiwan (large dark area in the lower right-hand section of the image).

Due to the interaction of the Kuroshio current with the ambient waters of the East China Sea and with the bottom topography a cold eddy is often encountered in this area. Also sea surface manifestations of oceanic internal waves are visible in the upwelling area which suggests that upwelling is a generation mechanism for internal waves.



Taiwan Strait

Latitude: 26° 15' N - Longitude: 121° 53' E

Sea surface temperature (SST) map derived from NOAA-11 AVHRR (Advanced Very High Resolution Radiometer) channel 4 data. Bright grey tones denote low SST values.

Clearly visible is a cold eddy northeast of Taiwan which corresponds well with the location of the dark patch visible on the previous ERS-1 SAR image. Inserted is into this map the location of the previous ERS-1 SAR scene.

The cold water surface gives rise to a stable marine boundary layer which makes it harder for the wind to generate small-scale sea surface roughness.

In addition, upwelling areas are areas of increased biological activity which give rise to an increased coverage of the ocean surface with natural surface films. The surface films damp the short surface waves (Bragg waves).

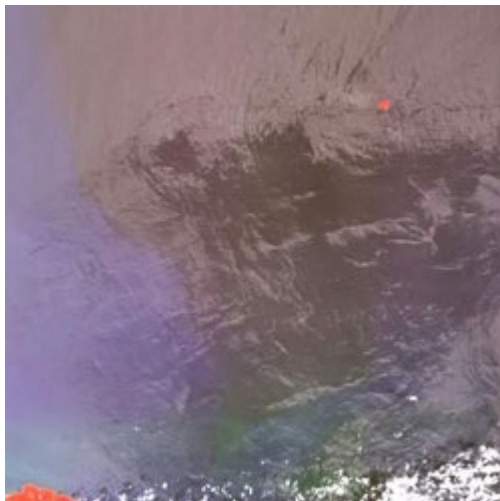
Thus both effects lead to a reduction of the radar backscattering. This is the reason why upwelling areas appear on radar images as areas of reduced image intensity.

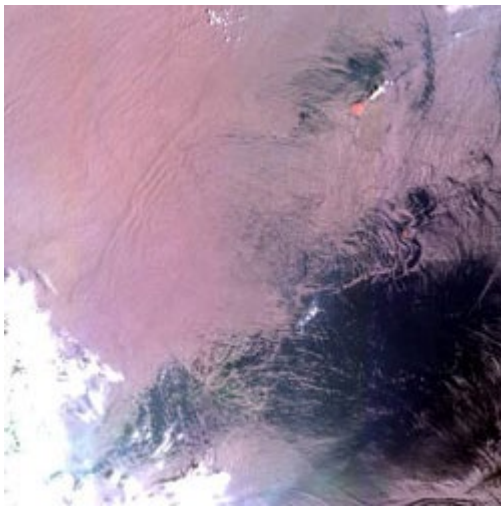
Taiwan

Latitude: 25° 29' N - Longitude: 121° 52' E

SPOT-2 image of the upwelling area northeast of Taiwan. The upwelling area lies in this image outside the sunglint area.

It is characterised by a reduced sea surface roughness and thus appears on this optical image as an area of reduced image intensity. The red spot visible in the upper section of the image is the island Pengchina.





Taiwan

Latitude: 25° 29' N - Longitude: 121° 54' E

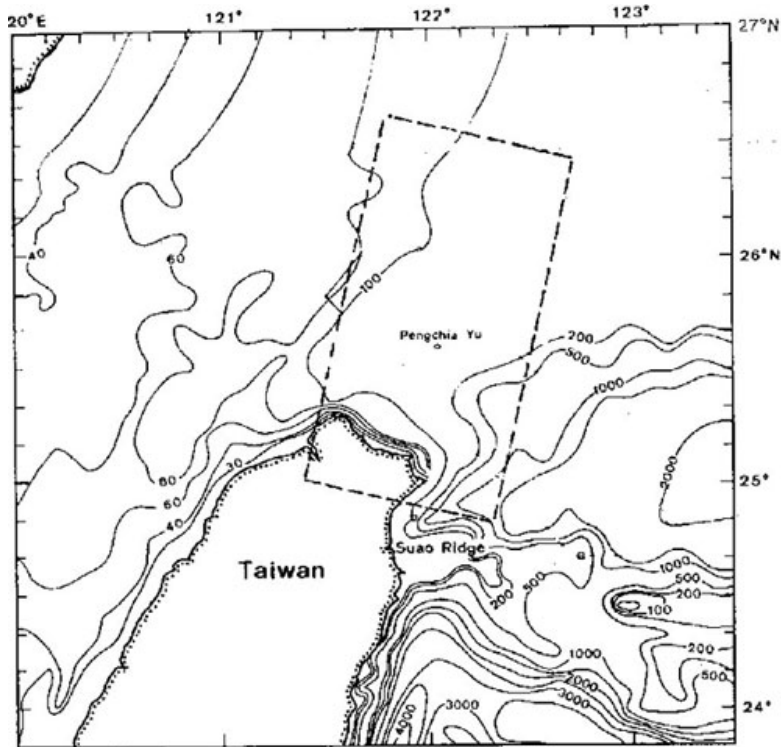
SPOT-2 image of the same area as in the previous SPOT-2 image, but imaged at a different time. Again, the upwelling area is characterised as an area of reduced image intensity.

Note the numerous internal wave features surrounding the upwelling area which indicates that it is a birth place for internal waves.

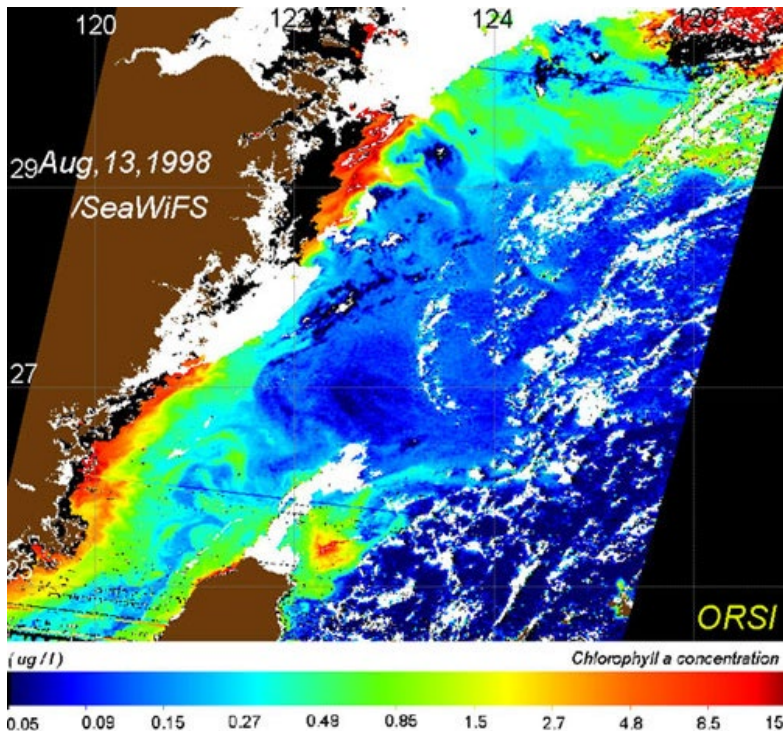
© CNES 2000 - [Spot Image](#) distribution

#	Orbit	Frame(s)	Satellite	Date	Time	Location
1	15785	3087-3105	ERS-1	23-Jul-1994	02:26	
2	30064	-	NOAA-11	22-Jul-1994	08:03	
3	Path: 300	299P2	SPOT 2	06-Apr-1999	02:53	
4	Path: 300	299P1	SPOT 2	09-Sep-1999	02:53	

Ancillary information



Map of the chlorophyll a concentration derived from SeaWiFS data of the American Seastar satellite. It clearly shows increased chlorophyll a concentration in the upwelling area north of Taiwan (This image was kindly provided by Prof. Ming-Xia He, Ocean Remote Sensing Institute, Ocean University of Qingdao, China).



Bathymetric map of the sea area north of Taiwan. The numbers to the isobath lines denote the depth in metres.

References

- Ajao, E.A. & Houghton, R.W., Coastal ocean of equatorial West Africa from 10°N to 10°S. In: *The Sea*, 11, edited by A.R. Robinson and K.H. Brink, John Wiley & Sons, Inc., Chapter 20, 605-631 (1998).
- Clemente-Colon, P. & Yan, X.-H., Observations of east coast upwelling conditions in synthetic aperture radar imagery, *IEEE Trans. Geosci. Remote Sens.*, 37, 2239-2248 (1999).
- Gong, G.-C., Lee Chen, Y.-L. & Liu, K.-K., Chemical hydrography and chlorophyll a distribution in the East China Sea in summer: implications in nutrient dynamics. *Cont. Shelf Res.*, 16, 1561-1590 (1996).
- Gong, G.-C., et al., Effect of the Kuroshio intrusion on the chlorophyll distribution in the southern East China Sea during spring 1993, *Contin. Shelf Res.*, 17, 79-94 (1997).
- Liu, K.-K., Gong, G.-C., Lin, S., Shyu, C.-Z., Pai, S.-C., Wie, C.-L. & Chao, S.-Y., Response of Kuroshio upwelling to the onset of northeast monsoon in the sea north of Taiwan: observations and numerical simulation, *J. Geophys. Res.*, 97, 12511-12526 (1992).
- Mitnik, L.M., Hsu, M.-K. & Liu, C.-T., ERS-1 SAR observations of dynamic features in the southern East-China Sea, *La mer*, 34, 215-225 (1996).
- Shillington, F.A., The Benguella upwelling system off Southwestern Africa. In: *The Sea*, 11, edited by A.R. Robinson and K.H. Brink, John Wiley & Sons, Inc., Chapter 20, 583-604 (1998).
- Schumann, E.H. Wind-driven mixed layer and coastal upwelling processes off the south coast of South Africa, *J. Marine Res.*, 57, 671-691 (1999).
- Smith, R.L., Upwelling, *Oceanography and Marine Biology, Annual Reviews*, 6, 11-46 (1968).